Analyses of the Behavior of Stimuli-Sensitive Microgel in SPR sensor

A Dissertation Submitted to Keio University
In Partial Fulfillment of the Requirement for the
Degree of Doctor of Philosophy

March 2008

Anan Jeenanong

Acknowledgements

The work presented in this thesis has been carried out at Polymer Science Laboratory, Center for Chemical Biology, School of Fundamental Science and Technology, Graduate School of Science and Technology, Keio University. I cannot do so without an appreciation for the contributions made by numerous individuals.

The respect and gratitude should be first given to my supervisor Professor Haruma Kawaguchi, who provided me with kind guidance, the opportunity, and the resources. I am grateful to him for devoting time for teaching me the skills of a researcher such as generating ideas with logical thoughts keeping the records, analyzing the data, presenting and writing the technical material in spite of his busy schedule. His logical and analytical thinking along with the deep involvement in my work has played a big role in shaping my approach towards the research. Indeed, I am fortunate to work under the guidance of a teacher with such a good personality that will be invaluable in my future development as an academic, a researcher, and a human being.

I would like to express my great appreciation to Professor Koji Suzuki, Associate Professor Keiji Fujimoto, and Associate Professor Atsushi Hotta; for their careful reviewing on my thesis book and serving on the supervisory committee for this thesis. Their comments and advises greatly improved the thesis.

This thesis would be also remiss without acknowledging the enormous contributions of Associate Professor Sanong Ekgasit of Chulalongkorn University. I was first introduced to the field of Physical Chemistry through his words and teachings. Although it was a short time to work with him, he has shown me the most unique efficiency and enthusiasm that have given me the initial motivation for being a good teacher in my future. His efforts and kindness throughout the years are the main reason that I was given this opportunity to come to Japan and approach to my Ph.D.

This work could not have been done without help and support of Mr. Mitani and the people who working at Central Service Facilities for Research, Keio University. I would like to thank them for providing us a great environment of research with best conditioned machinery.

I would also like to express my debt and gratitude to the many of my colleagues and friends. They include in particular the following: Dr. Sasiporn, Mr. Itthisek, Mr. Chutisant, Mr. Songkarn, Ms. Anwida, Ms Wongwanida, Mr. Phanu, and Mr. Amornsak. It gives me an immense pleasure to thank all my friends for their constant support, which made my days lively in Japan. I would like to thank all the members of Kawaguchi Laboratory and Fujimoto Laboratory, especially, Ms. Fang, Mr. Hattori, and Mr. Ishii, for teaching me basic experimental techniques. The friendships they made from this experience are very valuable to me. I feel I have been lucky to join this lab. I would also like to thank Ms. Umehara and Mr. Hara for teaching me about SPR. I appreciated all of the time they spend explaining SPR and helping with data analysis and troubleshooting. I would also like to thank my friend Dr. Ken for his helpful discussions about research.

My deepest thanks to my parents and my family whose unconditional support, encouragement and love has made it possible for me to achieve this. They are always a source of inspiration for me. Without their love and support I would not be the person that I am. I also would like to thank Ms. Busarakum, thank for your love and support. She has encouraged me with love and understanding, standing by me throughout the last three years even being far away.

Finally, I cannot forget to recognize the following financial supports during my Ph.D study: Keio Scholarship (2005-2008) and a Grant-in-Aid for the 21st Century COE program “Life Conjugated Chemistry, Keio University” from the Ministry of Education, Culture, Sports, Science, and Technology, Japan (2006-2007).

Anan Jeenanong

6 February 2008

Contents

Chapter 2
SPR response of stimuli-sensitive microgel on sensor chip

Chapter 3

Effect of swelling degree on SPR response in standard SPR chip

Chapter 4

Protein Adsorption to 2D-arrayed microgels on SPR chip

List of tables

Table

List of figures

Figure

2.13 AFM views of the poly(NIPAM-*co*-AAc) microgels on SAM surface prepared from various buffers, (a) glycine buffer (pH 9.5), (b) NaCl aq. (pH 5.7), and (c) citrate buffer (pH 3.2) at 40°C.

2.14 Calculated mean square electric fields (MSEFs) of their resonance angles of SPR pass through in different positions of spherical microgel as shown in side view (a) and top view (b). Solid lines show MSEF decay profiles of microgels in various positions; A, B, and C. A dashed line is the MSEF in solution without microgel. The inset is added for clarity, the inset shows the discontinuities of the evanescent field amplitudes at the Au/SAM and SAM/gel interfaces.

2.15 Difference in mean square electric fields between solution and microgel for calculating SPR response. It is shown as the shadow area in the figure.

2.15 The comparison of SPR responses between calculated (Cal) and experimental (Exp) responses.

2.16 The comparison of SPR responses between calculated (Cal) and experimental (Exp) ones.

3.1 Polymer segment distributed along with the solvent in the liquid lattice

3.2 Degree of swelling of poly(NIPAM-*co*-AAc) as a function of ionic strength at 20°C

3.3 Sensorgrams of microgels as a function of temperature in various buffer solutions. 25 μl of analyte was injected with a flow rate of 5 μl/min in SPR running buffer. The same chip was used in all experiments for keeping unchanged number of microgels on the chip surface.

3.4 Morphology of microgel in different shape (a) Flat film microgel and (b) Spherical microgel

3.5 Schematic shows the different evanescent wave between passing thought in microgel film ($\langle E^2 \rangle_x$) and buffer solution (without binding microgel, $\langle E^2 \rangle_{0,x}$). The difference area (shadow area) is integrated and used to calculated SPR response based on evanescent wave.

3.6 Mean square electric fields in buffer solution and microgel system; (a) film and (b) spherical models. The SPR response corresponds to the shadow area in each figure.

3.7 Morphology of microgels in different buffers; (a) the spherical microgels on the chip in citrate buffer (b) the gel films on the chip in both of NaCl aq., and (c) glycine buffer. Solid and dashed lines are shapes at 20°C and 40°C, respectively.

Abbreviations

AAc	Acrylic acid
AFM	Atomic Force Microscopy
APS	Ammonium Persulfate
ATR	Attenuated Total Reflection
BIS	*N*,*N'*-Methylene(bisacrylamide)
Cal	Calculated value
DLS	Dynamic Light Scattering
DSC	Differential Scanning Calorimetry
Exp	Experimental value
H.D	Hydrodynamic diameter
KPS	Potassium Persulfate
LCST	Lower Critical Solution Temperature
MSEF	Mean Square Electric Field
NIPAM	*N*-isopropylacrylamide
PBS	Phosphate Buffered Saline
PCS	Photon Correlation Spectroscopy
Poly(NIPAM)	Poly(*N*-isopropylacrylamide)
Poly(NIPAM-*co*-AAc)	Poly(*N*-isopropylacrylamide-*co*-acrylic acid)
RII	Refractive Index Increment
RU	Response Unit
SAM	Self Assembled Monolayer
SAN	Small-Angle Neutron Scattering
SEM	Scanning Electron Microscopy
SDS	Sodium Dodecyl Sulfate
SP	Surface Plasmon
SPR	Surface Plasmon Resonance
TEM	Transmission Electron Microscopy
VPTT	Volume Phase Transition Temperature
2D	Two Dimensional

Abstract

This dissertation is aimed to understand how Surface Plasmon Resonance (SPR) sensor detects the stimuli-sensitive behavior of microgels. Chapter 1 gives a detailed background of SPR and microgels. Chapter 2 describes the information of SPR response of poly(*N*-isopropylacrylamide-*co*-acrylic acid) microgels on sensor chip by changing environmental conditions (i.e., ionic strength, pH, and temperature). The attachment of microgel was carried out with different SPR sensor chips. Atomic Force Microscopy (AFM) was a tool for exploring an attachment behavior and a surface density of the microgels at different conditions. SPR simulation based on evanescent field theory was introduced the quantitative expression that described the relationship between SPR response and physicochemical valuables (i.e., refractive index, evanescent field strength, and the number of binding microgels). The effect of swelling behavior of constant numbered microgels bound on SPR sensor was presented in Chapter 3. Although the number of binding microgels was fixed, the conformation of binding microgels or swelling behavior due to changing pH and/or temperature has significant effect on SPR response. Two different models (i.e., flat film microgels and spherical microgels) in SPR simulation could explain how the difference in conformation of binding microgels and swelling degree of microgel affects the SPR response. Since the poly(NIPAM-*co*-AAc) microgels could attach strongly onto the SPR sensor chip, in Chapter 4 we fabricated two dimensional (2D) arrayed microgel, which offered the surface to study the protein adsorption at different pHs and temperatures. A series of poly(NIPAM-*co*-AAc) with different acrylic acid contents were prepared for human immunoglobulin G (IgG) adsorption analysis. The IgG adsorption onto 2D-arrayed microgel was compared to that of the microgel dispersion system. The IgG adsorption depended on AAc contents in microgel and environmental conditions. Since the SPR sensor can observe the binding event in real-time, we used the 2D-arrayed microgel to study the kinetic adsorption of IgG. In addition, the adsorption of IgG has been also monitored by using SPR imaging. The different thickness in each spot indicated the strength of the affinity of IgG to the microgel.

Chapter 1
Introduction

Hydrogels are essential stimuli-responsive or smart polymeric systems that have been widely used in different biological applications, such as the delivery of therapeutics, cell culture, tissue engineering, bioseperations, sensors or actuator systems. These polymers respond to small external stimuli with large changes in their properties. The external stimuli may be temperature, pH, electric field, chemicals, or ionic strength and the responses are large changes in the properties such as shape, surface characteristics, and solubility.

The swelling behavior of hydrogels is an important property for a variety of applications. Generally, the swelling property of polymer is reflected by the swelling ratio, the ratio of the weight of the swollen sample to the weight of the dry one. Factors affecting the swelling ratio mainly involve the chemical structure, the degree of crosslinking, the specific stimuli, and the solvent concentration and quality. Several models have been suggested to describe the relationships between structures and properties for polyelectrolyte hydrogels. There are many tools for measuring the swelling behavior of hydrogels. Surface plasmon resonance (SPR) spectroscopy is surface-sensitive due to the evanescent field of the surface plasmon. An electromagnetic wave travels along the interface between a metal and a dielectric. Its electric field decays exponentially into both materials over a distance of a few hundred nanometers. The resulting data are a direct measure of the local average refractive index of the dielectric close to the surface, and with Fresnel calculations either the thickness or the refractive index of thin films at an interface can be determined. Furthermore, a time-dependent measurement mode enables the detection of changes in the local average dielectric constant due to the adsorption of molecules onto the surface or changes in film properties due to an external trigger. Since the swelling degree of hydrogels also related to the change of refractive index of hydrogel, an interesting information about stimuli-sensitive behavior under various environmental conditions might be observed by SPR measurement.

1.1 Overview of Surface Plasmon Resonance

As early as 1909, Sommerfeld had introduced the concept of electromagnetic surface waves as a solution of Maxwell's equations for an interface between a non-conducting and a conducting medium; he dealt with the problem of wave propagation in radio telegraphy.[1] Experimental evidence for the existence of electromagnetic surface waves on a metal/dielectric interface surface plasmon (SP) waves was found in the 1950's by experiments with fast electrons passing through metal foils. In 1957, Ritchie assigned the observed characteristic energy losses of the electrons to the excitation of SP waves.[2] In 1960, Stern and Ferell had derived the resonance conditions for these modes and called them "surface plasmons".[3]

The excitation of SP waves by light was introduced by Otto in 1968.[4] The waves were resonantly excited by means of an attenuated total reflection (ATR) setup. The resonant excitation of SP waves is called surface plasmon resonance (SPR). In the Otto-configuration, the evanescent field of totally reflected light couples via an air gap to the SP waves on a silver substrate. However, it was the work of Kretschmann that gave the way to a practical application and commercial use of SPR. Also in 1968 he discovered that SP waves can also be excited on top of a silver film deposited on a glass substrate by light being totally reflected on the backside of the silver film, being reflected at the interface glass/silver.[5] Thus the Kretschmann configuration allowed the separation of the elements needed for excitation and detection spatially from the sensing region.

In the early 1980's, Nylander *et al.* and Liedberg *et al.* have demonstrated that SPR in the Kretschmann-configuration is well suited for both gas and biomolecular sensing purposes.[6-7] From there, it took to1990 until a commercial product came into the market, which made use of the distinct properties of SP waves: Pharmacia Biosensor (Sweden) introduced the BIAcore biosensor based on SPR.[8] Since then biosensors based on SPR have developed from instruments for a few interested scientists into widespread analytical tools.[9-11] Their success can be attributed to their ability to detect biomolecular interactions in real time without the need for any labeling. Today, SPR biosensors are routinely used for the analysis of protein-protein, antigen-antibody and protein-peptide interactions. Although the instruments are merely able to handle a small number of samples simultaneously, the current post-

genomic era of proteomics[12] can accomplish a further push for this technique if instrument developers can succeed in merging SPR detection technique with real high-throughput capabilities. In this context, the development of so-called imaging SPR is promising.[13-15]

The resonant excitation of surface plasmon waves on a metal film -in biosensing applications usually gold- by totally internal reflected light can be observed as a minimum in the intensity of the reflected light at a certain angle of incidence, the resonance angle ΘSPR. This phenomenon is very sensitive to the refractive index on top of the metal film; changes of the refractive index lead to a shift in the resonance angle. Surface plasmon waves are charge density oscillations on a metal surface and therefore an electric field is associated with them. The electric field is exponentially decaying with increasing distance from the surface. Typically, the decay length or penetration depth of the electric field makes up a third to a half of the exciting wavelength, e.g. for $\lambda = 784$nm the penetration depth for gold/water amounts to 324nm. Hence, SPR is an evanescent wave technique, with maximum sensitivity at the interface: only changes of the refractive index in close proximity to the gold surface alter the resonance angle.[17-18] By tracking the shift of the resonance angle, the deposition of molecules on the surface can be followed in real time. Since the change in refractive index is probed, no labeling of the molecules is necessary. Affinity biosensing makes use of these properties for the investigation of biochemical binding processes between immobilized biomolecules on the sensor surface and analyte biomolecules supplied in solution: monitoring of the interaction in real time enables the user to deduce kinetic and affinity constants of the reaction from the experimental data.[18]

However, an important prerequisite for the success of the method is a chemically tailored sensor interface which has to fulfill several tasks:

− Stable (covalent) immobilization of biomolecules as receptors

− Providing an environment which maintains the unique biological function of the immobilized biomolecules (specific interaction with their biological counterpart)

− Prevention of non-specific adsorption

Often, hydrogels are employed to achieve the desired characteristics: hydrogel functionalised surfaces provide a biocompatible 3D matrix for covalent biomolecule immobilisation. Compared to a flat surface the three dimensional structure allows a higher number of receptor molecules per area unit in addition to lower orientational

requirements for the receptors. Furthermore, the entropy elasticity of polymers may play an important role in reducing non-specific adsorption.[19]

Frequently, dextran, a α-1,6-linked polyglucose with 1,2- and 1,3-branchings is employed.[20-21] For instance, the "standard" sensor surface for the Biacore biosensor employs a dextran hydrogel that is carboxymethylated to the extent of one carboxyl group per glucose residue and is about 100 to 150nm thick.[22-24] For immobilisation of biomolecules the carboxyl groups are converted into activated esters which are reactive towards primary amino functions. These surfaces are well established for routine analysis comprising the determination of 9 the active concentration of analyte molecules and the measurements of reaction kinetics and affinity constants.[10] However, the actual shape and size of carboxymethylated dextran gels can change due to electrostatic repulsive forces between the carboxyl groups, depending on the pH and ionic strength of the solutions the hydrogel is in contact with.[25] Furthermore, the dextran matrix provides binding sites in a three-dimensional arrangement. This is raising the question about the dynamics of binding site occupation and the resulting biomolecule density distribution normal to the surface. In spite of its exponential decay, the evanescent SP wave field is probing refractive index changes in the entire dextran hydrogel. Therefore, the SPR response is also affected by the actual density profile in the hydrogel. These issues are addressed in theoretical papers,[26-28] but there is no direct experimental evidence of how these layer properties influence the SPR signal respectively to what extent these effects actually occur.

Although dextran fulfils the required tasks satisfactorily in many respects, synthetic hydrophilic polymers are attractive alternatives as they offer some potential advantages. First, they may be more resistant to harsh chemical conditions (strong acids, fouling etc.), since in particular those polymers exhibiting exclusively C-C bonds in their backbone. Second, they allow the synthesis of polymers with new physical properties by tailoring their structure. Impressive examples for the potential provided by tailored hydrogels are so-called thermo-responsive or thermo-sensitive hydrogels.[29] The behavior of thermo-responsive polymers in aqueous media often contradicts intuition because they generally exhibit a lower critical solution temperature (LCST). Upon heating, when the temperature increases beyond a certain value commonly referred to as “cloud point”, they precipitate from solution. Thermo-responsive hydrogels should undergo an analogous transition even under the

particular conditions existing in confined space at a surface.[30] Such a behavior is of special interest for applications at sensor surfaces because it allows to switch their properties, or to introduce new functionalities. However, there is no experimental proof for the effect at an interface, yet.

1.2 Fundamentals of Surface Plasmon Resonance

Electromagnetic waves guided along the boundary of two media with different dielectric constants are called evanescent waves. Their characteristic feature is the propagation along the interface. They do not transport energy into the adjacent media. However, the electric field of an evanescent wave penetrates into the adjacent media, decaying exponentially with distance from the interface. If one of the media is a dielectric and the other is a metal, these evanescent waves are called surface plasmon (SP) waves or surface plasmon oscillations, because collective oscillations of the free electrons of the metal are associated with these waves. Surface plasmon waves can be resonantly excited by internally reflected p-polarized light. The resonant excitation of surface plasmons is observable as a minimum in the intensity of the reflected light at a certain angle of incidence "the resonance angle θ_{SPR}" and is called surface plasmon resonance (SPR).[31]

For a comprehensive derivation of surface plasmon waves as electromagnetic modes of an interface dielectric D/metal M the reader may be referred to.[31-32] Here, the fundamental properties of SP waves on an interface between two semi-infinite media D and M are to be mentioned (Figure 1.1)

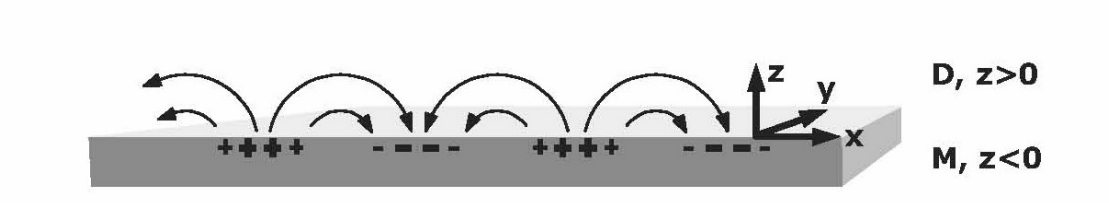

Figure 1.1 Scheme of a p-polarized surface wave and its electric field on the interface between two semi-infinite media. D: dielectric, M: metal. The oscillating charge density being associated with the electromagnetic wave is indicated

On an interface as sketched in Figure 1.1, the electric field E

$$E=E_0.e^{i(k_x x-\omega t)}.\begin{Bmatrix}\begin{pmatrix}1 & 0 & \frac{k_x}{k_{zD}}\end{pmatrix}.e^{-ik_{zD}z};z>0\\ \begin{pmatrix}1 & 0 & \frac{-k_x}{k_{zM}}\end{pmatrix}.e^{+ik_{zM}z};z<0\end{Bmatrix} \quad (1.1)$$

And the magnetic field H

$$H=\frac{\omega}{c}E_0.e^{i(k_x x-\omega t)}.\begin{Bmatrix}\begin{pmatrix}0 & \frac{-\varepsilon_D}{k_{zD}} & 0\end{pmatrix}.e^{-ik_{zD}z};z>0\\ \begin{pmatrix}0 & \frac{\varepsilon_M}{k_{zM}} & 0\end{pmatrix}.e^{+ik_{zM}z};z<0\end{Bmatrix} \quad (1.2)$$

Fulfill Maxwell's equations and the continuity relations for the tangential electric and magnetic field components and for the normal components of the electric displacement, when $k_x^2+k_{zj}^2=\varepsilon_j.\left(\frac{\omega}{c}\right)^2$, $j:D,M$

$$k_x=\frac{\omega}{c}.\left(\frac{\varepsilon_M.\varepsilon_D}{\varepsilon_M+\varepsilon_D}\right)^{1/2} \quad (1.3)$$

with ω the angular frequency, c the speed of light in vacuum, k_x and k_z the wave vector components, $\varepsilon_D = \varepsilon_D(\omega)$ the frequency dependent dielectric function of the dielectric and $\varepsilon_M = \varepsilon_{rM}(\omega)-i\varepsilon_{iM}(\omega)$ the complex dielectric function of the metal. The dielectric functions are related to the refractive indices by $\varepsilon_D(\omega) = n_D(\omega)^2$ and $\varepsilon_M = (n-ik)^2$.

In the Kretschmann-configuration, SP waves on top of a thin metal film deposited on a glass substrate are resonantly excited by totally reflected light.[5] Their field probes the dielectric properties of the medium on top of the metal film.

At angles larger than the critical angle totally reflected light forms an evanescent wave which penetrates the thin metal film. The evanescent light field can couple to SP waves, since the wave vector of light in glass is increased by the factor n_{glass}. The x-component of the light wave penetrates the interfaces without alteration and can be adjusted by varying the angle of incidence Θ (see Figure 1.2)

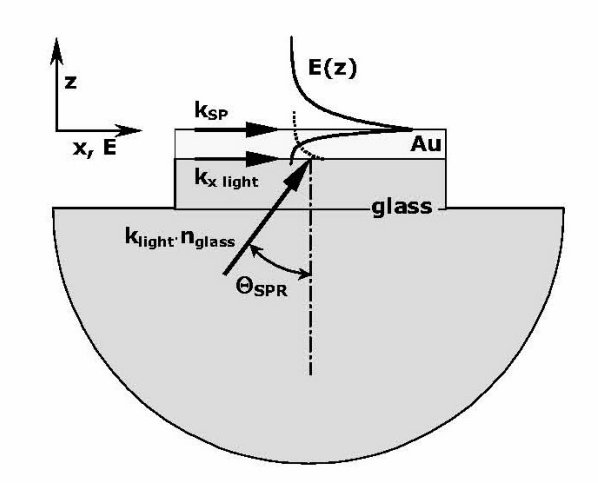

Figure 1.2 Excitation of surface plasmon waves by internally reflected light in the Kretschmann configuration. A gold coated glass slide is optically coupled to a glass prism. At the resonance angle $\cup_{SPR}$ the projection of the light wave vector in glass $k_{x\ light}$ is equal to the wave vector of the surface plasmon wave k_{SP}. The dashed line indicates the evanescent light field which is penetrating the gold film and exciting the SP waves. The exponentially decaying electric field E(z) of the SP wave is also sketched. Since the SP waves are excited resonantly their electric field is enhanced (resonance amplification)

At the particular angle of incidence Θ_{SPR} -the resonance angle- the SP waves are resonantly excited by the evanescent light field, because the resonance conditions are fulfilled: $\omega_{light} = \omega_{SP}$ and $k_{x\ light}(\Theta_{SPR}) = k_{SP}$. Although equation 1.3 must be modified for the Kretschmann-configuration,[34-35] it holds as a good approximation, thus

$$\Theta_{SPR} = \arcsin\left[1/n_{glass}\cdot\left(\frac{\varepsilon_M.\varepsilon_D}{\varepsilon_M+\varepsilon_D}\right)^{1/2}\right] \qquad (1.4)$$

1.3 SPR theory Based on Evanescent Wave

For a stratified medium with plane boundaries consisting of *N* isotropic layers, the medium is placed between a high refractive index prism and a dielectric substrate. A schematic illustration of the system is shown in Figure 1.3 The prism is transparent and has a dielectric constant of ε_P. The dielectric substrate with a semi-infinite thickness has a complex dielectric constant of $\hat{\varepsilon}_D$. The j^{th} layer of the stratified

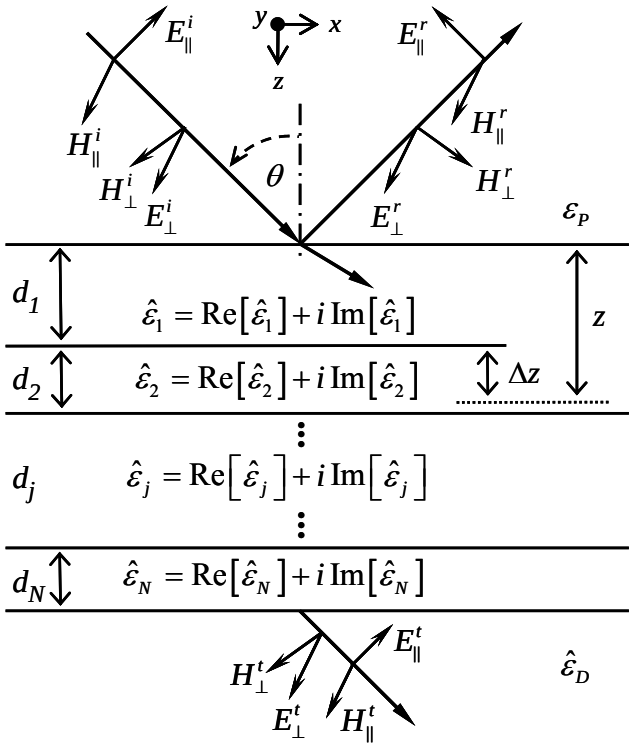

Figure 1.3 Schematic illustration shows the interaction between a plane wave and a stratified medium. Sign conventions for parallel (||) and perpendicular (⊥) polarized radiation are illustrated

medium has a thickness of d_j and a complex dielectric constant of $\hat{\varepsilon}_j$. When an incident beam of wavelength λ impinges at the prism/multilayer interface with an angle of incidence θ, the Fresnel reflection and transmission coefficients of the system are given by: [36]

$$r_{\parallel,\perp} = \frac{\left(M_{11} + M_{12}q_D\right)q_P - \left(M_{21} + M_{22}q_D\right)}{\left(M_{11} + M_{12}q_D\right)q_P + \left(M_{21} + M_{22}q_D\right)} \qquad (1.5)$$

$$t_{\parallel,\perp} = \frac{2q_P}{\left(M_{11} + M_{12}q_D\right)q_P + \left(M_{21} + M_{22}q_D\right)} \qquad (1.6)$$

where || indicates parallel-polarized radiation, ⊥ indicates perpendicular-polarized radiation. M_{mn} is an element of the characteristic matrix M(2x2) of the plane boundary stratified layers. This matrix M is given in terms of material characteristics and experimental parameters by:

$$M = \prod_{j=1}^{N} \begin{bmatrix} \cos\left(k_{zj}d_j\right) & \dfrac{-i}{q_j}\sin\left(k_{zj}d_j\right) \\ -iq_j\sin\left(k_{zj}d_j\right) & \cos\left(k_{zj}d_j\right) \end{bmatrix} \qquad (1.7)$$

where $i=\sqrt{-1}$, $q_j = k_{zj}/\hat{\varepsilon}_j$ for parallel-polarized radiation, and $q_j = k_{zj}$ for perpendicular- polarized radiation. k_{zj} is the z-component of the wavevector in the j^{th} layer and is given by $k_{zj}=\left[\left(2\pi/\lambda\right)^2\hat{\varepsilon}_j - k_{xP}^2\right]^{1/2}$. k_{xP} is the x-component of the wavevector in prism and is given by $k_{xP}=\left(2\pi/\lambda\right)\left[\varepsilon_P \sin^2\theta\right]^{1/2}$. The reflectance and transmittance are given in terms of the Fresnel reflection and transmission coefficients, respectively, according to: [36]

$$R_{\parallel}=\left|r_{\parallel}\right|^2 \quad \text{and} \quad T_{\parallel}=\frac{\mathrm{Re}\left[k_{zD}/\hat{\varepsilon}_D\right]}{k_{zP}/\varepsilon_P}\left|t_{\parallel}\right|^2 \quad \text{: for parallel polarization} \tag{1.8}$$

$$R_{\perp}=\left|r_{\perp}\right|^2 \quad \text{and} \quad T_{\perp}=\frac{\mathrm{Re}\left[k_{zD}\right]}{k_{zP}}\left|t_{\perp}\right|^2 \quad \text{: for perpendicular polarization} \tag{1.9}$$

The electromagnetic fields (the magnetic field and the electric field) at a distance z from the prism, which located within the l^{th} layer of the stratified medium, are given in terms of the wavevector and the Fresnel reflection and transmission coefficients by the following expressions.[36]

For parallel polarization:

$$\left\langle H_{yz}^2\right\rangle=\left|U_{\parallel z}\right|^2,\ \left\langle E_{xz}^2\right\rangle=\frac{\varepsilon_P}{\left(2\pi/\lambda\right)^2}\left|V_{\parallel z}\right|^2,\left\langle E_{zz}^2\right\rangle=\frac{k_{xP}^2}{\left(2\pi/\lambda\right)^2\left|\hat{\varepsilon}_j\right|^2}\left|U_{\parallel z}\right|^2 \tag{1.10}$$

with

$$\begin{bmatrix}U_{\parallel z}\\ V_{\parallel z}\end{bmatrix}=\begin{bmatrix}\cos\left(k_{zl}\Delta z\right) & i\dfrac{\hat{\varepsilon}_l}{k_{zl}}\sin\left(k_{zl}\Delta z\right)\\ i\dfrac{k_{zl}}{\hat{\varepsilon}_l}\sin\left(k_{zl}\Delta z\right) & \cos\left(k_{zl}\Delta z\right)\end{bmatrix}\prod_{j=l}^{N}\begin{bmatrix}\cos\left(k_{zj}d_j\right) & -i\dfrac{\hat{\varepsilon}_j}{k_{zj}}\sin\left(k_{zj}d_j\right)\\ -i\dfrac{k_{zj}}{\hat{\varepsilon}_j}\sin\left(k_{zj}d_j\right) & \cos\left(k_{zj}d_j\right)\end{bmatrix}\begin{bmatrix}t_{\parallel}\\ \dfrac{k_{zD}}{\hat{\varepsilon}_D}t_{\parallel}\end{bmatrix}H_{\parallel}^i \tag{1.11}$$

For perpendicular polarization:

$$\left\langle H_{xz}^2\right\rangle=\frac{1}{\left(2\pi/\lambda\right)^2}\left|V_{\perp z}\right|^2,\ \left\langle H_{zz}^2\right\rangle=\frac{k_{xP}^2}{\left(2\pi/\lambda\right)^2}\left|U_{\perp z}\right|^2,\ \left\langle E_{yz}^2\right\rangle=\left|U_{\perp z}\right|^2 \tag{1.12}$$

with

$$\begin{bmatrix}U_{\perp z}\\ V_{\perp z}\end{bmatrix}=\begin{bmatrix}\cos\left(k_{zl}\Delta z\right) & \dfrac{i}{k_{zl}}\sin\left(k_{zl}\Delta z\right)\\ ik_{zl}\sin\left(k_{zl}\Delta z\right) & \cos\left(k_{zl}\Delta z\right)\end{bmatrix}\prod_{j=l}^{N}\begin{bmatrix}\cos\left(k_{zj}d_j\right) & -\dfrac{i}{k_{zj}}\sin\left(k_{zj}d_j\right)\\ -ik_{zj}\sin\left(k_{zj}d_j\right) & \cos\left(k_{zj}d_j\right)\end{bmatrix}\begin{bmatrix}t_{\perp}\\ k_{zD}t_{\perp}\end{bmatrix}E_{\perp}^i \tag{1.13}$$

where Δz is the distance of z from the $l^{th}/(l\text{-}1)^{th}$ interface (i.e., $\Delta z = z - \sum_{j=1}^{l-1} d_j$, see Figure 1.3), $H_{\parallel}^{i}$ is the magnetic field of the incident radiation with parallel polarization while $E_{\perp}^{i}$ is the electric field of the incident radiation with perpendicular polarization. For parallel-polarized radiation, $H_{\parallel}^{i}$ is given in term of $E_{\parallel}^{i}$ by $H_{\parallel}^{i} = \sqrt{\varepsilon_P} E_{\parallel}^{i}$.[36] Since the surface plasmon resonance phenomena can only be observed with a parallel-polarized radiation, Equations 1.8 and 1.10 will be employed for the calculations of the reflectance and the electromagnetic field of the system.

The electric fields for parallel polarization are using for SPR response simulation. We calculated mean square electric field entering into the microgel phase ($\left\langle \mathrm{E}^2 \right\rangle_x$) and buffer solution (without binding microgel, $\left\langle \mathrm{E}^2 \right\rangle_{0,x}$) via this equation

$$\left\langle \mathrm{E}^2 \right\rangle_x \text{ or } \left\langle \mathrm{E}^2 \right\rangle_{0,x} = \left\langle E_{xz}^2 \right\rangle + \left\langle E_{zz}^2 \right\rangle \qquad (1.14)$$

SPR has been recently used to determine the film thickness[37-39] swelling ratio of thin polymer layers,[40-44] in biological sensing[45-48] and to study the conformational dynamics[49] of polymers. It is a surface sensitive technique based on the detection of refractive index changes in a thin dielectric layer on top of a noble metal surface and probed by the evanescent field of a laser beam. SPR instrument set-up can also be used for the investigation of thick films (dry thickness > 500 nm) by using Optical Waveguide Spectroscopy (OWS). Reflected intensity versus time scans from SPR gives information on the kinetics of swelling, which is inaccessible by other techniques. Surface sensitivity of this technique is due to the evanescent field of the surface plasmon. The latter is an electromagnetic wave traveling along the interface between the metal and a dielectric. Its electric field decays exponentially into both materials over a distance of few hundred nanometers. Reflected intensity versus angle scans when analyzed by Fresnel calculations results in simultaneous determination of refractive index and film thickness of hydrogel thin layer. The BIAcore biosensor based on SPR set up has developed for the analysis of biomolecual interactions. The instrument set up showed in Figure 1.4.

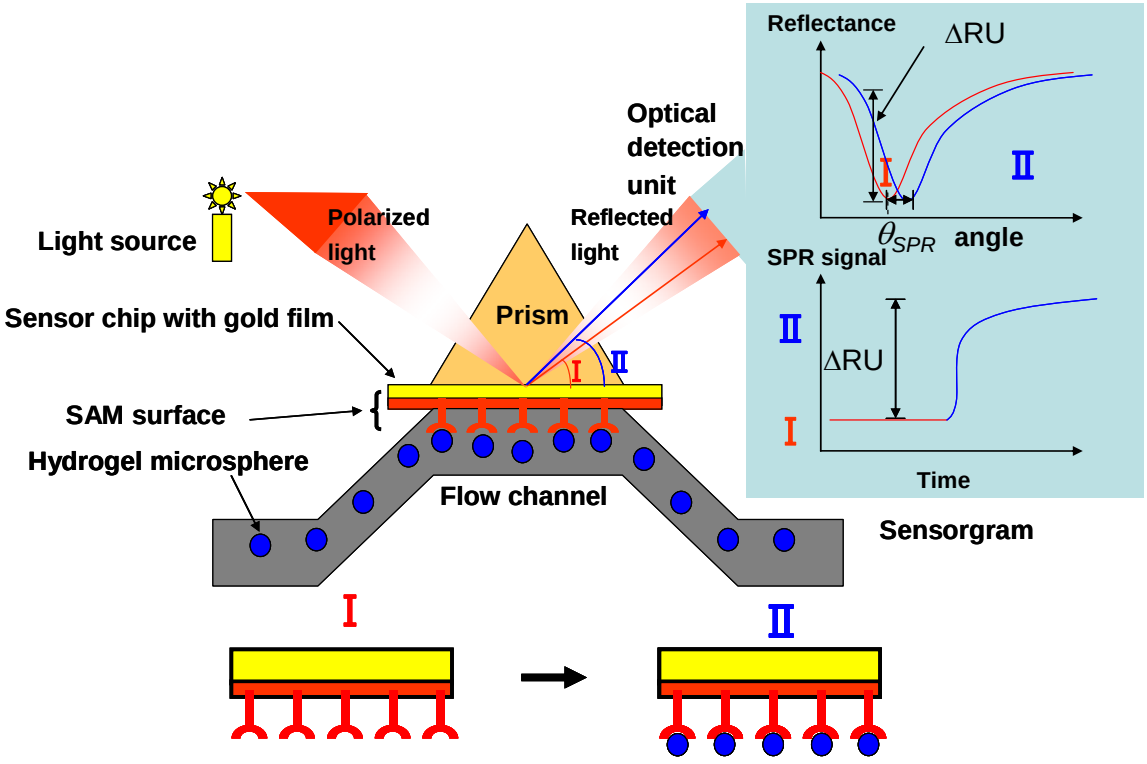

Figure 1.4 SPR detection caused by biospecific binding of ligand in solution to an immobilized receptor

1.4 Characteristics of Evanescence wave and SPR response simulation

Based on the evanescent wave calculation, we use the change of evanescent wave resulting of binding microgel for calculating SPR response in microgel system. According to the change of evanescent field strength is very sensitive to the refractive index on the top of the metal film, the decay of evanescent field strength is using for calculating the SPR response in microgel system. The strong surface plasmon wave-generated evanescent field is governed by experimental parameters (i.e., angle of incidence and wavelength of the coupled radiation) and material characteristics (i.e., complex refractive indexes of metal film, dielectric substrate and thickness of metal and dielectric films). The magnitude and decay characteristic of the evanescent field are very sensitive to changes in any of the governing parameters. This unique characteristic makes us to use evanescent field for simulating SPR response in microgel system. In general, if there is film onto SPR sensor chip surface, the

evanescent wave will be decreased. The decrease of evanescent wave also occurs in the buffer solution beyond the microgel, as shown in Figure 1.5.

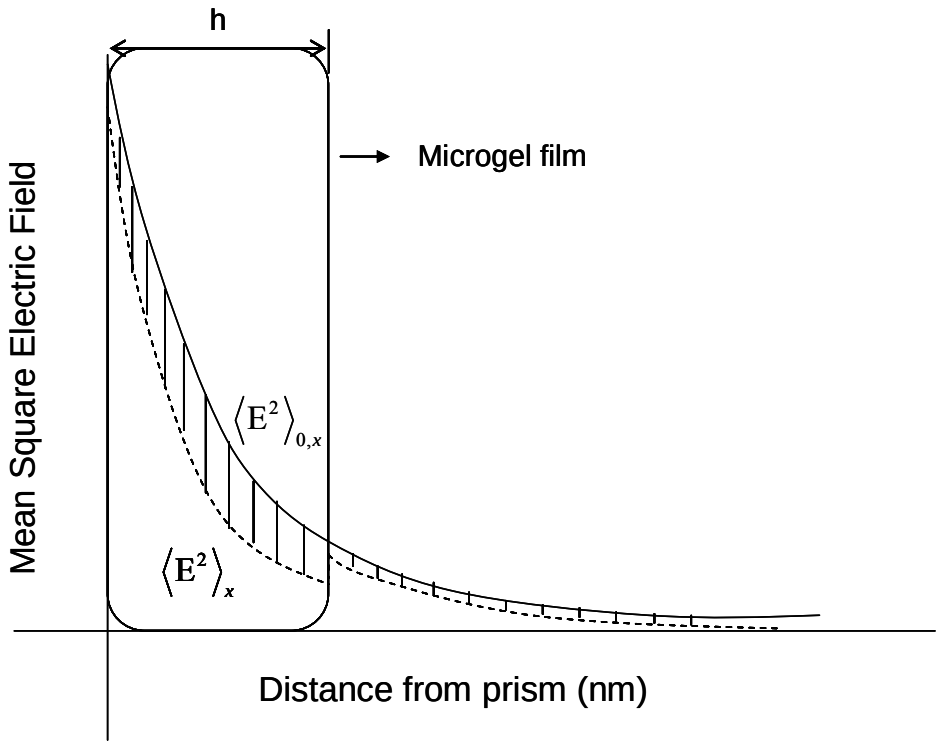

Figure 1.5 Schematic shows the different evanescent wave between passing thought in microgel film ($\langle E^2 \rangle_x$) and buffer solution (without binding microgel, $\langle E^2 \rangle_{0,x}$). The difference area (shadow area) is integrated and used to calculated SPR response based on evanescent wave.

To calculate the SPR response based on evanescent wave, we have to calculate the SPR angle using Frenel reflection and transmission equation (i.e., via eq. 1.8).[36] Then, the SPR angle is used to calculate electric fields for parallel polarization (i.e., via eq. 1.11). The mean square electric field (i.e., $\langle E^2 \rangle_x$ or $\langle E^2 \rangle_{0,x} = \langle E_{xz}^2 \rangle + \langle E_{zz}^2 \rangle$) in each medium (i.e., gold, microgel, and buffer solution medium) using for SPR simulation could calculate from eq 1.14. All calculations were done by mathematica 6.0 programming.

When a surface of SPR chip is covered with a flat gel film with surface area of *S* and thickness of h, the increment of SPR response caused by the film is expressed in the following equation:

$$\text{SPRt} = S\int_0^\infty \left[\langle E^2 \rangle_{0,x} - \langle E^2 \rangle_x \right] dx \qquad (1.15)$$

where $\langle E^2 \rangle_{0,x}$ and $\langle E^2 \rangle_x$ are the mean square electric fields at *x* (i.e., the distance from SAM/gel interface) in buffer and swollen gel systems, respectively.

Decay characteristics of mean square electric fields (MSEFs) associated with the parallel-polarized radiation with absence of flat film microgel $\langle E^2 \rangle_{0,x}$ or presence of flat film microgel $\langle E^2 \rangle_x$ show in Figure 1.5.

1.5 SPR imaging

More recently, SPR microscopy (SPRM), also, referred to as "SPR imaging" (SPRI), has started to be used for the same types of measurements, but with high spatial resolution. Since the measurements are done simultaneously over the entire are radiated by the light or imaged onto the detector array (typically a charge-coupled device (CCD) array), combining SPR imaging with patterned microarrays of biomolecules allows for very high throughput analyses of biomolecular binding. Thus, SPRM has been used to measure the binding of DNAs and RNAs to DNA arrays, of DNA-binding proteins to dsDNA arrays, of proteins to protein and peptide arrays, and even of small ligands to protein arrays. Just like SPR spectroscopy, SPR imaging can be used for determining the on- and off-rates and equilibrium binding constants of all these types of interactions, only now in high throughput (>1000 interactions simultaneously). Since the amount of biomaterial needed to make on 100 μm spot on an SPR active surface is tiny, and since the same solution can be used to monitor > 1000 spots simultaneously, this provides not only a huge saving in time, but also a tremendous cost savings for the precious biomolecules used for these assays. More importantly, since the buffer and temperature and many other variables are exactly the same for each spot in such an analysis, this approach offers an improvement in measurement reliability relative to 1000 independent measurements by the simpler SPR spectroscopy. Table 1.1 summarizes some of the advantages of SPR imaging for such analyses.

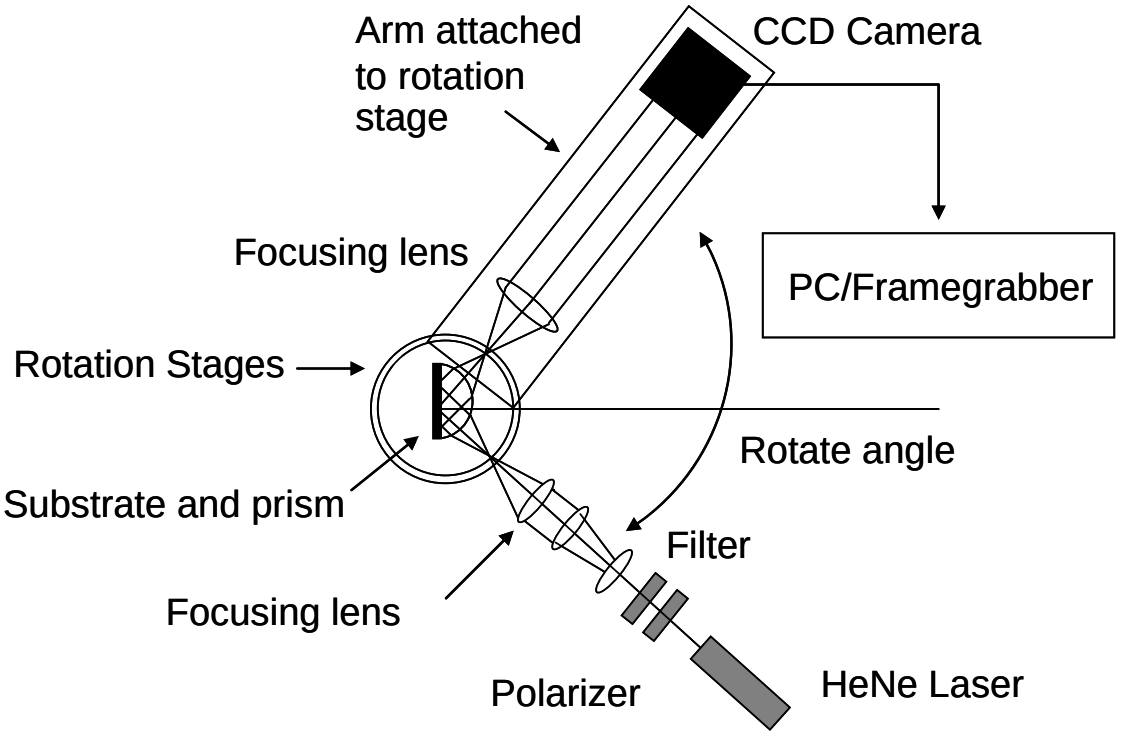

Figure 1.6 Design of SPR imaging

Table 1.1

Advantages of SPR imaging for high-throughput bioaffinity assays

- Simultaneous monitoring of different area/interactions
- Label-free detection
- Absolute quantification of binding amounts and ratios
- Kinetic measurements with ~1 s time resolution
- Detection limit: ~80 fg, or ~1 attomole (<1 million molecules) for 60-kDa proteins
- Can detect small ligands (<300 Da) interacting with >1000 different proteins simultaneously
- Near perfect referencing for removing spurious signals due to changes in index of refraction of buffer solutions, temperature, etc.
- Time response and absolute quantitative nature render analyses of concentrations much more reliable, and make control experiments much easier to design
- Requires much less of the precious biomolecules than normal SPR:

- On-chip receptors: requires only enough of each for spotting ~1 nL droplet onto microarray
- Solution-phase biomolecules in the flow cell: requires 1000-fold less, since >1000 interactions probed with every injection to cell

-SPR-active chips typically compatible with inexpensive but reliable robotic spotters
-Timely: many new methods for spotting protein arrays and arrays of other receptors on gold have recently been developed

Table 1.2

Example potential applications of SPR imaging for high-throughput bioaffinity analyses

- Analyses of protein and ligand concentrations with protein or antibody arrays
- Analysis of concentrations of DNA-binding proteins from small cell colonies with dsDNA arrays
- Screening for ligands that bind to proteins: drug discovery
- Screening for substrates (peptides) for catalysis by proteases or kinases, and the relative reaction rates of different peptides
- Searches for cofactors in all sorts of protein binding events
- Fundamental research in proteomics, neurobiology, and cell biology
- Arrays designed for early disease diagnostics, and other clinical applications

However, there are several disadvantages for SPR imaging, shown in Table 1.2. Perhaps the most important is that, without signal amplification in any way, one requires a minimum of ~0.1% of the surface receptors to be occupied to detect their presence. Thus, to achieve the advantages in Table 1.1, one requires a concentration of the biomolecular binding partner in solution that is at least $K_d/1000$, where K_d is the equilibrium dissociation constant for the interaction of interest. However, a number of methods have been developed for amplification that dramatically relaxes this limitation, as outlined below. Another disadvantage is that the metal surface must be functionalized with a bioreceptor in a way that avoids non-specific adsorption. Non-specific adsorption can lead to false signals and biosensor fouling. Finally,

biomolecules immobilized onto SPR sensor surfaces do not always retain their native bioactivity and, with some immobilization schemes, only a small fraction of the immobilized biomolecules is active. This can effect the determination of binding stoichiometry (biomolecules bound per receptor). The stoichiometry can also be influenced by the proximity of other receptors in the adlayer, especially when the analyte is a large biopolymer.[50]

SPR imaging provides the quantitative data as obtained in biosensing with SPR spectroscopy (i.e., amount adsorbed versus time), but it has the very important added feature of monitoring adsorption with a spatial resolution down to ~4 μm over a large area of a sensing surface.[51-59]

In most SPR imaging, an expanded and collimated polarized and monochromatic light beam (often a He-Ne laser, but sometimes a narrow-pass filtered white light) travels through a prism and an attached glass slide coated with a thin gold film, and reflects from the gold/solution interface at an angle greater than the critical angle.[51-59] The reflected light intensity from the illuminated area of the surface is monitored at the specular angle, typically by a CCD detector array. In any case, each pixel on the CCD array maps into a specific location on the gold surface, and provides the surface information about that spot on the surface. The spatial contrast in an SPR imaging image comes from the heterogeneity in the complex dielectric due to difference in refractive index near the surface at different lateral positions across the surface. This leads to changes across the surface in reflected intensity at an incident angle near the resonance angle. If an adsorbate has a different refractive index than the solvent, its binding to the surface can thus be detected in a spatially resolved way simply by monitoring changes in reflected light intensity at the pixel(s) of interest. Since the pixels on CCD array are all sampled simultaneously in modern instrumentation, this allows for very high throughput studies of adsorbed amount versus position on the surface, ideally compatible with the probing of micro arrays of biomolecules.[51, 57,59-78]

1.6 Atomic force microscopy (AFM)

Atomic force microscopy is one of many scanned probe microscopy techniques used to image the surface. AFM operates by measuring attractive or repulsive force between a tip and the sample.[79] The atomic force microscope (AFM)

probes the surface of sample with a sharp tip, a couple of microns long and often less than 100 A° in diameter. The tip is located at the free end of a cantilever that is 100 to 200 μm long. Forces between the tip and the sample surface cause the cantilever to bend, or deflect. A laser beam is focused on the back of the cantilever, and the deflection of the cantilever translates to a deflection in the laser beam. A detector measures the cantilever deflection as the tip is scanned over the sample, or the sample is scanned under the tip. The measured cantilever deflections allow a computer to generate a map of surface topography. In non-contact mode, the AFM derives topographic images from measurements of attractive forces; the tip does not touch the sample.[80] AFMs can achieve a resolution of 10 pm, and unlike electron microscopes, can image samples in air and under liquids.

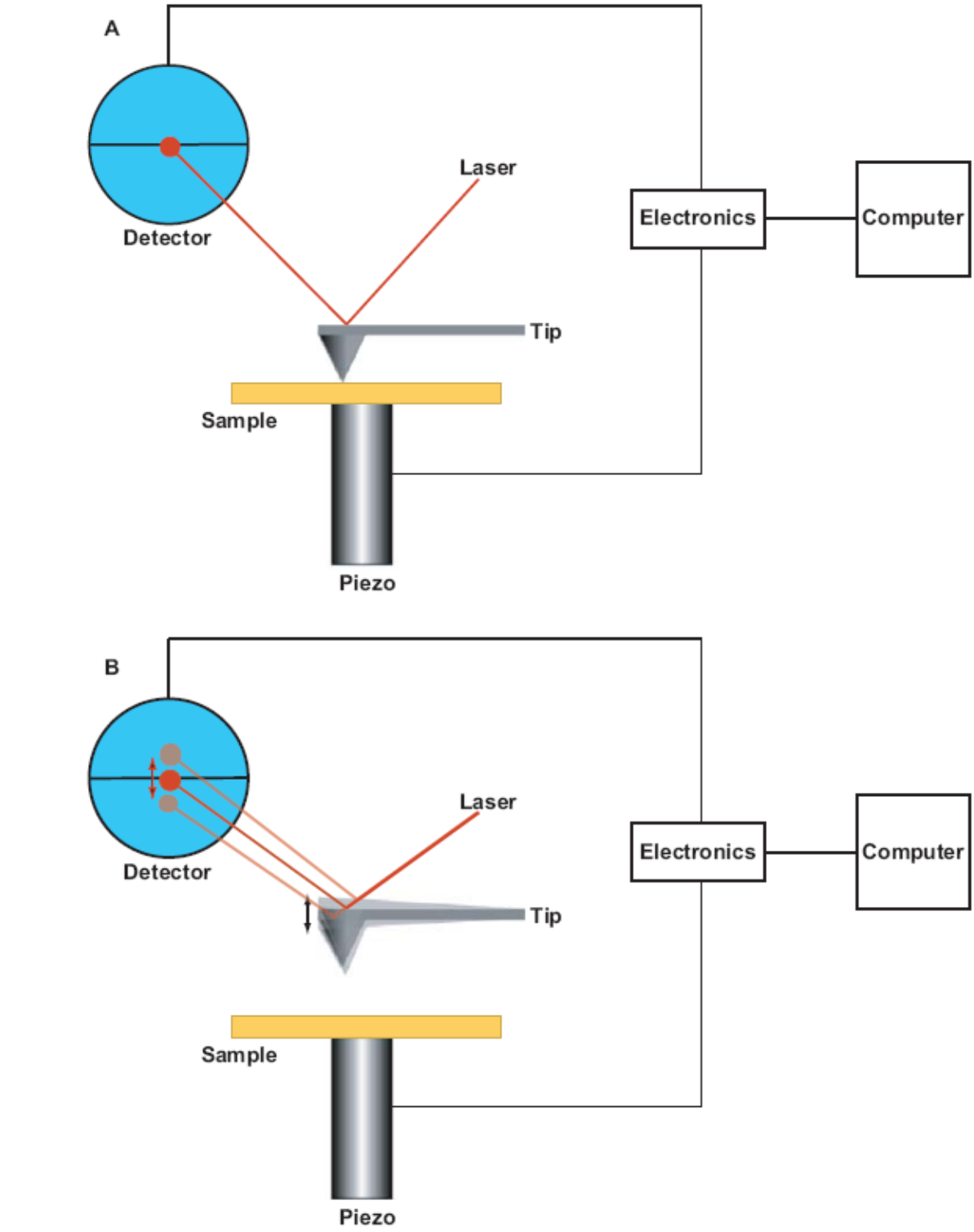

Figure 1.7 Schematics of (A) contact and (B) non-contact mode atomic force microscopy. A laser reflected off the back of the cantilever, focused on a photodetector is used for feedback. In contact mode, the position of the laser spot on the photodetector is recorded and simultaneously used in the feedback mechanism. In non-contact mode, the amplitude of the laser modulation on the photodetector is recorded and simultaneously used in the feedback mechanism.

1.7 Overview of sensitive hydrogel

Temparature-reponsitive polymers and gels have gained great scientific and technological importance, and the characteristics of these materials have been studied extensively for application such as drug delivery,[81] cosmetics,[82] coatings,[83] lubricants,[84] food,[85] and oil recovery.[86] One of the most intensively studied polymer in this field is poly(*N*-isopropylacrylamide) (poly(NIPAM)).[87] Poly(NIPAM)-based microgels exhibit an extreme response to change in temperature. Poly(NIPAM) has a lower critical solution temperature (LCST) in water at 32°C,[88] at which the polymer reversibly switches from a fully soluble, hydrophilic random coil to an insoluble one.[89-97]

Poly(N-isopropylacrylamide) belongs to a general class of materials called associating polymers, which contain in their chemical structure both hydrophilic and hydrophobic groups that form intra and inter molecular associations. Poly(NIPAM) hydrogel are temperature-sensitive and they undergo a discrete phase transition at their LCST. Below this temperature, the polymer is hydrophilic and soluble, and above LCST it is hydrophilic and becomes collapsed. For a linear flexible polymer chain in solution, there has been much debate concerning the major determinant of the coil-to-globule transition, whether "hydrophobic effects" and/or "hydrogen bonding effects" are dominant in general in aqueous solutions.[89] Some authors[90-93] favor the breakdown of polymer-water "hydrogen bonding" interactions in controlling the macromolecular contraction whereas others[94-99] attribute the chain collapse to changes in the "hydrophobic effect", which induces local structure in the solvent molecules surrounding the hydrophobic substituents of the polymer. A third group group of authors[100-105] argues that the LCST of the thermoresponsive polymers is associated with changes in both "hydrogen bonding" and "hydrophobic interactions" within the interacting polymer solvent system. According to the last group, at the molecular level the phase transition of temperature-sensitive polymers is a change from hydrated random coil to hydrophobic globule. As the temperature rises and approaches the phase transition point, the first step of the phase separation is the breaking up of the relatively strong hydrogen bonds, formed around the polymer coil between water molecules and the NH or C=O groups of the temperature-sensitive polymers, followed by the collapse of the polymer molecule into a hydrophobic globule. Polymer-polymer interactions are responsible for the aggregation and the

subsequent precipitation of the polymer out of solution is taking place since hydrogen bonding becomes weaker and breaks as the temperature is raised.[106-107]

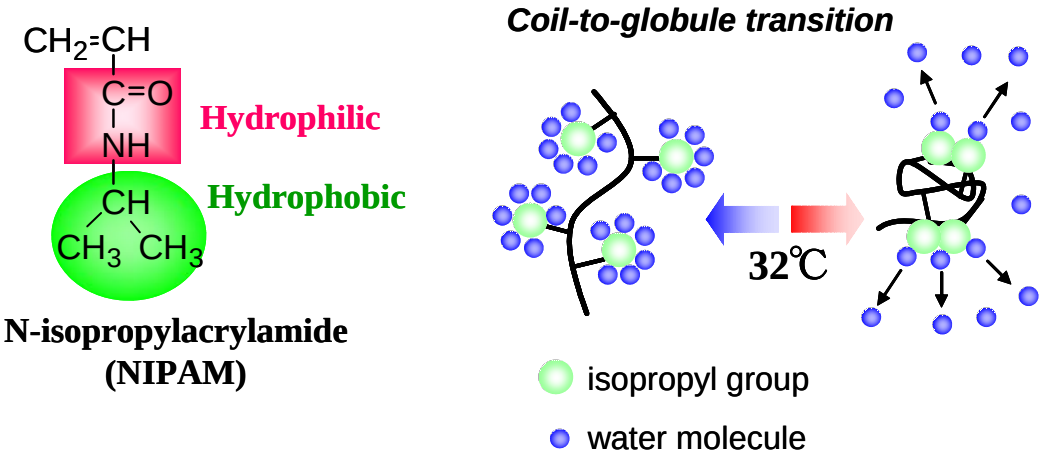

Figure 1.8 Molecular structure of *N*-isopropylacrylamide (NIPAM) and thermal study of the coil-to-globule transition of poly(NIPAM) solution

However, for some purposes, hydrogel systems are required to have a combination of two or more stimuli-responsive abilities. Numerous other monomers are available that can be added to the hydrogel structure in order to render the structure responsive to numerous other stimuli such as electrical current, magnetic field, pH. Hydrogel can also be easily rendered multifunctional by the polymerization of two or more functional monomers into the network structure. Performing this copolymerization results in a hydrogel that changes its salvation state in response to multiple stimuli where the energetics involved in responsivity are dictated by the component of the network that has the strongest interaction with water. Hydrogel swelling/deswelling behavior has been described previously by numerous theories including Flory-Huggins theory.[108]

Hydrogels can be classified as neutral or ionic based on the type of repeating units or the nature of the side chains on the polymer backbone. They can be homopolymer or copolymer networks based on the preparation approach. The most important property for hydrogels is the stimuli-sensitivity depending on the external conditions, which include pH, temperature, pressure, ionic strength, electromagnetic radiation, ultrasonic energy, buffer composition, the concentration of glucose, stress and strain, and photo.[109] These conditions dramatically affect the swelling behavior, network structure, permeability and mechanical strength of hydrogels. Such

intelligent materials open the door for novel applications in the areas of nanotechnology (actuators, substrates), surgical implants and tissue engineering, due to hydrogel's unique ability to undergo phase transitions under the influence of small stimuli.

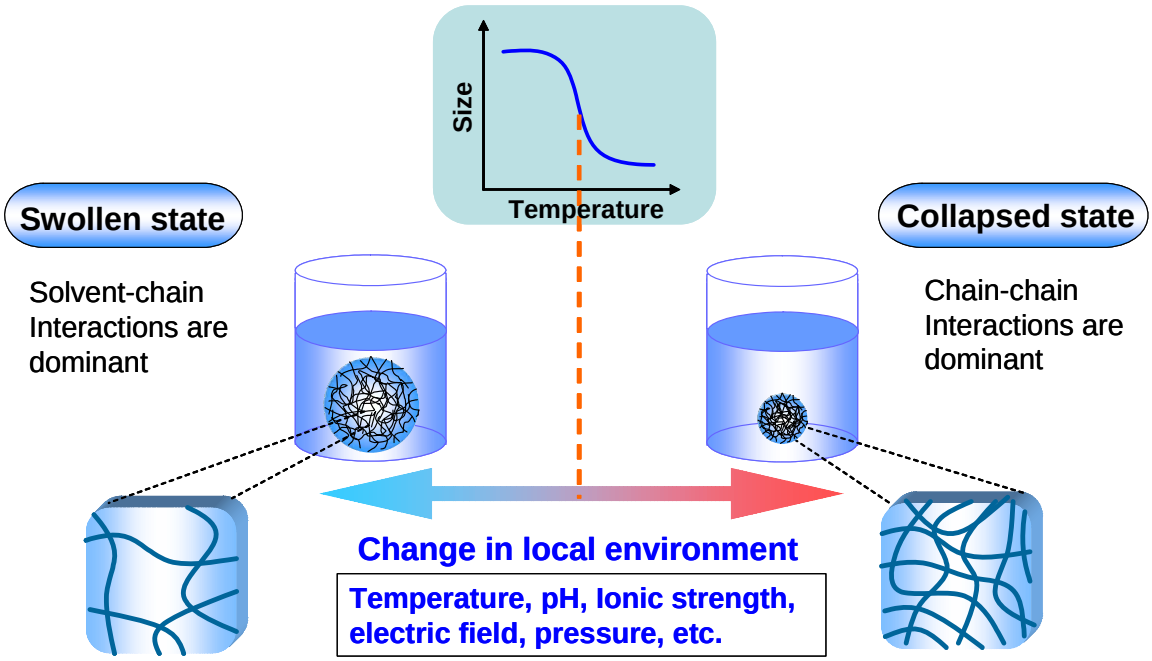

Figure 1.9 Schematic of swollen and collapsed state of microgel under stimuli

The pH-sensitive hydrogels exhibit swelling or deswelling behavior with changes of pH values in the surrounding medium. The swelling behavior may be due to one of the following mechanisms: (1) changes in the hydrophobic-hydrophilic nature of chains; (2) inter- and intramolecular complexation by hydrogen bonding, or (3) electrostatic repulsion. All these mechanisms are closely related to the protonation phenomena of the ionizable moieties on the polymer backbone or the side chains. In the first case, ionization makes the hydrophobic polymer network more hydrophilic because the ionized structure usually posses more hydrophilicity which can imbided more water into the matrix. In the second case, ionization results in the breaking up of the hydrogen bonds that exist in the polymeric matrix in the unionized state, leading to the hydrogel swelling. In the third case, the ionization provides the electrostatic repulsion among charges present on the polymer chain to keep the chains apart and

allow more water absorbing into the loose structure. In all these cases, the kinetics of the swelling process and the equilibrium extent of swelling are affected consideratbly by several factors, such as ionic strength of the medium, buffer composition, presence of salts.[110] Other factors, such as the crosslinking ratio, solvent quality, chemical structure of monomers, and the synthesized conditions also influence the structure formation and the swelling behavior of hydrogels.

pH-sensitive hydrogels can be divided into anionic and cationic depending on the nature of pendant groups in the network, which show sudden or gradual changes in their dynamic and equilibrium swelling behavior as a result of pH changes. Anionic gels often contain carboxylic or sulfonic acid. When the pH value of surrounding medium rises above its pK_a, the ionized structure will provide increased electrostatic repulsion between chains and the hydrophilicity of network. Under these conditions, hydrogels are capable of uptaking large amounts of water and forming very loose structure. In contrast, cationic hydrogels usually contain pendent group such as amines. As pH values lower than the pK_b, the amine group change from NH_2 to NH_3^+, resulting in the increased hydrophilicity, strong electrostatic repulsion, and high swelling ratio.

Temperature-sensitive hydrogels have received considerable attention for uses in bioseparations, drug delivery, and diagnostics due to the ability of hydrogels to swell or shink as a result of temperature change in the surrounding fluid.[111] Based on the transition mechanism, these hydrogels can be classified into categories: negatively temperature-sensitive gels and positively temperature-sensitive.[112]

Positive hydrogels have an upper critical solution temperature (UCST). If the temperature is below the UCST, the hydrogels contract and release solvent from the matrix. In contrast, the swelling behavior of negative hydrogels is attributed to the lower critical solution temperature (LCST). A temperature above LCST results in a collapsed structure for hydrogels. For the thermo-reversible gels, the polymer chains are not covalently crosslinked and the gels may undergo sol-gel phase transition, instead of swelling-shrinking transitions.

1.7.1 Negatively temperature-sensitive gels

For most polymers, the water solubility increases with increasing temperature. Negatively temperature-sensitive gels, however, have a critical parameter LCST. That means these gels shrink as the temperature increases above the LCST and swell at the lower temperature. The structures of some of those polymers are shown in Figure 1.10

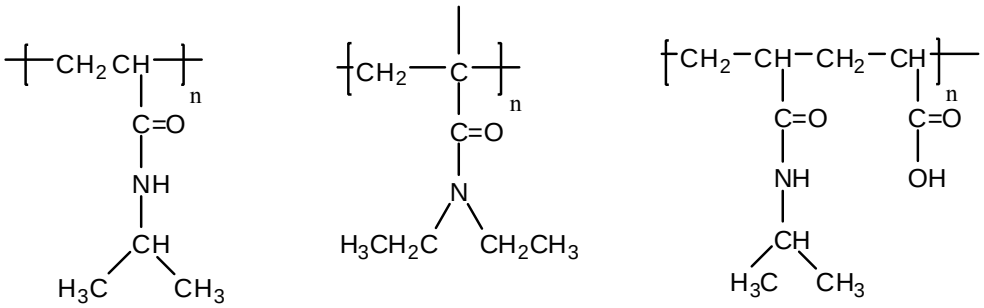

Poly(NIPAM) Poly(DEAAm) Poly(NIPAM-co-AAc)

Figure 1.10 Structures of negatively temperature-sensitive hydrogels

Some of the earliest work with negatively temperature-sensitive hydrogels was done by the Tanaka's group.[113] Poly(*N*-isopropylacrylamide) (Poly(NIPAM)) is the best example of a negatively temperature-sensitive hydrogel, which is made of polymer chains containing a mixture of hydrophobic and hydrophilic segments. At lower temperatures, water interacts with the side chains through the hydrogen bonds between water molecules and the hydrophilic parts, -CONH-. These hydrogen bonds lead to enhanced dissolution and well swelling in water.[114-115] As the temperature is increased to higher LCST, the hydrophobic interactions among hydrophobic segments, $-CH(CH_3)_2$, become stronger, while hydrogen bonds become weaker. These interactions result in the shrinking of the hydrogels due to inter-polymer chain association.[112] Hirotsu et al.[116] worked with crosslinked poly(NIPAM) and determined that the LCST of poly(NIPAM gel was 34.38°C. However, the response rate to external temperature changes of typical poly(NIPAM) hydrogel is low, which limits its applications. Kabra et al.[117] synthesized fast temperature-response poly(NIPAM) gels by using a phase separation technique. Preparation of gels at temperatures above LCST[118] or below the freezing point[119] results in an enhanced shrinking rate. Gas blowing[120] and radiation[121] may produce porous structures leading to fast response. Other successful approaches to achieve a high temperature-

response rate using poly(ethylene glycol)s as pore-forming agents,[122] interpenetrating poly(vinyl alcohol) within the hydrogel network, using aqueous sodium chloride solution as the reaction medium for gel preparation, and carrying out polymerizations in mixed sucrose solutions. These approaches could significantly increase the response rate since these reaction mediums induce the phase separation of gel system. For example, the fully deswelling time could be reduced to 2 min when the hydrogel preparation was carried out in aqueous glucose solutions.[114-115]

LCST is a very important parameter for negatively thermo-sensitive gels. LCST could be increased by mixing a small amount of ionic copolymers in the gels[123] or by changing the solvent composition.[124] In general, as the polymer chains contain more hydrophobic constituents, LCST moves to a lower temperature. Thus, incorporating a hydrophilic monomer, acrylic acid (AAc), into the poly(NIPAM) backbone is a good approach to modulate the properties of poly(NIPAM) gels[125]. Copolymerization of NIPAM with different monomers results in hydrogels with versatile properties. However, an increased hydrophilic content in the copolymer network can reduce its temperature sensitive.[126-127] In order to improve the temperature sensitive of copolymers, several researchers have prepared poly(NIPAM) based copolymers. Okano and coworkers[128] developed an exquisite method to prepare graft hydrogels of poly(NIPAM). Small poly(NIPAM) molecules were grafted with the main chain of the crosslinked poly(NIPAM). Above the LCST, hydrophobic regions in the network structure made the gels dehydrate to a collapse state. At temperature below LCST, the gels could transform into a fully swollen conformation in less than 20 min, which was much faster than that of comparable gels without graft chains. This group also proposed an incorporating carboxylate method to promote gel shrinking.[129] 2-carboxyisopropylacrylamide (CIPAM) was incorporated into poly(NIPAM) gels to induce rapid shrinking in response to small temperature increases. In contrast, poly(NIPAM-co-AAc) copolymer gels lose their temperature sensitivity with the introduction of only a few mode percent of AAc. Zhang et al.[125] synthesized poly(NIPAM-co-AAc) gels in an alkaline solution to achieve the improved oscillating swelling properties. There has also been significant interest in the synthesis of poly(NIPAM) based hydrogels by other methods such as graft-, block- or comb-copolymerization. Such systems show promise for rapid and abrupt or oscillatory release of drugs, peptides, or proteins, because their swelling is relatively fast.[130-132]

Recently, efforts have been made to prepare multifunctional hydrogels responding to more than two stimuli, such as the pH and temperature sensitive hydrogels. Chen and Hoffman[133] prepared poly(NIPAM-co-AAc) gels, which exhibited temperature- and pH-sensitive behavior. These gels were able to respond rapidly to both temperature and pH changes. The temperature- and pH-dependent swelling behaviors were better defined in the graft copolymers than in random copolymers containing similar amounts of components. Tian et al.[134] developed a hydrogel of poly(NIPAM-co-AAc) modified by a small amount of hydrophobic comonomers in *tert*-butanol solutions. The hydrogels with a suitable 2-(*N*-ethylperfuorooctanesulfoamido) ethyl acrylate content showed good pH and temperature sensitivity. Similar work was done by Peppas group.[135] The interpenetrating gels of poly(NIPAM) and Poly(MAA) exhibited the ability of responding to temperature and pH conditions. Additionally, the transition conditions were determined at a pH value of approximately 5.5 and a temperature range of 31-32°C.

Negatively temperature-sensitive hydrogels have been studied extensively and these materials can be used in a variety of applications, including controlled drug delivery, immobilized-enzyme reactors, separation process, and biochips. In a monolithic device, an on-off drug release profile could be obtained based on the reversible thermo-sensitivity of hydrogels[136-137] which involve crosslinked poly(NIPAM-co-BMA), and inter-penetrating poly(NIPAM) and poly(tetramethyleneether glycol) (poly(TMEG). In order to increase the mechanical strength of hydrogels, Okano and coworkers incorporated a hydrophobic comonomer, BMA into NIPAM gels and investigated the on-off release profile of indomethacin from the matrices in response to a stepwise changing temperature. The hydrophobicity of the comonomer influenced the shrinking process and thus controlled the release behavior of the therapeutic agent dispersed in the matrix.[138] Negatively temperature-sensitive gels are also utilized for controlled delivery of highly sensitive therapeutic agents, such as peptides and proteins. Peppas et al.[139] developed a hydrogel of inter-penetrating poly(NIPAM) and poly(MAA) and studied the release kinetics of bioactive streptokinase.

1.7.2 Positively temperature-sensitive gels

Certain hydrogels formed by IPNs show positive thermosensitivity. IPNs of PAA and polyacrylamide (polyAAm) or poly(AAm-co-BMA) have positive temperature dependence. IPNs composed of PAA and PAAm may shrink at low temperatures because of the interpolymer complexes formed by hydrogen bonding. The complexes dissociate at higher temperatures due to breaking of hydrogen bonds, and the gels rapidly swell above the UCST.[140] Katono et al.[141] compared the temperature dependent swelling behavior of poly(AAm-co-BMA), the IPNs of poly(AAm-co-BMA) with PAA, and the random copolymer gel poly(AA-co-AAm-co-BMA). The IPNs and the random gels showed the distinctly different profiles of temperature dependence, although both had the positive temperature dependence. Only the IPNs showed a sigmoidal alteration with a transition zone. The swelling of those hydrogels was reversible, responding to stepwise temperature changes. This resulted in reversible changes in the release rate of a model drug, ketoprofen, from a monolithic device.

1.8 Microgel applications

The major applications of thermoresponsive microgel particles have been in the surface coating industry[142-144] and particularly in the automotive industry.[145] In addition such structures have been used for improving the rheological properties of paints[146] and the performance of films.[147] Microgels have also found wide application in other areas such as protein,[148-149] cells[150] and enzyme immobilization[151-154] but also show promise in the printing industry[155] and for oil recovery from petroleum reservoirs.[156] In addition, microgel dispersions have potential use as environmentally sensitive optoelectronic devices.[157-158] The controlled uptake and release of large molecules has been also demonstrated.[156,159-160] Thermosensitive microgels having either cationic or anionic surface charge groups have been shown to have potential applications for the removal of ionic cantaminants from waste water.[156] The applications related with the use of microgel systems are schematically summarized in Figure 1.11

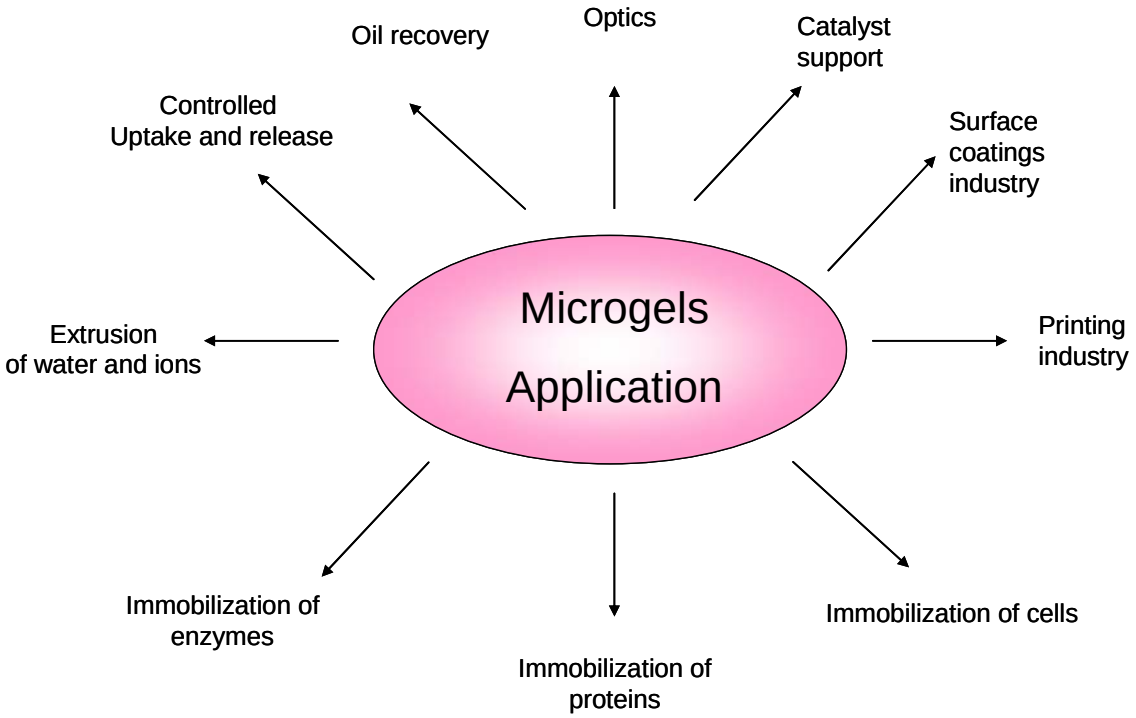

Figure 1.11 Applications of microgels

Table 1.3 Experimental Techniques for microgel characterization

Experimental techniques	Measurement
Transmission Electron Microscoy (TEM)	Particle size and shape[148,161-162]
Scanning Electron Microscopy (SEM)	Particle size and shape[163-164]
Static Light Scattering	Particle molecular weight[165-166]
Photon Correlation Spectroscopy Or Dynamic Light Scattering	Hydrodynamic size[167-170]
Gel Permeation Chromatography	Weight and Number Average [166] Molecular Weight
Ultracentrifugation	Weight Average Molecular Weight[171]
Conductometric and Potentiometric titration	Surface charge[169-172]
Small Angle X-ray Scattering (SAXS)	Internal Structure[173]
Small Angle Neutron Scattering (SANS)	Internal Structure[170,173]
Atomic Force Microscopy (AFM)	Surface morphology[170]
Turbidimetric methods	Stability of microgel dispersion[159]
High Sensitivity Differential Scanning Calorimetry	Thermodynamic Properties[174]
Differential Scanning Calorimetry	Thermodynamic Properties[168,175]
Bohlin Rheometer	Rheological measurements[175]
Surface Plasmon Resonance (SPR)	Volume phase transition[176]

The first reported investigation of the interaction of biological molecules with poly(NIPAM) microgels was by Kawaguchi et al. [177] who described the temperature-dependent sorption and desorption of hyman γ globulin. Figure 1.12 shows that the maximum protein binding occurs at low pH and 40°C which is above the LCST. Below the LCST of poly(NIPAM) or the volume phase transition temperature of poly(NIPAM) particles in an aqueous medium, that is, around 32°C, the particles adsorbed less protein. This was attributed to the fact that the particles hold a large amount of water in the particle and their surface is hydrophilic enough to suppress the adsorption of protein. On the other hand, above 32°C the particle deswell and their surface becomes hydrophobic and, consequently, susceptible to adsorption of a large amount of protein. Electrostatic force plays an essential role for the protein adsorption on poly(NIPAM) particles. Particles were prepared by use of ionic initiators, persulfate, having anionic charges on the surfaces. The charges were distributed dilutedly in the inside of particles below 32°C but concentrated above 32°C.

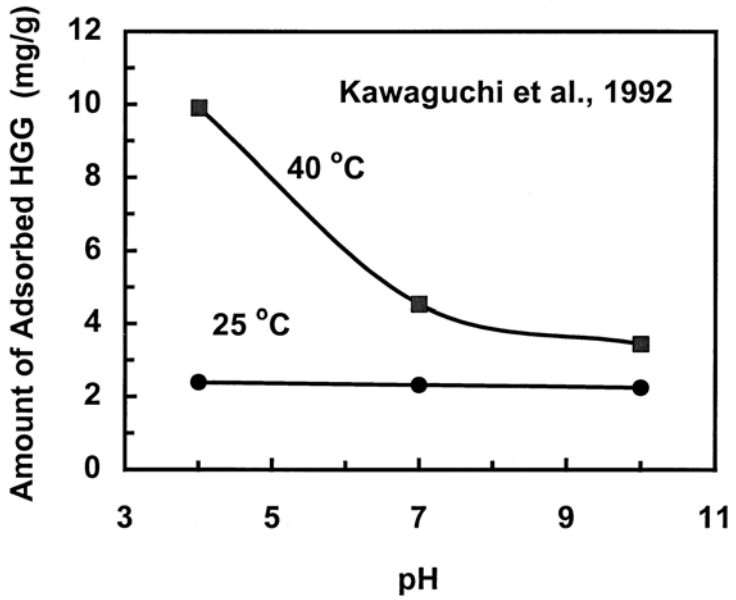

Figure 1.12 Influence of pH and temperature on human gamma globulin adsorption onto polyNIPAM microgels. Adapted from Kawaguchi et al.[177]

The studies, summarized above involved the physical sorption of protein to poly(NIPAM) microgel. A number of recent reports have addressed the properties of enzymes covalently bonded to microgels. Shiroya et al[178] grafted trypsin and peroxidase to poly(NIPAM) microgels. The enzyme activity went down when

temperature was raised above the LCST. This was explained by decreased substrate diffustion rates and by “trapping of the enzyme in the surface layer”. On the other hand, temperature-independent enzyme activities were obtained when the enzymes were attached to the microgel via PEG spacers. Presumably the spacers isolate the enzymes from the temperature-sensitive poly(NIPAM) domains.

1.9 Objective and overview of this thesis

In this thesis, the behavior of poly(NIPAM-*co*-AAc) microgel was investigated with surface plasmon resonance (SPR), specifically utilizing the particular properties of evanescent field theory: the change of exponential decay of mean square electric field with binding microgel. The motivation of this thesis is to explain the effect of physicochemical parameter of anionic thermosensitive microgels on SPR response. We proposed the SPR simulation based on the evanescent wave to explain the swelling degree of microgel in dispersion system. Poly(NIPAM-co-AAc) microgels at different pHs, salts, and temperatures were used for the study of the attachment behavior. The different attachments or the number of binding microgel resulting of difference in swelling behavior affected on the SPR response. In addition, we could see the microgel bound onto the SPR sensor chip strongly. This result could be applied to study the swelling degree by changing temperature while the number of binding microgel was fixed. The research introduces the quantitative expression that describes the relationship between the SPR response and refractive index of the microgel system. We expected that SPR simulation based on evanescent field could explain the effect of salt, pH, and temperature, providing the difference in conformation or morphology of binding microgel, on SPR response. The difference in conformation of binding microgel (i.e., flat film microgel or spherical microgel) has a different sensitivity on SPR response. Moreover, the protein adsorption onto 2D-arrayed microgel has been studied in this thesis. 2D-arrayed microgel created responsitive surface for a study of protein adsorption. We compared the IgG adsorption between onto 2D array on the chip and onto microgel in dispersion system. The kinetic parameter for IgG adsorption could be investigated in our system.

The research described in the following Chapters pertains to the effects of physicochemical parameters of anionic thermosensitive microgels on SPR response. The physicochemical parameters include refractive index, evanescent field strength,

and the number of binding microgels. We figured out how the swelling degree of microgel affects the SPR response.

Chapter 2 described the influence of ionic strength, pH, and temperature on the binding behavior and SPR response of poly(NIPAM-co-AAc) microgels. The swelling degree provided the difference in the size and the number of binding microgel on chip. According to our SPR simulation, we found that the number of microgel was the dominant factor determining the SPR response.

In Chapter 3, we discussed the effect temperature on the swelling degree of poly(NIPAM-co-AAc) microgels by using the same chip (i.e., the same chip binding the number of microgels). In Chapter 2, we found the microgel could bind onto chip strongly. Then, we designed the unchanged number of binding microgels to study the swelling degree as the function of temperature. SPR simulation could explain how the difference in conformation of binding microgel and swelling degree of microgel affects the SPR response by keeping unchanged number of binding microgels.

In Chapter 4, after the fundamental study of binding microgels onto the SPR chip system has studied in Chapter 2 and Chapter 3, we applied to modify microgel surface which having the different acrylic acid content to study the binding of IgG. The result from the new microgel surface system was compared to that of the microgel dispersion. Moreover, we also observed the kinetics of IgG adsorption onto microgel surface on the SPR chip, and multiple region adsorptions could be monitored by using SPR imaging.

References

[1] Sommerfeld, A. *Annal. Phys.* **1909**, *28*, 665.

[2] Ritchie, R. H. *Phys. Rev.* **1957**, *106*, 874.

[3] Stern, E. A.; Ferrell, R. A. *Phys. Rev.* **1960**, *120(1)*, 130.

[4] Otto, A. *Zeitschrift fur Physik*. **1968**, *216*, 398.

[5] Kretschmann, E.; Raether, H. *Z. Naturforsch*. **1968**, *23a*, 2135.

[6] Nylander, C.; Liedberg, B.; Lind, T. *Sens. Actuators*. **1982**, *3*, 79.

[7] Liedberg, B.; Nylander, C.; Lundstrom, I. *Sens. Actuators*. **1983**, *4*, 299.

[8] Liedberg, B.; Nylander, C.; Lundstrom, I. *Biosens. Bioelectron.* **1995,** *10*, i-ix.

[9] Homola, J.; Yee, S. S.; Gauglitz, G. *Sens. Actuators, B* **1999**, *B54*, 3.

[10] Rich, R. L.; Myszka, D. G. *Curr. Opin. Biotechnol.* **2000**, *11*, 54.

[11] Hall, D. *Anal Biochem.* **2001**, *288*, 109.

[12] Humphery-Smith, I.; Blackstock, W. *J. Protein Chem.* **1997**, *16(5)*, 537.

[13] Steiner, G.; Sablinskas, V.; Hubner; Kuhne, C.; Salzer, R. *J. Mol. Struct.* **1999**, *509*, 265

[14] Brockman, J. M.; Nelson, B. P.; Corn, R. M. *Annu. Rev. Phys. Chem.* **2000**, *51*, 41.

[15] Johansen, K.; Arwin, H.; Lundstrom, I.; Liedberg, B. *Rev. Sci. Instrum.* **2000**, *71*, 3530.

[16] Stenberg, E.; Person, B.; Roos, H.; Urbaniczky, C. *J. Colloid Interface Sci.* **1991**, *143(2)*, 513.

[17] Liedberg, B.; Lundstrom, I.; Stenberg, E. *Sens. Actuators, B* **1993**, *11*, 63.

[18] Fivash, M.; Towler, E. M.; Fisher, R. J. *Curr. Opin. Biotechnol.* **1998**, *9*, 97.

[19] Lee, J. H.; Lee, H. B.; Andrade, J. D. *Prog. Polym. Sci.* **1995**, *20*, 1043.

[20] Elam, J. H.; Nygren, H.; Stenberg. M. *J. Biomed. Mat. Res.* **1984**, *18*, 953.

[21] Piehler, J.; Brecht, A.; Geckeler, K. E.; Gauglitz, G. *Biosens. Bioelectron*. **1996**, *11(6/7)*, 579.

[22] Löfås, S.; Johnsson, B. *J. Chem. Soc., Chem. Commun.* **1990,** 1526.

[23] Fägerstam, L. G.; Frostell-Karlsson, Å.; Karlsson, R.; Persson, B.; Rönnberg, I. *J. Chromatogr.* **1992**, *597*, 397.

[24] Earp, R. L.; Dessy, R. E. *Surface Plasmon Resonance in Commercial Biosensors* G. Ramsay Ed. New York, John Wiley & Sons.

[25] Karlsson, R.; Fält, A. *J. Immunol Methods*. **1997**, *200*, 121.

[26] Schuck, P. *Biophys. J.* **1996**, *70*, 1230.

[27] Witz, J. *Anal. Biochem.* **1999**, *270*, 201.

[28] Wofsy, C.; Goldstein, B. *Biophys. J.* **2002**, *82*, 1743.

[29] Peppas, N. A.; Langer, R. *Science* **1994**, *263*, 1715.

[30] Zhu, P. W.; Napper, D. H. *Macromo. Chem. Phys.* **1999**, *200*, 698.

[31] Raether, H. *Surface Plasmon on Smooth and Rough Surfaces and on Gratings*, 136, Hamburg, Springer-Verlag.

[32] Boardman, A. D. *Hydrodynamic Theory of Plasmon-Polaritons on Plane Surfaces, in Electromagnetic Surface Modes* **1982**, New York, John, Wiley & Sons.

[33] Zhizhin, G. N.; Moskalova, M. A.; Shomina, E. V.; Yakovlev, V. A. *Surface Electromagnetic Wave Propagation on Metal Surfaces, in Surface Polaritons*, **1982**, Amsterdam, North-Holland Publishing Company: 93.

[34] Kretschmann, E. *Z. Physik.* **1971**, *241*, 313.

[35] Chen, W. P.; Chen, J. M. *J. Opt. Soc. Am.* **1981**, *71(2)*, 189.

[36] Hansen, W. N. *J. Opt. Soc. Am.***1968**, *58,* 380.

[37] Barrett, D. A.; Hartshorne, M. S.; Hussain, M. A.; Shaw, P. N.; Davies, M. C. *Anal. Chem.* **2001**, *73*, 5232.

[38] Balamurugan, S.; Mendez, S.; Balamurugan, S. S.; Brien II, M. J. O.; Lopez, G. P. *Langmuir* **2003**, *19*, 2535.

[39] Li, X.; Wei, X.; Husson, S. M. *Biomacromolecules* **2004**, *5*, 869.

[40] Kuckling, D.; Harmon, M. E.; Frank, C. W. *Macromolecules* **2002**, *35*, 6377.

[41] Harmon, M. E.; Kuckling, D.; Pareek, P.; Frank, C. W. *Langmuir* **2003**, *19*, 10947.

[42] Harmon, M. E.; Kuckling, D.; Frank, C. W. *Macromolecules* **2003**, *36*, 162.

[43] Knoll, W. *Annu. Rev. Phys. Chem.* **1998**, *49*, 569.

[44] Kumar, A.; Kamihira, M.; Galaev, I. Y.; Iijima, S.; Mattiasson, B. *Langmuir* **2003**, *19*, 865.

[45] Brockmann, J. M.; Fernandez, S. M. *American Laboratory*, **2001**, 37.

[46] Zhang, Z.; Menges, B.; Timmons, R. B.; Knoll, W.; Forch, R. *Langmuir* **2003**, *19*, 4765.

[47] Mark, S. S.; Sandhyarani, N.; Zhu, C.; Campagnolo, C.; Batt, C. A. *Langmuir* **2004**, *20*, 6808.

[48] Lahav, M.; Vaskevich, A.; Rubinstein, I. *Langmuir* **2004**, *20*, 7365.

[49] Sarkar, D.; Somasundaran, P. *Langmuir* **2004**, *20*, 4657.

[50] Shumaker-Parry, J. S.; Campbell, C. T.; Stormo, G. D.; Silbaq, F. S.; Aebersold, R. H. *Proceedings of SPIE photonics west conference,* San Jose, CA: SPIE; **2000**.

[51] Shumaker-Parry J. S.; Campbell, C. T.; *Anal Chem*. **2004**, *76(4),* 907.

[52] Rothenhausler, B.; Knoll, W. *Nature*. **1988**, *332*, 615.

[53] Knoll, W. *Annu Rev Phys Chem*. **1998**, *49*, 569.

[54] Berger C. E. H.; Kooyman, R. P. H.; Greve, J.; *Rev. Sci. Instrum*. **1994**, *65*, 2829.

[55] Zizlsperger, M.; Knoll, W. *Prog. Colloid Polym Sci.* **1998**, *109*, 244.

[56] Aust, E. F.; Sawodny, M.; Ito, S.; Knoll, W. **1994**, *16*, 353.

[57] Thiel, A. J.; Frutos, A. G.; Jordan, C. E.; Corn, R. M.; Smith, L. M. *Anal Chem.* **1997**, *69(24)*, 4948.

[58] Lyon, L. A.; Holliway, W. D.; Natan, M. J. *Rev Sci Instrum.* **1999,** *70*, 2076.

[59] Smith, E. A.; Corn, R. M. *Appl Spectrosc.* **2003**, *57(11)*, 320A.

[60] Zizlsperger, M.; Knoll, W. *Prog. Colloid Polym Sci.* **1998**, *109*, 244.

[61] Nelson, B. P.; Grimsrud, T. E.; Liles, M. R.; Goodman, R. M.; Corn, R. M. *Anal. Chem.* **2001**, *73(1)*, 1.

[62] Brockman, J. M.; Nelson, B. P.; Corn, R. M. *Annu Rev Phys Chem* **2000**, *51*, 41.

[63] Brockman, J. M.; Frutos, A. G.; Corn, R. M. *J. Am. Chem. Soc.* **1999**, *121(35)*, 8044.

[64] Jordan, C. E.; Frutos, A. G.; Thiel, A. J.; Corn, R. M. *Anal. Chem.* **1997**, *69(24)*, 4939.

[65] Li, Y. A.; Wark, A. W.; Lee, H. J. Corn, R. M. *Anal. Chem.* **2006**, *78(9)*, 3158.

[66] Fang, S.; Lee, H. J.; Wark, A. W.; Kim, H. M.; Corn, R. M. *Anal Chem.* **2005,** *77(20)*, 6528.

[67] Lee, H. J.; Li, Y.; Wark, A. W.; Corn, R. M. *Anal. Chem.* **2005**, *77(16)*, 5096.

[68] Frutos, A. G.; Corn, R. M. *Anal. Chem.* **1998**, *701*, A449.

[69] Nelson, B. P.; Frutos, A. G.; Brockman, J. M.; Corn, R. M. *Anal. Chem.* **1999**, *71*, 3928.

[70] Lee, H. J.; Wark, A. W.; Corn, R. M. *Langmuir*, **2006**, *22(12)*, 5241.

[71] Lee, H. J.; Wark, A. W.; Corn, R. M. *Anal Chem.* **2005**, *77(23)*, 7832.

[72] Lee, H. J.; Wark, A. W.; Goodrich, T. T.; Fang, S. P.; Corn, R. M. *Langmuir*, **2005**, *21(9)*, 4050.

[73] Goodrich, T. T.; Lee, H. J.; Corn, R. M. *Anal. Chem.* **2004**, *76(21)*, 6173.

[74] Wegner, G. J.; Wark, A. W.; Lee, H. J.; Codner, E.; Saeki, T.; Fang, S. P. *Anal. Chem.* **2004**, *76(19)*, 5677.

[75] Goodrich, T. T.; Lee, H. J.; Corn, R. M. *J. Am. Chem. Soc.* **2004**, *126(13)*, 4086.

[76] Shumaker-Parry, J. S. Aebersold, R.; Campbell, C. T. *Anal. Chem.* **2004**, *76(7)*, 2071.

[77] Shumaker-Parry, J. S.; Zareie, M. H.; Aebersold, R.; Campbell, C. T. *Anal. Chem.* **2004**, *76(4)*, 918.

[78] Piscevic, D.; Lawall, R.; Veith, M.; Liley, M.; Okahata, Y.; Knoll, W. *Appl. Surf. Sci.* **1995**, *90(4)*, 425.

[79] Binnig, G.; Quate, C. F.; Gerber, C. *Phys. Rev. Lett.* **1986**, *56*, 930.

[80] Albrecht, T. R.; Grutter, P.; Horne, D.; Rugar, D. *J. Appl. Phys.* **1991**, *69*, 668.

[81] Dhara, D.; Nisha, C. K.; Chatterji, P. R. *J. Macromol. Sci., Pure Appl. Chem.* **1999**, *A36*, 197-210.

[82] Zaldivar, D.; Peniche, C.; Gallardo, A.; Sanroman, J. *Biomaterials* **1993**, *14*, 1073-1079.

[83] Martin, B. D.; Ampofo, S. A.; Linhardt, R. J.; Dordick, J. S. *Macromolecules* **1992**, *25,* 7081-7085.

[84] Eddington, D. T.; Beebe, D. J. *Adv. Drug Deliv. Rev.* **2004**, 199-210.

[85] Qiu, Y.; Park, K. *Adv. Drug Deliv. Rev.* **2001**, *53*, 321-339.

[86] Yan, Q.; Hoffman, A. S. *Poly. Commun.* **1995**, *36*, 887-889.

[87] Beebe, D. J.; Moore, J. S.; Bauer, J. M.; Yu, Q.; Liu, R. H.; Devadoss, C.; Jo, B. H. *Nature* **2000**, *404*, 588-590.

[88] Wu, X. S.; Hoffman, A. S.; Yager, P. *J. Polym. Sci. Pol. Chem.* **1992**, *30*, 2121-2129.

[89] Schild, H. G.; Tirrel D. A. *Polymer Preprints (ACS) 30*, 350.13

[90] Walker, J. S. and Vause, C. A. *Sci. Am.* **1987**, *90*, 256.

[91] Prange, M. M.; Hooper, H. H.; Prausnitz, J. M. *AIChe J.*, **1989**, *35*, 803.

[92] Otake, K.; Inomata, H.; Konn, M.; Saito, S. *Macromolecules*, **1990**, *23*, 283.

[93] Schild, H. G.; Tirrell, D. A. *J. Phys. Chem.* **1990**, *94*, 4352.

[94] Fujishije, S.; Kubota, K.; Ando, I. *J. Phys. Chem.*, **1989**, *93*, 3311.

[95] Kubota, K.; Fujishige, S.; Ando, I. *Polymer Journal*. **1990**, *22*, 15.

[96] Inomata, H.; Goto, S.; Saito, S. *Macromolecules*, **1990**, *23*, 4887.

[97] Feil, H.; Bae, Y. H.; Feijen, J.; Kim, S. W. *Macromolecules*, **1993**, *26*, 2496.

[98] Shibayama, M.; Mizutani, S.; Nomura, S. *Macromolecules*, **1996**, *29*, 2019.

[99] Favier, A.; Ladaviere, C.; Charreyre, M.-T.; Pichot, C. *Macromolecules*, **2004**, *37*, 2026.

[100] Inomata, H.; Goto, S., Saito, S. *Macromolecules* **1990**, *23*, 4887.

[101] Winnik, F. M. *Macromolecules* **1990**, *23*, 233.

[102] Winnik, F. M. *Macromolecules* **1990**, *23*, 1647.

[103] Feil, H.; Bae, Y. H.; Feijen, J.; Kim, S. W. *Macromolecules* **1993**, *26*, 2496.

[104] Volpert, E.; Selb, J.; Candau, F. *Polymer* **1998**, *39*, 1025.

[105] Lin, S.-Y.; Chen, K.-S.; Liang, R.-C. *Polymer* **1999**, *40*, 2619.

[106] Fujishige, S.; Kubota, K.; Ando, I. *J. Phys. Chem.* **1989**, *93*, 3311.

[107] Boutris, C.; Chatzi, E. G.; Kiparissides, C. *Polymer*. **1997**, *38*, 2567.

[108] Flory, P. J. *Principles of Polymer Chemistry, Cornell Unversity Press, Ithaka*. **1953**.

[109] Peppas, N. A., *J. Bioact. Compat. Polym.* **1991**, *6*, 241.

[110] Hariharan, D.; Peppas, N. A., *Polymer*. **1996**, *37*, 149.

[111] Peppas, N. A.; Bures, P.; Leobandung, W. *European J. Pharm. And Biopharm*. **2000**, *50*, 27.

[112] Qiu, Y.; Park, K. *Adv. Drug Delivery Rev*. **2001**, *53*, 321.

[113] Tanaka, T. *Phys. Rev. Lett*. **1978**, *40*,820.

[114] Zhang, J. T.; Cheng, S. X.; Zhuo, R. X. *J. Polym. Sci., Part A: Polym. Chem.* **2003**, *41*, 2390.

[115] Zhang, J. T.; Cheng, S. X.; Huang, S. W.; Zhuo, R. X. *Macromolecular Rapid Comm*. **2003**, *24*, 447.

[116] Hirotsu, S.; Hirokawa, Y.; Tanaka, T. *J. Chem. Phy.* **1987**, *87*, 1392.

[117] Kabra, B. G.; Gehrke, S. H.; Hwang, S. T.; Ritschel, W. A. *J. Appli. Polym. Sci.* **1991**, *42(9)*, 2409.

[118] Wu, X. S.; Hoffman, A. S. *J. Polym. Sci., Part A: Polym. Chem.* **1992**, *30*, 2121.

[119] Zhang, X. Z.; Zhuo, R. X. *Macromolecular Chem. Phy.* **1999**, *200*, 2602.

[120] Nakamoto, C.; Motonaga, T.; Shibayama, M. *Macromolecules* **2001**, *34*, 911.

[121] Chen, J.; Park, H.; Park, K. *J. Biomed. Mater. Res.* **1999**, *44*, 53.

[122] Zhang, X. Z.; Zhuo, R. X. *Eur. Polym. J.* **2000**,*36*, 2301.

[123] Yu, H.; Grainger, D. W. *J. Appl. Polym. Sci.* **1993**, *49*, 1553.

[124] Suzuki, Y.; Tomonaga, K.; Kumazaki, M.; Nishio, I. *Polym. Gels Netw* **1996**, *4*, 129.

[125] Zhang, X. Z.; Yang, Y. Y.; Wang, F. J.; Chung, T. S. *Langmuir* **2002**, *18(6)*, 2013.

[126] Beltran, S.; Baker, J. P.; Hooper, H. H.; Blanch, H. W.; Prausnitz, J. M. *Macromolecules* **1991**, *24*, 549.

[127] Feil, H.; Bae, Y. H.; Feijen J.; Kim, S. W. *Macromolecules* **1993**, *26*, 2496.

[128] Kaneko, Y.; Nakamura, S.; Sakai, K.; Kikuchi, A.; Aoyagi, T.; Sakurai, Y.; Okano, T. *Polym. Gels Network.* **1998**, *6*, 333.

[129] Ebara, M.; Aoyagi, T.; Sakai, K.; Okano, T. *J. Polym. Sci. Part A: Polym. Chem.* **2001**, *39(3)*, 335.

[130] Yoshida, R.; Uchida, K.; Kaneko, Y.; Sakai, K.; Kikcuhi, A.; Sakurai, Y.; Okano, T. *Nature* **1995**, *374*, 240.

[131] Kaneko, Y.; Saki, K.; Kikuchi, A.; Sakurai, Y.; Okano. *Macromol. Symp.* **1996**, *109*, 41.

[132] Inoue, T.; Chen, G.: Nakamae, K.; Hoffman, A.S. *Polym Gels Network*. **1997**, *5*, 561.

[133] Chen, G. H.; Hoffman, A. S. *Nature* **1995**, *373*, 49.

[134] Tian, Q.; Zhao, X.; Tang, X.; Zhang, Y. *J. Appli. Polym. Sci.* **2003**, *87(14)*, 2406.

[135] Zhang, J.; Peppas, N. A. *Macromolecules* **2000**, *33*, 102.

[136] Bae, Y. H.; Okano, T.; Kim, S. W. *Pharm. Res.* **1991**, *8*, 531.

[137] Okano, T.; Bae, Y. H. *J. Control. Release* **1990**, *11*, 255.

[138] Yoshida, R.; Sakai, K.; Ukano, T.; Sakurai, Y.; Bae, Y. H. *J. Biomater. Sci. Polym. Ed.* **1991**, *3*, 155.

[139] Peppas, N. A.; Sahlin, J. J. *Biomaterials* **1996**, *17*, 1553.

[140] Klenina, O. V.; Fain, E. G. *Polym. Sci.* **1981**, *23*, 1439.

[141] Katono, H.; Maruyama, A.; Sanui, K.; Okano, T.; Sakurai, Y. *J. Control. Release* **1991**, *16*, 215.

[142] Murata, M. *Surfaces* **1980**, *18*, 99.

[143] Nakayama, H. *Journal of Adhesion Society in Japan* **1982**, *18*, 451.

[144] Aihara, T.; Nakayama, Y. *Progress in Organic Coatings* **1986**, *14*, 103.

[145] Bradna, P.; Stern, P.; Quadrat, O; Snuparek, J. *Colloid and Polymer Science* **1995**, *273*, 324.

[146] Wolfe, M. S. *Polymeric Materials for Science Engineering* **1989**, *61*, 398.

[147] Bromley, C. W. A.; Downing, S. B.; Taylor, D. W. *Advance in Organic Coatings Science. Technical Series* **1989**, *12*, 21.

[148] Kawaguchi, H.; Fujimoto, K.; Mizuhara, Y. *Colloid and Polymer Science* **1992**, *270(1)*, 53.

[149] Fujimoto, K.; Mizuhara, Y.; Tamura, N.; Kawaguchi, H. *Journal of Intelligent Material Systems and Structures* **1993**, *4(2)*, 184.

[150] Achiha, K.; Ojima, R.; Kasuya, Y.; Fujimoto, K. *Polymer for Advanced Technologies* **1995**, *6*, 534.

[151] Seitz, U.; Pauly, H. E. *Angewandte Macromolekulare Chemie* **1979**, *76/77*, 319.

[152] Williams, A.; Pryce, R. J. *UK Patent GB*, **1989**, *2(215)*, 335A.

[153] Shiroya, T.; Tamura, N.; Yasui, M.; Fujimoto, K.; Kawaguchi, H. *Colloids and Surfaces B: Biointerfaces* **1995**, *4*, 267.

[154] Yasui, M.; Shiroya, T.; Fujimoto, K.; Kawaguchi, H. *Colloids and Surfaces B: Biointerfaces* **1997**, *8*, 311.

[155] Sasa, N.; Yamaoka, Y. *Advanced Materials* **1994**, *6*, 417.

[156] Snowden, M. J.; Thomas, P.; Vincent, B. *Analyst* **1993**, *118*, 1367.

[157] Sawai, T.; Yamazaki, S.; Kariyama, Y.; Aizawa, M. *Macromolecules* **1991**, *24(8)*, 2117.

[158] Weissman, J. M.; Sunkara, H. B.; Tse, A. S.; Asher, S. A. *Science* **1996**, *274*, 950.

[159] Snowden, M. J. *Journal of Chemical Society, Chemical Communications* **1992**, 803.

[160] Kato, T.; Fujimoto, K.; Kawaguchi, H. *Polymers Gels and Networks* **1994**, *2*, 307.

[161] Kawaguchi, H.; Fujimoto, K.; Saito, M.; Kawasaki, T.; Urakami, Y. *Polymer International* **1993**, *30(2)*, 225.

[162] Hatto, N.; Cosgrove, T.; Snowden, M. J. *Polymer* **2000**, *41(19)*, 7133.

[163] Chai, Z.; Zheng, X.; Sun, X. *Journal of Polymer Science, Pary B: Polymer Physics* **2003**, *41(2)*, 159.

[164] Xiao, X. –C., Chu, L. –Y.; Chu, W. –M.; Chen, S.; Wang, R.; Xie, X.-C.; Xiao, X. –C. *Langmuir* **2004**, *20(13)*, 5247.

[165] Antonietti, M.; Sillescu, H.; Schmidt, M.; Schuch, H. *Macromolecules* **1988**, *21(3)*, 736.

[166] Kunz, D.; Burchard, W. *Colloid and Polymer Science* **1986**, *264(6)*, 498.

[167] Hirose, Y.; Amiya, T.; Hirokawa, Y.; Tanaka, T. *Macromolecules* **1987**, *20*,1342.

[168] Lopez, V. C.; Raghavan, S. L.; Snowden, M. J. *Reactive and Functional Polymers* **2004**, *58(3)*, 175.

[169] Wu, X.; Pelton, R. H.; Hamielec, A. E.; Woods, D. R.; McPhee, W. *Colloid and Polymer Science* **1994**, *272(4)*, 467.

[170] Kratz, K.; Hellweg, T.; Eimer, W. *Polymer* **2001**, *42*, 6631.

[171] Nieuwenhuis, E. A.; Pathmamanoharan, C.; Vrij, A. *Journal of Colloid and Interface Science* **1981**, *1(81)*, 196.

[172] Stacey, K. A.; Weatherhead, R. H.; Williams, A. *Macromolecular Chemistry* **1980**, *181*, 2517.

[173] Seelenmeyer, S.; Deike, I.; Rosenfeldt, S.; Norhausen, Ch.; Dingenouts, N.; Ballauff, M.; Narayanan, T.; Lindner, P. *Journal of Chemical Physics* **2001**, *114(23)*, 10471.

[174] Murray, M. J.; Charlesworth, D.; Swires, L.; Riby, P.; Cook, J.; Chowdhry, B.; Snowden, M. J. *Journal of the Chemical Society-Faraday Transactions* **1994**, *13(90)*, 1999.

[175] Ole Kiminta, D. M.; Luckham, P. F.; Lenon, S. *Polymer* **1995**, *36(25)*, 4827.

[176] Harmon, M. E.; Jakob, T. A. M.; Knoll, W.; Frank, C. W. *Macromolecules* **2002**, *35*, 5999.

[177] Kawaguchi, H.; Fujimoto, K.; Mizuhara, Y.; *Colloid Polym. Sci.* **1992**, *270*, 53-57.

[178] Shiroya, T.; Tamura, N.; Yasui, M.; Fujimoto, K.; Kawaguchi, H. *Colloid Surf. B.* **1995**, *4*, 267.

Chapter 2
SPR response of stimuli-sensitive microgel on sensor chip

2.1 Introduction

Much attention has been focused on polyelectrolyte-type hydrogels that undergo large changes in the degree of swelling in response to small variations in swelling medium.[1-3] Temperature and pH have been the solution variables of greatest interest, primarily because these variables change (or can be changed) in typical physiological, biological, and chemical systems. Temperature- and pH-sensitive gels have been suggested for use in variety of novel applications including controlled drug delivery,[4-5] immobilized enzyme reactors,[6] and separation processes.[7] Variations in solution, such as ionic strength or pH induce a change in network ionization and a corresponding change in swelling capacity. The swelling-deswelling makes such hydrogels interesting for applications ranging from controlled drug delivery to solute separation.[8,9] There are numerous models that describe the relationship between structure and properties for polyelectrolyte hydrogels.[10,11] Small-angle neutron scattering (SANS) technique has been used to study the microscopic structure of poly(NIPAM-co-AAc) and swelling behavior affected by pH and salt concentration. The bulk behavior of these hydrogels is widely studied and they show an isotropic swelling. However, thin microgel layers on a substrate show a swelling behavior which constrained in some way. Therefore, size, morphology, response time, and transition temperature of thin microgels are the most important parameters in technological applications. Since the swelling degree relates to the change of size and refractive index, Surface Plasmon Resonance (SPR) spectroscopy, which can detect the change in the local average refractive index due to the adsorption of molecules onto the surface, is introduced to monitor the swelling behavior at different conditions.

The volume phase transition in the stimuli sensitive hydrogels is important for applications.[4-7] The majority of applications requires the use of hydrogel at surfaces

and interfaces. Therefore, the behavior of bulk hydrogel may not be necessarily extended to these types of geometries. In this Chapter, our focus will be on the effect of physicochemical parameters of anionic thermosensitive microgels on SPR response. The effect of ionic strength and pH on swelling degree provided the difference in size of microgels and the number of binding microgels. Combination of SPR and AFM measurement can explore the attachment behavior and surface density of the microgels under various conditions. In the microgel system, even if the concentration of dispersed microgels is the same in various solutions, the interaction between particles and between particle and substrate is different. We propose SPR simulation to describe the effects of physicochemical valuables (i.e., refractive index, evanescent field strength, and the number of binding microgels) on SPR response. We expect that SPR and AFM could be used to explore how the external stimuli, such as ionic strength, pH, and temperature affects on the swelling behavior of the microgels. SPR simulation based on evanescent field introduced the quantitative expression that described the relationship between SPR response and physicochemical valuables.

2.2 Influence of salts on swelling behavior

The influence of salts, detergents and organic solvents on polymer thermoprecipitation from aqueous solution has been studied since the 1960's, albeit mainly for molecules such as poly(ethylene glycol) and poly(vinylpyrrolidone).[12-16] Since a rather delicate free energy balance involving hydrophobic, hydrophilic and H-bridge mediated interactions determines the solubility of a given polymer in water, the salt effect is hardly surprising. The interpretation of the observed effects usually based on the assumption of an interaction of the co-solute with the dissolved polymer or influence of the co-solute on the solvent water. Simple salts, e.g., are generally assumed to exert their influence by acting on the water structure (salting in/salting out) and the resulting behavior can be interpreted as a consequence of the "hydrophobic effect".[17]

The addition of a simple salt generally results in a decrease of the cloud point temperature ("salting out" effect).[14-16,18-20]

The cosolute effect has already been observed more than 100 years ago and the phenomenon has been named as the Hofmeister effect.[21] The Hofmeister effect refers to an ordered sequence of ions, the *Hofmeister series*, also called the *Lyotropic*

series.[22-26] The Hofmeister series originally categorized salts in regard to their "salting out" potential toward proteins from aqueous solution.[12,21-22,27] Starting from the anion that has the greatest ability of "salting in" some hydrophobic proteins, the Hofmeister series goes as follows: ClO_4^- > SCN^- > I^- > NO_3^- > Br^- > Cl^- > CH_3COO^- > $HCOO^-$ > F^- > OH^- > HPO_4^- > CO_3^{2-} > SO_4^{2-}.[28] The anions in the series can be divided into two classes defined by the position of chloride, which can be treated as a median.[15] The anions on the left hand side of chloride in the above mentioned series are *chaotropic ions* (water structure breakig), which exhibit weaker interaction with water than water ifself. The ions on the right hand side of chloride are *cosmotropic* (water structure making), which exhibit strong interactions with water. A similar series holds for cations, but their effect on stabilizing macromolecules is generally smaller than that of the anions. [22,29] It has been already reported that some salts, the chaotropic agents, increase the critical solution temperature CST ("salting in" effect), where other salts, the cosmotropic ones, decrease the CST ("salting out" effect). [20,30] The observed "salting out" process can be explained as a combination of several effects (i.e., changes of the water structure in the polymer hydration sheath and changes of the interactions between the polymer and the solvent, due to the presence of salts.[31-33] It is known that the addition of electrolytes to water changes the normal hydrogen bound water structure. Several models have been proposed for the structure of water in the presence of ionic solutes. [16-17,27,34-35]. According to the model of Frank and When Frank[23] for aqueous salt solutions, water consists of three regions:

- A region: It is composed of water molecules which are immobilized through ionic-dipole interactions
- B region: It is consists of water molecules partially ordered by the electric field of region A, being more random in organization than "normal" water
- C region: Consists of "normal" water.

The extent of region B is a measure of the ability of the ion to destroy water structure. In general, small and polyvalent ions have large A regions and are called *structure makers* or "positively hydrated". On the other hand, large and monovalent ions have small A regions and large B regions and are called *structure breakers* or "negatively hydrated". It is known that the addition of structure breakers to water decreased the viscosity of the solutions and vice versa. This is the reason why the phase transition phenomenon of aqueous polymer solutions is associated with changes in the normal structure of water induced by electrolytes (i.e., salts).

Saito et al.[36] investigated transition temperature (T_c) of poly(NIPAM) hydrogels in the presence of different salts. They reported that the transition was strongly dependent upon the anionic species deriving from introduced salt; however, T_c was almost independent of cationic species (Na^+, K^+). They assigned such behavior to the mentioned structure-making or structure-breaking effects induced by addition of different salts.

The influence of salts on stimuli sensitive polymer solution is widely known (for example salting out effect). Upon salt addition, dissociated salt ions are immediately surrounded by water, forming associated molecules, what is similar to the effect observed in case of alcohol-mixture with low alcohol content. Partial dehydration of poly(NIPAM) chain appears and polymer becomes more hydrophobic. This effect leads to the lowering of its phase separation temperature. This phenomenon is more produced to so-called strong "salting out" agents. The strength of "salting out" of the given salt corresponds to its position in the classical Hofmeister series, which is the ranking of ions toward their ability to precipitate a mixture of hen egg white proteins.[37-38]

The influence of salts on T_c of poly(NIPAM) was investigated by Borisow et al.[39] Two salts were chosen: sodium chloride (NaCl) and ammonium sulphate ($(NH_4)_2SO_4$). It was observed that phase separation temperature decreases almost linearly with increasing salt concentration, where this effect was more pronounced when ammonium sulphate was added. The phase separation temperature for 1% (w/w) solution of poly(NIPAM) was lowered by 8°C as the result of addition of 0.5 mol/l sodium chloride, where only 0.2 mol/l of ammonium sulphate gave the same result The differences were attributed to the stronger association of bigger ions or "divalent effect".

Polyelectrolytic gels are swollen at very low ionic strength due to repulsion among the charged groups. By increasing the ionic strength the repulsive forces can be screened, which causes the gel to shrink.[40]

There have been many reports of attempts to control the thermally induced volume phase transition of *N*-alkylacrylamide gels, for example through the use of mixed solvent,[41-42] the addition of salt,[28,43-44] the copolymerization of an electrolyte monomer[41] and the addition of surfactants.[41,43-44]

Park and Hoffman[45] were the first to demonstrate that aqueous NaCl can induce volume phase transition in non-ionic poly(NIPAM) hyrogels. They monitored the effect of a series of sodium salts and concluded that the chloride ion is responsible for this transition.

2.3 Experiments

2.3.1 .Microgel preparation.

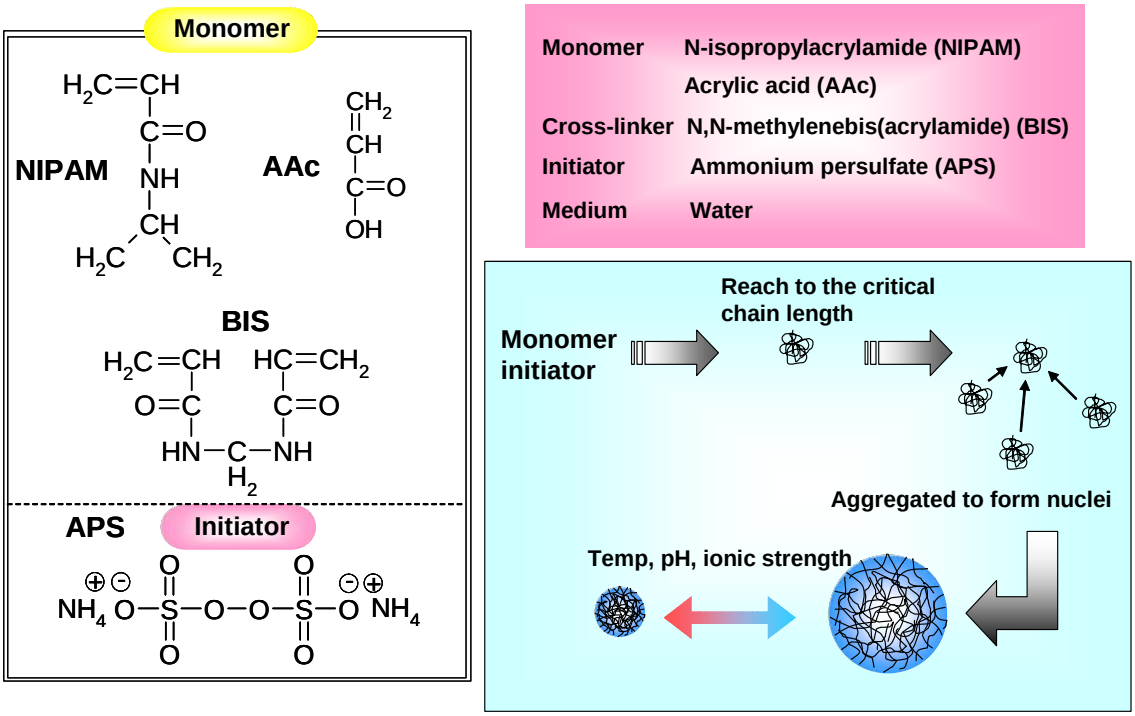

Figure 2.1 Chemicals and mechanism of precipitation polymerization of poly(NIPAM-*co*-AAc)

The details of temperature induced free-radical precipitation polymerization used in these studies are as follows. Sodium dodecyl sulfate (SDS) was used as the stabilizing surfactant while ammonium persulfate (APS) was used as the free radical initiator. The 0.3169g NIPAM monomer (main monomer), 0.0252g acrylic acid/ (comonomer), 0.109g BIS (cross-linker) and 0.06g SDS were dissolved in 100 ml of distilled water.[46-.47] This dissolved solution was continuously stirred in a three-neck, 200mL round-bottom flask. This solution was heated to 70°C while being purged with N_2 gas. This purging was necessary to remove any dissolved oxygen that could act as a free-radical scavenger that may interfere with the polymerization process. Thirty

minutes later, the reaction was initiated by adding a solution of APS. The solution turned turbid within 10 minutes, indicating successful initiation. The reaction proceeded for approximately 5 hours under a constant stream of nitrogen gas. Following synthesis, the microgels were cooled and then dialyzed for 2 weeks against distillated water with a daily exchange of fresh water. The resulting polymer microgels were refined by dialysis followed by repetitive centrifugation-decantation-redispersion and finally dispersed in PBS buffers containing 50, 100, 150, and 200 mM NaCl. The hydrodynamic sizes of the microgels were determined by photo correlation spectroscopy (PCS, PARIIIs, Ohtsuka Electronics). A scheme depicting microgel synthesis using this technique is illustrated in Figure 2.2 This synthetic process results in the fabrication of monodisperse microgel particles.

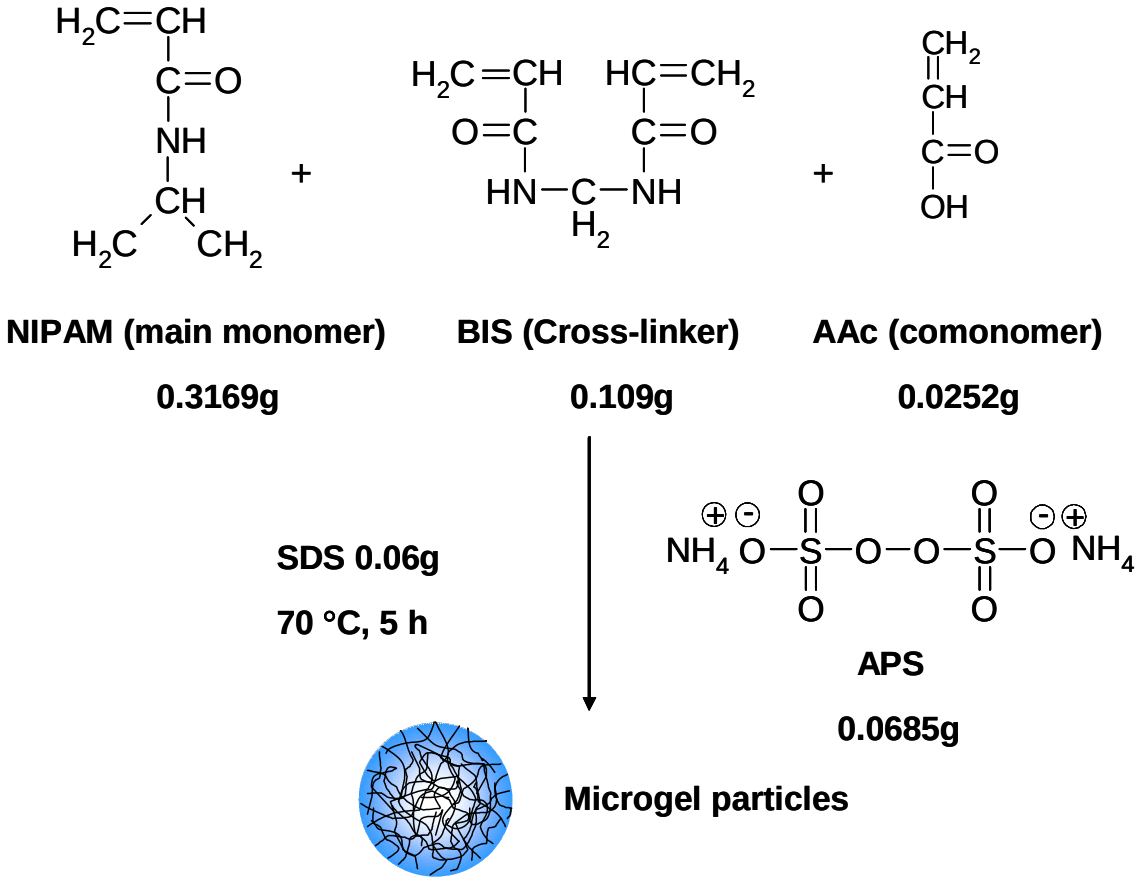

Figure 2.2 Synthesis scheme for poly(NIPAM-*co*-AAc) microgel particles. The monomer, acrylic acid comonomer, and surfactant (SDS) are all dissolved in distillated water and this solution is heated to 70°C. The polymerization is then initiated by addition of the free-radical initiator (APS).

This route by which these microgels grow in solution is a typical nucleation, aggregation and growth mechanism.[48] An illustration of this mechanism is shown in Figure 2.3. It is important to note that all of these syntheses are carried out at 70°C, which is a temperature well above the LCST of the polymer. This high temperature allows the thermal free-radical initiator (APS) to act effectively. It also aids in the nucleation process. Once the free-radical initiator is added to the heated monomer solution, growing oligoradical chains are formed immediately. These chains keep growing until a critical chain length is reached, after which these chains hydrophobically collapse upon themselves forming precursor particles. The reason for this collapse is because the polymer phase separates at temperature above its LCST, It is onto these precursor particles that other growing oligoradical chains can attach, thereby forming growing particles that keep maturing until all of the monomer has been exhausted. The size of these microgel particles can be tuned by modulating the concentration of stalbilizing surfactant as well as initiator. Typically, higher surfactant concentration results in smaller microgels and vice versa.

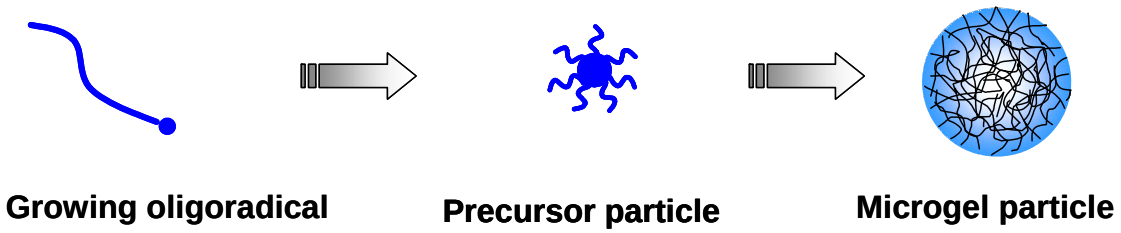

Figure 2.3 Schematic depicting the mechanism by which poly(NIPAM) based microgel particle grow during free-radical precipitation polymerization. Once initiator is added to the heated monomer solution, growing oligoradicals forms precursor particles. To these precursor particles, other growing oligoradicals can attach until all monomer is exhausted, resulting in the formation of colloidally stable microgel particles.

2.3.2 Preparation of buffer solutions

Preparation of Buffers with different NaCl concentrations

A series of Phosphate-buffered saline (PBS) buffers with different sodium chloride concentrations was prepared by dissolving 0.05, 0.1, 0.15, and 0.2 mol NaCl in 0.01 mol Na_2HPO_4 and 0.01 mol NaH_2PO_4 in 1L water.

Preparation of solutions with ionic strength 0.02 (I=0.02)

NaCl aqueous (NaCl aq.) solution was prepared by dissolving 0.02 mol L^{-1} NaCl in water. Glycine buffer was prepared by dissolving 0.05 mol crystalline glycine and 0.015 mol NaCl in 1L water. The pH was adjusted to 9.5 by adding 5 ml of 1 N NaOH. Citrate buffer was prepared by dissolving 0.02 mol citric acid 1-hydrate and 0.02 mol sodium citrate 2-hydrate in 1L water. The pH was adjusted to 3.2 by adding 0.1 mol L^{-1} citric acid.

2.3.3 SPR Chip Surface Modification.

Gold-coated glass slides were used as the substrate for binding of microgels. The glass slides were cleaned with piranha solution (H_2O_2/H_2SO_4 = 1:3 by volume) and thoroughly rinsed with Milli-Q water and ethanol sequentially. The Au sensor chip was covered with amine-terminated self-assembled monolayer (SAM) by immersing into 50 mM ethanolic solution of 11-amino-1-undecanethiol hydrochloride for 24h at room temperature.

2.3.4 SPR experiment

All SPR experiments were performed on a Biacore2000 biosensor (BIAcore, Sweden). The dimensions and volume of the cell are (l x w x h = 2.4 x 0.5 x 0.05 mm) and 60 pl., respectively. All experimental data were evaluated by BIAevaluation 3.1.

Each SAM chip was placed in a Biacore2000 first, and then SPR running buffer was run until the system reached the steady state. Secondly, the SAM surface was washed with 5-μl injections of 10 mM NaOH solution twice before the binding process of microgels was started. Thirdly, 50 μl dispersions of 0.4069 wt% Poly(NIPAM-*co*-AAc) microgels were injected and measured at 20°C. And finally, in order to regenerate the surface 100 mM NaOH aqueous solution was injected twice for 1 min at the end of each experiment. Response arising from the microgels attached onto chip was taken as the difference between the SPR signals before and after interaction. Data analysis of sensorgrams was performed using BIAevaluation software.

2.3.5 Surface characterization

After measuring SPR, the microgels bound on SAM surface of SPR sensor chip were observed by atomic force microscopy (AFM) in contact mode with a SPR300/SPI3700 (SII Nano-Technology Inc.)

The size and shape of dried particles were also characterized by field emission scanning electron microscopy (FE-SEM, S-4700, Hitachi Ltd.). The particle arrays on SPR sensor chip were sputter-coated with platinum/palladium before examination.

2.3.6 Measurements of the Electrophoretic Mobility of Microgels

The electrophoretic mobility of microgels was measured at ionic strength of 0.02 (I=0.02) in various buffers (citrate buffer, NaCl aq, and glycine buffer) by using Zeta potential analyzer (ZEECOM). The measurement was repeated at least 5 times.

2.4 Results and Discussion

2.4.1 Precipitation Polymerization to form Anionic thermosensitive microgel

Poly(NIPAM-*co*-AAc) microgel was prepared by the aqueous free-radical precipitation copolymerization of NIPAM, AAc and BIS, using APS as initiator, and SDS as surfactant. After removing surfactant by dialysis, hydrodynamic diameters were determined by photon correlation spectroscopy (PCS). The microgels were monodisperse soft particles with diameters less than 200 nm (see Table 2.1). The microgels were stable in dispersion due to electrostatic and steric stabilization. Electrostatic stabilization was originated from sulfate and carboxyl groups (i.e., ammonium persulfate initiator and acrylic acid comonomer, respectively). Monodispersity of particles was achieved by SDS, which enhanced colloidal stability during the sensitive nucleation stage.

Table 2.1 Hydrodynamic diameter of poly(NIPAM-*co*-AAc) microgel in two dispersing media at 20 °C

Medium	Weight average diameter ($D_{w,}$ nm)	Number average diameter ($D_{n,}$ nm)	Polydispersity index (D_w/ D_n)
Water	189.2	181.2	1.04
PBS	183.3	180.7	1.01

Figure 2.4 shows the SEM view of the microgels, which were dried from the dispersion in the 150 mM NaCl of PBS buffer. According to Figure 2.4, the microgels are not fully spherical shape due to a heterogeneous contraction of the size during evaporating of buffer. Small dots represent crystals of salt remaining in the dry sample. The average diameter of dry microgel is 103.4 nm. It is about 60% of hydrodynamic diameter. It indicates that the volume decreased by 80% during evaporating buffer if a contraction took place isotropically. Such large shrinkage might cause unsymmetrical shape of dry microgel.

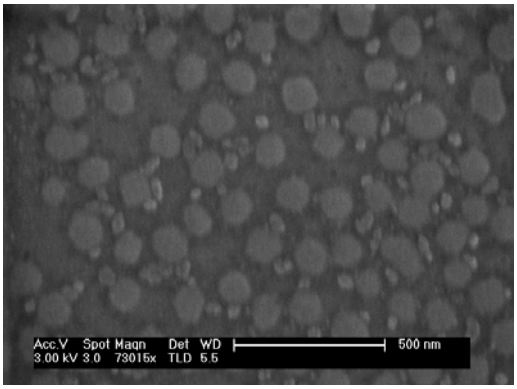

Figure 2.4 SEM view of the poly(NIPAM-*co*-AAc). It shows that the diameter of microgel in dry state is 103.4 nm. Small cubes in the fugure are salt crystal.

2.4.2 Ionic strength- and temperature--responsitiveness of microgel

Figure 2.5 shows temperature dependence of hydrodynamic diameter of poly(NIPAM-*co*-AAc) microgels in 50, 100, 150, and 200 mM NaCl. In the medium with 200 mM NaCl, microgels did not disperse stably and their hydrodynamic

diameter could not be measured exactly. According to Figure 2.5, the hydrodynamic size of microgels decreased with increasing temperature at various NaCl concentrations. At higher temperatures the hydrogen bonds among water molecules break, and there is an expulsion of water from the interior of the microgels. Then, hydrophobic interaction between polymer molecules occurs and the microgels become shrunken. As the salt concentration increased, the sizes of microgels under swollen (i.e., 20°C) and shrunken states (i.e., 40°C) decreased. The presence of salts tends to disrupt the hydration structure of water molecules in the vicinity of the NIPAM side chains, which leads to gel collapsing.[23] As a result, the size of microgels decreased with increasing NaCl concentration in the buffer.

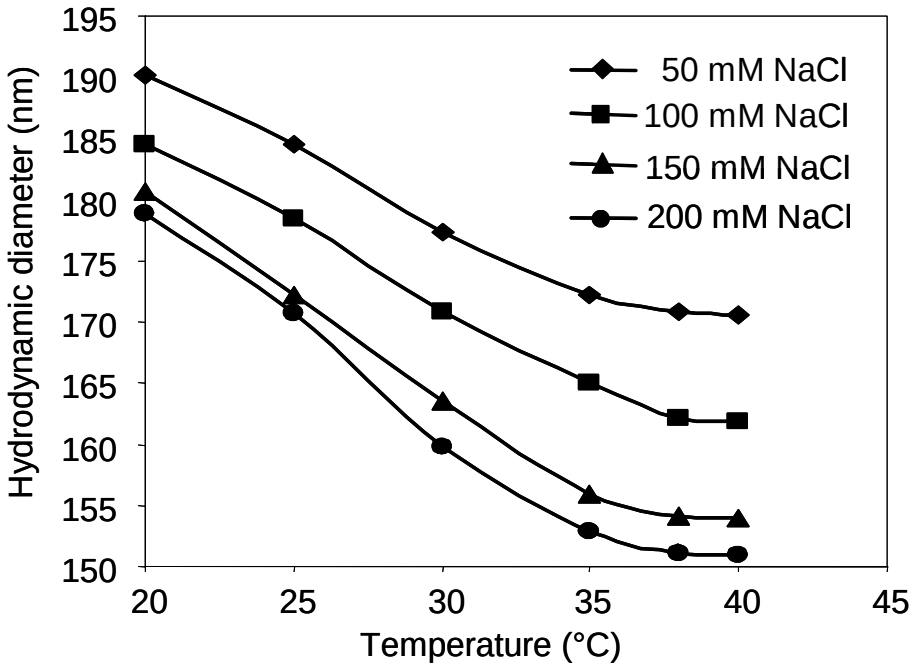

Figure 2.5 Hydrodynamic diameter of PNIPAM-*co*-AAc) in various NaCl concentrations

2.4.3 pH- and temperature-responsiveness of microgel

The average diameters of microgels in three kinds of solutions are shown in Table 2.2. As the polymerization progresses, the microgels in the dispersion medium are formed and stabilized by the surface charge originated from the initiator and the surfactant.[49-50] The particle formation seems to be governed by a homogeneous nucleation process, which can produce a very narrow particle size distribution provided that the particles have been formed in very early stage of the polymerization

process and subsequent growth has taken place without the formation of additional particles.[51]

Table 2.2 Hydrodynamic diameter and electrophoretic mobility of poly(NIPAM-*co*-AAc) microgel in various dispersing mediums at 20 °C with ionic strength 0.02.

Medium	pH	Weight average Diameter (D_w, nm)	Number average diameter (D_n, nm)	Polydispersity index (D_w/D_n)	Electrophoretic mobility ($\mu m\ s^{-1}V^{-1}$ cm)
Citrate buffer	3.2	139.8	137.6	1.02	-1.11
NaCl aq.	5.7	192.6	189.5	1.02	-2.67
Glycine buffer	9.5	197.4	194.5	1.01	-4.79

Table 2.2 shows pH dependence of hydrodynamic diameter of poly(NIPAM-*co*-AAc) microgels in three kinds of solutions (i.e., citrate buffer pH 3.2, NaCl aq pH 5.7, and glycine buffer pH 9.5) with ionic strength of 0.02 (I = 0.02). The size of microgels was the smallest in citrate buffer among three kinds of solutions. In low pH solution, acrylic acid on the network chain is noncharged, the microgels become shrunken due to loss of electrostatic repulsive force. With increasing pH (i.e., NaCl aq.), the acrylic acid on the network exhibits partial ionization to introduce some water molecules into the network, which makes the microgels expand. At high pH (i.e., glycine buffer), the microgels are fully charged. This causes high water absorbability, which makes the microgels swollen. As a result, the size of microgels increased with increasing pH of solution.

Information about the pH-dependent changes in surface properties of poly(NIPAM-*co*-AAc) had been obtained from the electrophoretic mobility measurement of the microgels dispersed in various pH buffers at I = 0.02. The electrophoretic mobility of poly(NIPAM-*co*-AAc) microgels in various buffers measured at 20°C are shown in the last column of Table 2.2. The obtained values were negative in all buffer solutions with I = 0.02. In the case of citrate buffer, the surface of microgels has the slightly negative charges originated from the sulfate groups (i.e., initiator and surfactant). In both of NaCl aq. and glycine buffer, the surfaces of microgels have large negative charges originated from acrylic acid as well as from sulfate groups. The dissociation of acrylic acid increases and the electrophoretic mobility becomes more negative as the pH of solutions increases.

2.4.4 Microgel binding on sensor chip

Dispersions of microgel were run through the channel of SPR sensor. Carboxyl group on the microgels seemed to be used for binding microgels onto SPR sensor chip through the reaction with amine group of 11-amino-1-undecanethiol hydrochloride SAM on the sensor chip. When regeneration solution was passed through the channel after binding microgels, SPR response was slightly decreased (see the arrow in Figure 2.6a). The slight decrease in SPR response was attributed to removal of microgels which were not bound directly onto SAM surface. Figure 2.6b shows an AFM view of the surface of chip taken out from the flow cell after SPR measurement. A plenty amount of microgels existed on SPR sensor chip even after the chip surface was rinsed with NaOH regeneration solution. This result showed us that the microgels were firmly bound onto the chip and the same chip would be usable repeatedly for SPR experiments keeping unchanged number of microgels on it.

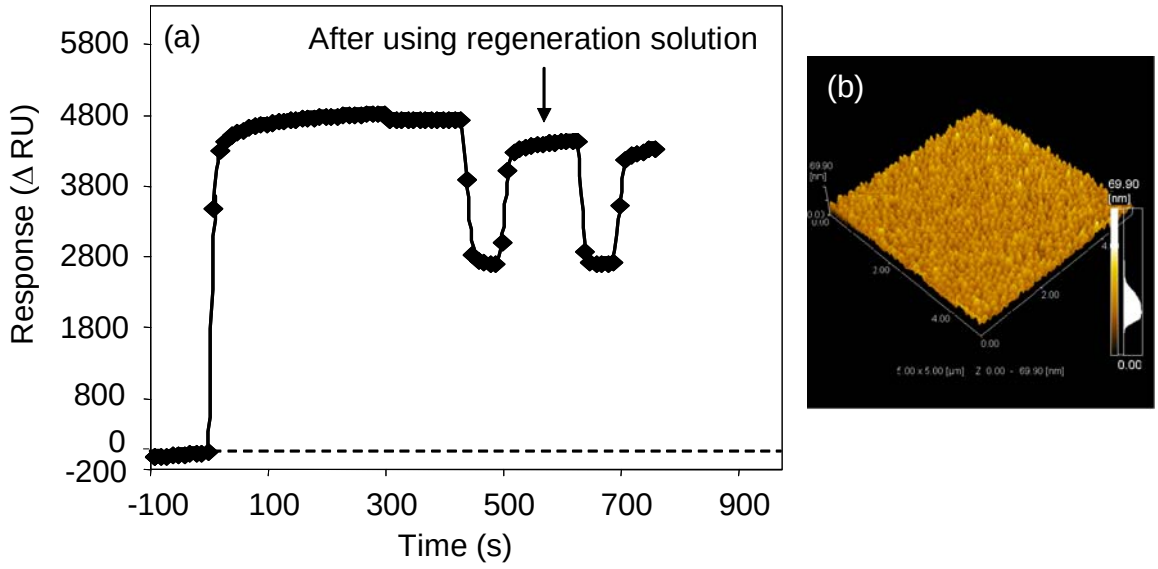

Figure 2.6 (A) A sensorgram of the microgels and (B) AFM image of poly(NIPAM-*co*-AAc) microgels in PBS buffer after using regeneration solution

The vertical axis of Figure 2.6 indicates SPR response in Δ(response unit) or (ΔRU) when microgels were bound on the chip. If the material bound is protein, SPR response in ΔRU can be converted to that in ng/μm^2. But such conversion is

impossible for environmentally sensitive microgels. So, the numerical values on vertical axis were expressed in ΔRU through this work.

The AFM images of SAM surfaces after being used for SPR measurements of binding microgels in different pH buffers are shown in Figure 2.6. The center-to-center distance of adjacent particles was also measured on AFM images. The hydrodynamic diamerter and center-to-center distance of microgels in three buffers are presented in Table 2.3. The round coincidence between hydrodynamic diameter and center-to-center distance implies that microgels were bound on the SPR chips keeping the same size and shape as in their dispersions. That is, the results suggested that the microgels were not deformed and hold their spherical swollen body on the chip.

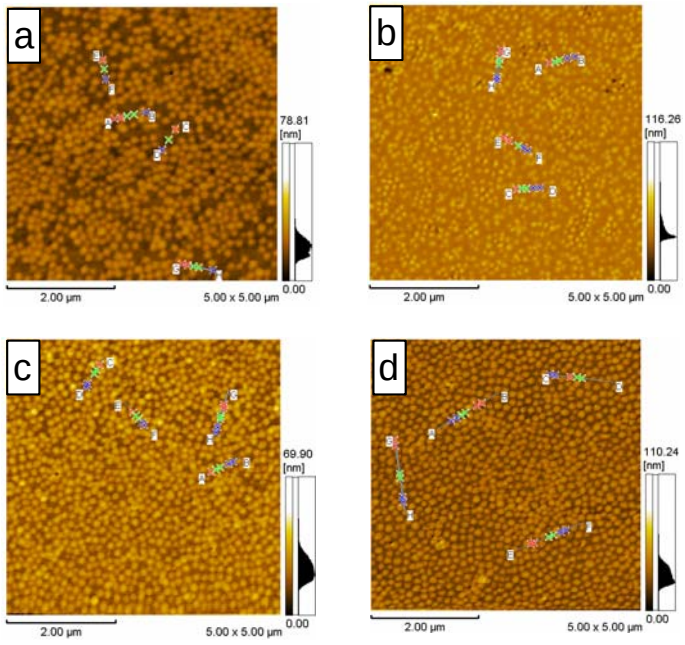

Figure 2.7 AFM views of the poly(NIPAM-*co*-AAc) microgels on SAM surface prepared from PBS with various NaCl concentrations, (a) 50, (b) 100, (c) 150, (d), and 200 mM NaCl at 20°C.

The AFM images of chip surfaces after being used for SPR measurements of binding microgels at different salt concentrations are shown in Figure 2.7. According to AFM images, the number of binding microgels increased as salt concentration increased. The disruption of the hydration structures around the NIPAM side chain due to the presence of salts leads to the gel collapsing[52] as well as the hydrophobic interaction of chains. Thus obtained small microgels were supposed to make a densely packed monolayer. As a result, the microgels in higher salt concentration gave the

greater number of binding microgels on the chip. The number of binding microgels, shown in the third row in Table 2.3, was calculated from the center-to-center distance and used for the simulation later.

Table 2.3 The number of binding microgel and average inter-particle distance in various NaCl concentrations

NaCl (mM)	50	100	150	200
Hydrodynamic diameter (nm) measured by DLS	190.2	184.5	180.6	178.9
Center-to-center distance (nm)* measured on AFM	204	188	174	170
Number of binding microgel (particles/μm^2)	36	45	48	51

* The Center-to-center distance of adjacent particle on the chip.

Table 2.4 Hydrodynamic diameter of microgels in buffers, center-to-center distance, and number of microgels bound on SPR chips

Medium	pH	Hydrodynamic diameter (nm)	Center-to-center distance (nm)	Number of binding microgels (particles/μm^2)
Citrate buffer	3.2	139.8	134.9	72
NaCl aq.	5.7	192.6	190.5	55
Glycine buffer	9.5	197.4	194.3	26

Table 2.4 includes the number of binding microgels in μm^2, which was counted on AFM view. The number of binding microgels increased as pH decreased. In citrate buffer (pH 3.2), little inter-chain electric repulsion makes the microgels shrank. The obtained small microgels made a densely packed monolayer on the chip. It was worth mentioning that direct interaction between citrate ion and SAM was negligible judging from negligible SPR response in citrate buffer itself. At high pH (i.e., glycine buffer) the microgels were swollen and repulsive to each other due to an

electrostatic repulsion. Therefore, the smaller number of binding microgels could be observed on the chip from higher pH solution.

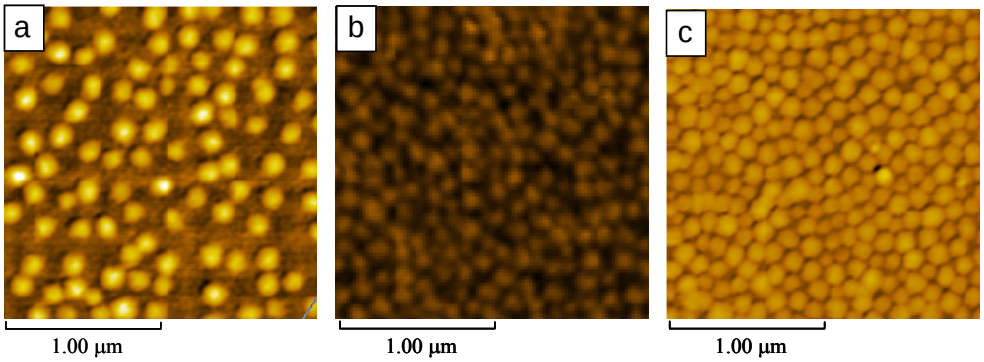

Figure 2.8 AFM views of the poly(NIPAM-*co*-AAc) microgels on SAM surface prepared from various buffers, (a) glycine buffer (pH 9.5), (b) NaCl aq (pH 5.7), and (c) citrate buffer (pH 3.2) at 20°C

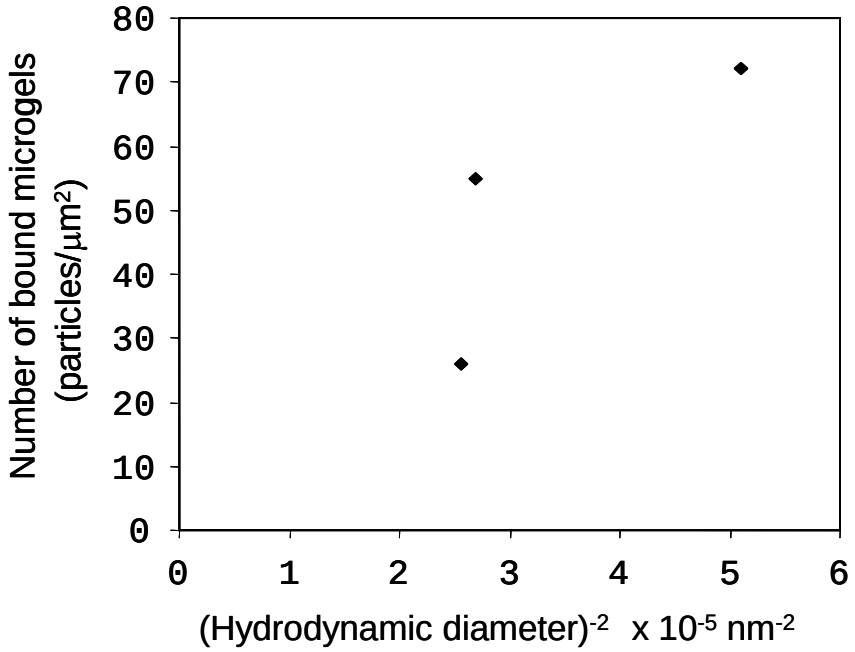

Figure 2.9 Relationship between the number of binding microgels on SAM surface and the hydrodynamic diameter in various solutions

The expected density of microgels could be calculated by reciprocal of hydrodynamic diameter^2 (i.e., (surface area of chip) $\propto$ (number of binding microgels) x (hydrodynamic diameter)^2) or density $\propto$ (H.D)$^{-2}$) if they were packed densely in

2D monolayer. Figure 2.9 shows the relationship between the counted number of binding microgels on SAM surface and the density of microgels expected from the hydrodynamic sizes in three buffers (i.e., citrate buffer, NaCl aq., and glycine buffer I=0.02). The smaller size in low pH gave the greater number of microgels bound on the chip although the number of binding microgels was not necessarily proportional to (hydrodynamic diameter)$^{-2}$. The discrepancy from proportionality resulted from loose packing of microgels in glycine buffer. It might be attributed to partial contribution of electrostatic repulsive force among highly charged microgels in glycine buffer.

2.4.5 Effect of ionic strength, pH and temperature on SPR response

2.4.5.1 The effect of salt on SPR response in microgel dispersion flow system

SPR measurements were done using a series of PBS buffers with different NaCl concentrations to study the effect of ionic strength on SPR response. Figure 2.10 represents SPR sensorgrams resulting from the microgel attached on SAM surface in PBS bufferes with various NaCl concentrations.

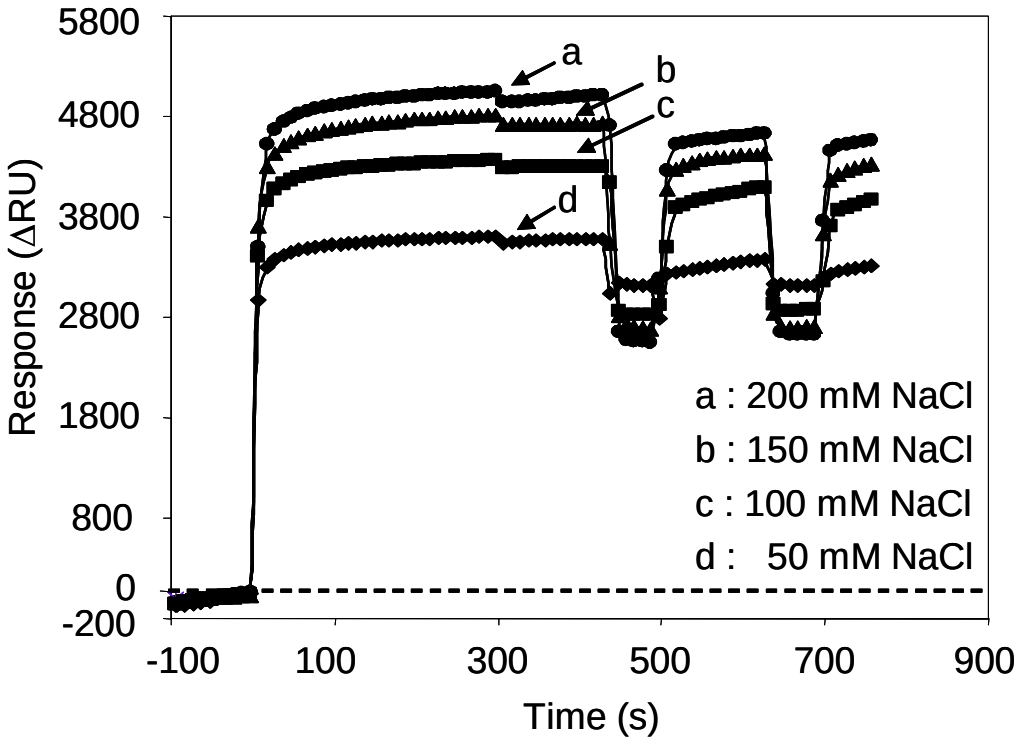

Figure 2.10 Sensorgrams of the microgels at concentrations of PBS in 50, 100, 150, and 200 mM NaCl. Injection volume of 0.0407% wt/wt the microgel was 25 μl at 20°C using a flow rate of 5 μl/min in SPR running buffer

The SPR response increased as NaCl concentration increases. The solution of 200 mM NaCl gave the highest SPR response. As mentioned in the previous section, microgels dispersion in 200 mM NaCl shrank to the smallest and attached in the largest amount on the chip. Both might be possible to contribute to the highest response because the small microgels with high polymer density could place themselves closely to the surface where the evanescent wave is strong so that SPR can be strong. The number of microgel bound on the chip, of course, affects SPR response in a proportional manner. There might be negative effect of small sized microgel on SPR response. The narrower space of microgel in evanescent wave field might cause smaller change of SPR response.

2.4.5.2 The effect of pH and temperature on SPR response in microgel dispersion flow system

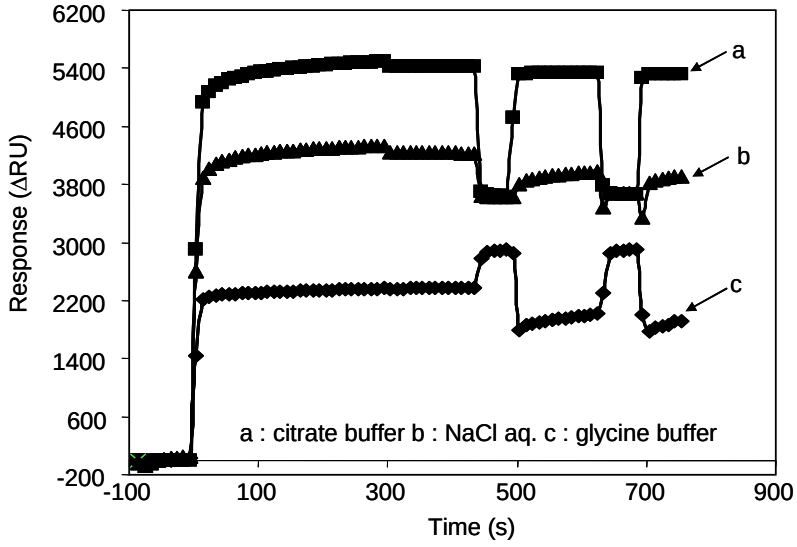

Figure 2.11 Sensorgrams of the microgels at concentrations of citrate buffer, NaCl aq., and glycine buffer. 25 μl of 0.042 (wt/wt) % microgel dispersion was injected at 20°C with a flow rate of 5 μl/min in SPR running buffer.

The behavior of microgels attaching onto the chip in various pH buffers was measured by SPR sensorgrams as shown in Figure 2.11. The SPR response increased as a pH decreased. The citrate buffer (pH 3.2) gave the highest SPR response. As mentioned in the previous section, microgel dispersion at low pH (i.e., in citrate buffer) shrank to the smallest and attached in the largest amount on the chip. So, the extent of the response seems to be proportional to the number of microgels bound on the SPR chip.

Poly(NIPAM-*co*-AAc) can exhibit temperature- and pH- sensitive properties. Temperature and pH dependence of SPR response were examined in this section.

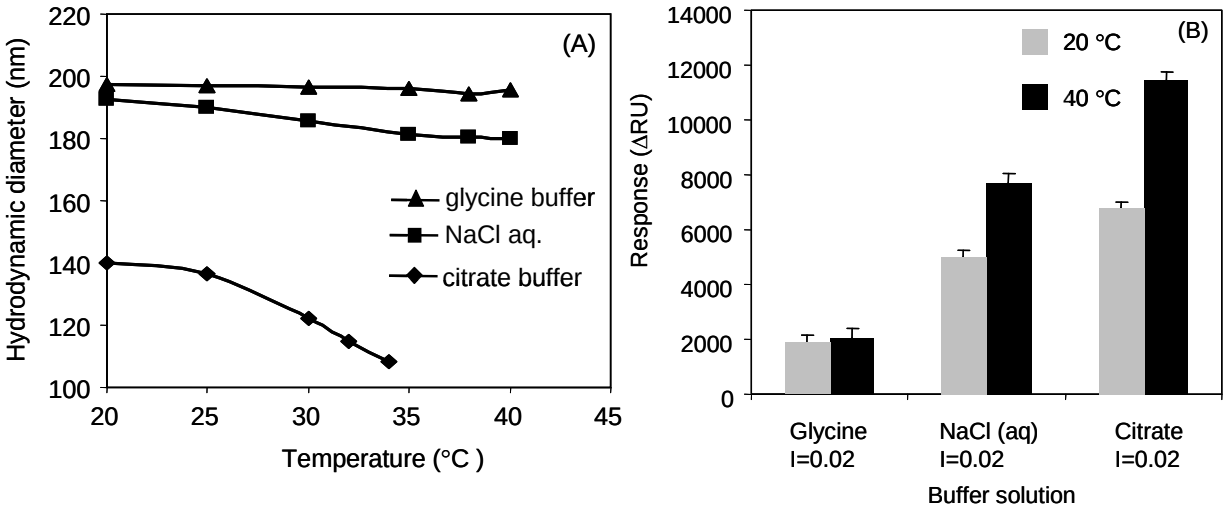

Figure 2.12 (A) Hydrodynamic diameter of PNIPAM-co-AAc) and (B) The comparison of SPR responses between 20°C and 40°C in various solutions with I = 0.02. The values are the mean of three experiments; error bars indicate the standard deviation.

To compare the binding of microgels onto the chip between 20°C and 40°C, the dispersions of microgels were injected into SPR cell at 40°C. The comparison of SPR response is shown in Figure 2.12B. There was insignificant difference in response between 20°C and 40°C in glycine buffer. According to Figure 2.12A, hydrodynamic size of microgels in glycine buffer little changed with increasing temperature due to full dissociation and disappearance of the thermosensitive property. There was no difference in the number of binding microgels at two different temperatures, shown in Figure 2.8a and Figure 2.13a. Therefore, there was no significant temperature dependence of SPR response in glycine buffer. In contrast, there were differences in response of binding microgels in both of NaCl aq. and

citrate buffer. In the case of NaCl aq., the larger response is due to larger number of particles bound on the chip at higher temperature. That is, the smaller size gave more densely packed monolayer and higher response. For citrate buffer, there is also a large difference in response between 20°C and 40°C. This is due to the aggregation of microgels at 40°C, as shown in Figure 2.13c. Electrostatic interactions between microgels in various buffer solutions play an important role in binding state of microgels on chip and consequently in SPR response.

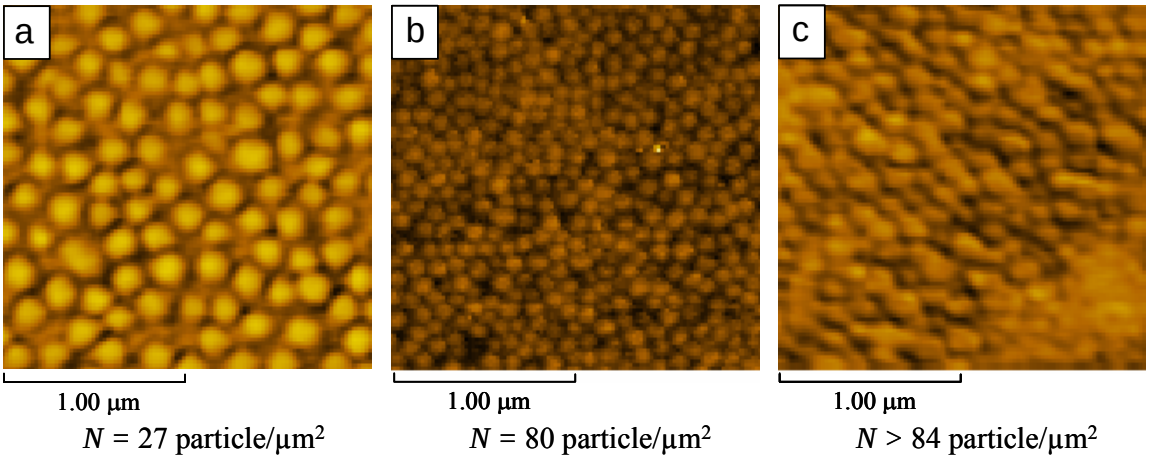

Figure 2.13 AFM views of the poly(NIPAM-*co*-AAc) microgels on SAM surface prepared from various buffers, (a) glycine buffer (pH 9.5), (b) NaCl aq. (pH 5.7), and (c) citrate buffer (pH 3.2) at 40°C.

To better understand the effect of physical parameters (i.e., the size, refractive index, and the number of binding microgels) on the SPR response, quantitative analysis of SPR simulation was examined.

2.4.6 SPR simulation of microgel on sensor chip in the flow of aqueous solutions at different salt concentrations and pHs

From above discussion, we have two factors, which might affect on SPR response, to be taken account for the simulation. The change in evanescent wave strength was caused by the binding microgel and the number of binding microgel. In this work, the simulation based on evanescent wave function was done based on the Fresnel reflection and transmission coefficients.[53] In our system, the most simple and widely employed experimental setup for excitation of the surface plasmon wave at the

metal/dielectric interface is employed according to the Kretschmann-Raether attenuated total reflection (ATR) configuration.[54] In this configuration, a thin gold film with an adhesion promoter, chromium, is deposited to the surface of a high refractive index, higher than that of the dielectric medium. In the simulation, the following dielectric constant (ε) and thickness (d) were used for glass / metal film / SAM / microgel / buffer; $\varepsilon_{glass} = 2.2831$, $\varepsilon_{Au} = -24.276+i1.68$, $d_{Au} = 45$ nm, $\varepsilon_{SAM} = 2.25$, $d_{SAM} = 2.2$ nm, $\varepsilon_{gel} = 1.8685$, $d_{gel} = 180.6$ nm, and $\varepsilon_{buffer} = 1.7853$, respectively, in 150 mM NaCl at 20°C with wavelength of 765 nm. (ε and d values in different buffers are not shown) The evanescent wave function was calculated according to these parameters. The strength and decay characteristic of the evanescent wave function are governed by the experimental parameters (i.e., polarization and wavelength of the incident radiation) and material characteristics (i.e., refractive index of prism, metal film and medium, and the metal film thickness).[54-56] When a dielectric medium changes from microgel layer to PBS buffer, a discontinuous decay takes place. For different salt concentration systems, the evanescent wave was calculated from each resonance angle depending on each salt concentration, and then SPR simulation in each salt concentration can be achieved.

Based on the evanescent wave calculation, we use the change of evanescent wave resulting of binding microgel for calculating SPR response in microgel system. According to the change of evanescent field strength is very sensitive to the refractive index on the top of the metal film, the decay of evanescent field strength is used for calculating the SPR response in microgel system. The strong surface plasmon wave-generated evanescent field is governed by experimental parameters (i.e., angle of incidence and wavelength of the coupled radiation) and material characteristics (i.e., complex refractive indexes of metal film, dielectric substrate and thickness of metal and dielectric films). The magnitude and decay characteristic of the evanescent field are very sensitive to changes in any of the governing parameters. This unique characteristic makes us to use evanescent field for simulating SPR response in microgel system. We assume that there are two possible conformations of binding microgel on the SPR sensor chip surface; these are spherical and flat shape. The difference in conformation provides the difference in the occupied volume, decay of evanescent field strength, and sensitivity. To calculate the SPR response based on evanescent wave, we have to calculate the SPR angle using Frenel reflection and

transmission equation (i.e., via eq. 1.8 in Chapter 1). Then, the SPR angle is used to calculate electric fields for parallel polarization (i.e., via eq. 1.11). The mean square electric field (i.e., $\left\langle \mathrm{E}^2 \right\rangle_x$ or $\left\langle \mathrm{E}^2 \right\rangle_{0,x} = \left\langle E_{xz}^2 \right\rangle + \left\langle E_{zz}^2 \right\rangle$) in each medium (i.e., gold, microgel, and buffer solution medium) using for SPR simulation could calculate from eq 1.14. All calculations were done by mathematica 6.0 programming.

In this Chapter, the binding microgels were bound onto the sensor chip with spherical shape in dispersion system. The SPR response simulation for spherical model was discussed in this Chapter. To obtain the resonance angle, θ_{SPR}, of each system, the angular dependence of the reflectivity was solved by *N*-phase system (i.e., prism, gold, SAM, microgel, solution phases) of Fresnel equation[53] (via eq. 1.8 in Chapter 1). Then, the mean square electric fields $\left\langle \mathrm{E}^2 \right\rangle_x$ and $\left\langle \mathrm{E}^2 \right\rangle_{0,x}$ given in terms of wave vector and the Fresnel reflection and transmission coefficients[53] at a distance *x* from SAM/gel interface, which are located within the each layer of the medium (i.e., SAM, microgel, and solution) are calculated by using refractive indexes of each medium and θ_{SPR} (via eq. 1.10 and 1.14 in Chapter 1).

The simulation was done assuming that evanescent wave entering a microgel goes straight through microgel phase. Each evanescent wave entering a microgel at each position, e. g., at A, B, or C in Fig. 2.14 (a) and (b), contributed to SPR response with the extent $\int [\left\langle \mathrm{E}^2 \right\rangle_{0,x} - \left\langle \mathrm{E}^2 \right\rangle_x] \, \mathrm{d}x$ ($\equiv \mathrm{A}y$, eq. 2.4) which is shown as the area surrounded by $\left\langle \mathrm{E}^2 \right\rangle_{0,x}$ and $\left\langle \mathrm{E}^2 \right\rangle_x$ (Figure 2.15).

$$\mathrm{A}_y = \int_0^\infty \left[\left\langle \mathrm{E}^2 \right\rangle_{0,x} - \left\langle \mathrm{E}^2 \right\rangle_x \right] \mathrm{d}x \qquad (2.4)$$

The refractive index of swollen microgel, which was used for the deduction of $\left\langle \mathrm{E}^2 \right\rangle_x$, was given as a function of volume fraction of the polymer $\phi_p = (r_{dry}/r_{HD})^3$ and solution (1- ϕ_p) by

$$\mathrm{n}_{gel} = \left[\mathrm{n}_p \times \phi_p + \mathrm{n}_m \times (1 - \phi_p) \right] \qquad (2.5)$$

where n_p and n_m are the refractive indexes of NIPAM in dry polymer[57] (=1.5) and the buffer, respectively.

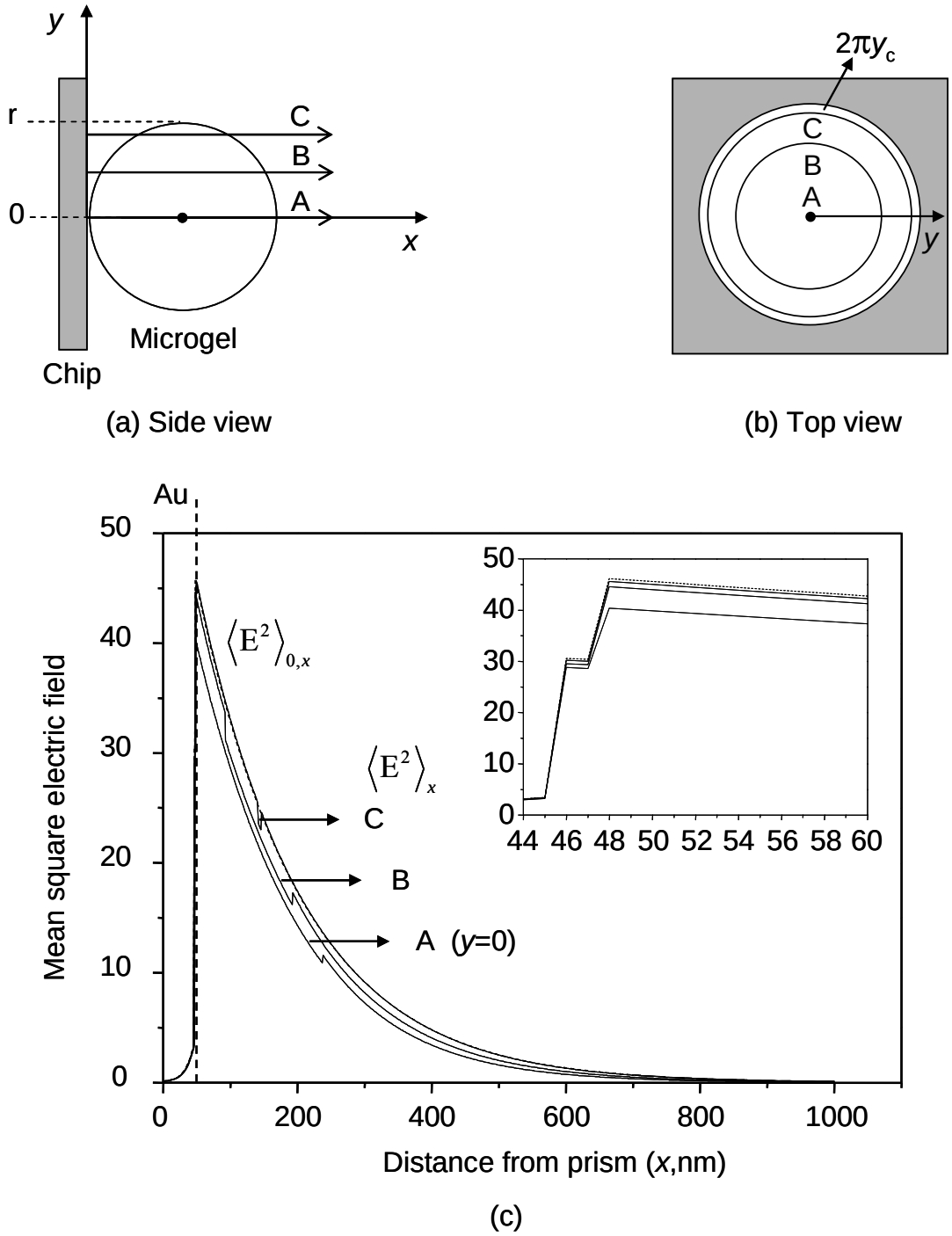

Figure 2.14 Calculated mean square electric fields (MSEFs) of their resonance angles of SPR pass through in different positions of spherical microgel as shown in side view (a) and top view (b). Solid lines show MSEF decay profiles of microgels in various positions; A, B, and C. A dashed line is the MSEF in solution without microgel. The inset is added for clarity, the inset shows the discontinuities of the evanescent field amplitudes at the Au/SAM and SAM/gel interfaces.

As presented in Figure 2.14c, which shows $\langle E^2 \rangle_x$ at resonance angle in microgel A-C, $\langle E^2 \rangle_x$ for A and B after passing through the microgel is smaller than $\langle E^2 \rangle_{0,x}$ in the range $x > 200$ nm. This means that the existence of the microgel affects $\langle E^2 \rangle_x$ not only in the inside of microgel but also in the buffer solution beyond the microgel. The inset of Figure 2.14c shows that the means square electric field amplitude at the SAM/microgel interface $\langle E^2 \rangle_{S/M}$ becomes smaller as the refractive index of the dielectric medium becomes greater. It decrease results from the increase of refractive index of microgel. there were differences in distribution of evanescent wave at different positions of passing through; we have to integrate all of distribution of evanescent wave for one particle. The total change of evanescent strength (SPRt) per microgel is obtained by integrating A*y* with y from 0 to r, and presented in Figure. 2.15

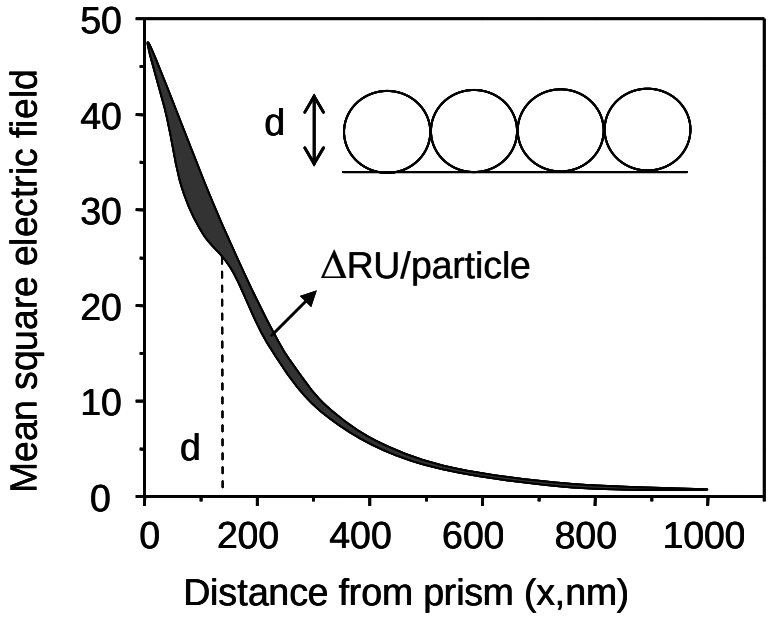

Figure 2.15 Difference in mean square electric fields between solution and microgel for calculating SPR response. It is shown as the shadow area in the figure.

Figure 2.15 shows the simulated SPR response for one particle. For all of microgels on sensor chip, the equation includes the terms of the number (N) of microgels bound onto chip.

$$SPRt = 2\pi N \int_0^r A_y y dy \qquad (2.6)$$

The mean square electric field amplitude at the SAM/Microgel interface $\langle E^2 \rangle_{S/M}$ becomes smaller as the refractive index of the dielectric medium becomes greater.[58-60] Its decrease corresponds to the increase of refractive index of microgel.

The calculated and experimental results are summarized in Table 2.5. According to the 7th row of Table 2.5, the absolute values calculated from eq. 2.6 were different from the experimental SPR response values because both based on different standards. The calculated values were multiplied by a fitting factor, *a* (= 3307.8/4.8 x 10^8), to set the calculated and experimental responses to the same value at 50 mM NaCl.

Table 2.5 Parameters of the microgel in different NaCl concentrations

NaCl (mM)	50	100	150	200
N (particle/μm^2)	36	45	48	51
n_{gel}	1.3618	1.3647	1.3669	1.3683
n_{buffer}	1.3354	1.3358	1.3362	1.3367
θ_{SPR}	69.14	69.37	69.55	69.67
$\langle E^2 \rangle_{S/M}$	40.395	39.779	39.325	39.038
ΔRU in eq.5	1.74 x 10^7	2.16 x 10^7	2.39 x 10^7	2.54 x 10^7
Cal. (RU)	3307.8	4120.2	4547.4	4844.9
Exp. (RU)	3307.8	3964.9	4322.7	4558.7

* A SIA kit Au glass ε_{glass} = 2.2831 are employed as a coupling prism, and radiation from a HeNe laser ($\lambda = 765$nm) is coupled to the sensor chip. The gold film ε_{Au} = -24.276+*i*1.68 is employed as a coated thin film on glass as a thickness of 45 nm. The dielectric constant of SAM is ε_{SAM} = 2.25 with 2.2 nm of thickness.[61] Diameter of microgel in dry state is 103.4 nm measured by SEM (see Figure 2.5). $\langle E^2 \rangle_{S/M}$ is evanescent field amplitude at SAM/Microgel interface.

The increase of the NaCl concentration in buffer affected two terms in eq. 2.6 The N increased with increasing salt concentration but the integral term in eq. 2.6 was almost constant for four solutions with different NaCl concentrations. The independence of integral term from NaCl concentration was the result of

compensation between the increase in the refractive index and the decrease in the volume of micorgel bound onto chip.

The comparison of responses between experiment and calculation are shown in Figure 2.16 It showed that the simulated SPR response was close to each experimental response. This result indicated that the eq. 2.6 could explain the experimental results.

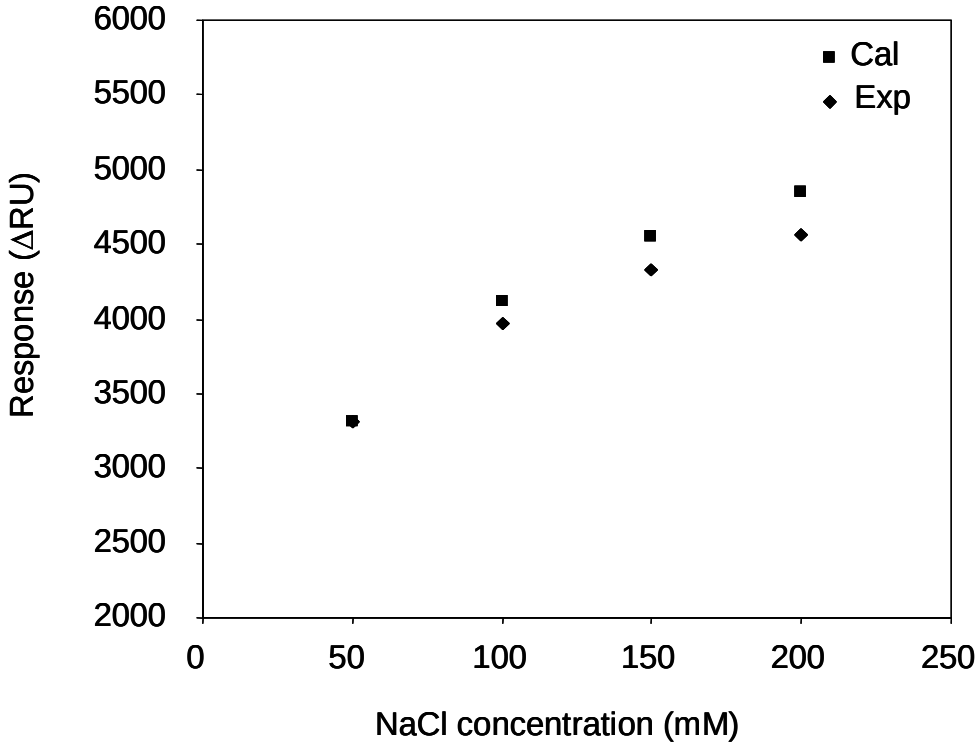

Figure 2.16 The comparison of SPR responses between calculated (Cal) and experimental (Exp) responses.

The calculated values are shown in Table 2.6 with the data necessary for the calculation. The decrease in pH affected the number of microgels bound to chip significantly. Microgels have inter- and intra-particle electrostatic repulsive force, wide area and low number density on chip at high pH whereas the low repulsive force, narrow area, and high number density at low pH. Nevertheless, the integrated terms (i.e., $\int_0^r A_y y dy$) in eq. (2.4) were little different among three systems. Therefore, SPRt was mainly decided by N. Thus, the citrate buffer system had the largest N and the largest SPRt, and glycine buffer system had the smallest N and the smallest SPRt. Table 2.6 includes experimental values of SPR response at three pHs in the last row. SPRt values in Table 2.6 were different from the experimental values. The SPRt

values were multiplied by a fitting factor, *a* (= 1910.5/7.24 x 10^8), to set the calculated and experimental values of SPR response to the same value in glycine buffer system. The comparison of response between experiment and calculation is shown in Figure 2.17 It showed that the simulated SPR response was close to each experimental response. This result indicated that eq. 2.6 could explain the experimental results satisfactorily.

Table 2.6 The simulation parameters and SPR responses in three buffer solutions

Medium	Citrate buffer pH 3.2	NaCl aq. pH 5.7	Glycine buffer pH 9.5
H.D (nm)	139.8	192.6	197.4
n_{gel}	1.3988	1.3606	1.3543
n_{buffer}	1.3298	1.3298	1.3298
θ_{SPR}	71.49	68.57	68.37
$\int_0^t A_y y dy$	4.48x10^6	4.31x10^6	4.43x10^6
^{0}SPRt	2.03x10^9	1.49x10^9	7.24x10^9
Cal. (ΔRU)	5353.1	3936.2	1910.5
Exp. (ΔRU)	5327.1	3912.1	1910.5

* A SIA kit Au glass ε_{glass} = 2.2831 are employed as a coupling prism, and radiation from a HeNe laser (λ = 765nm) is coupled to the sensor chip. The gold film ε_{Au} = -24.276+*i*1.68 is employed as a coated thin film on glass as a thickness of 45 nm. The dielectric constant of SAM isε_{SAM} = 2.25 with 2.2 nm of thickness.[61] Diameter of microgel in dry state is 103.4 nm measured by SEM.

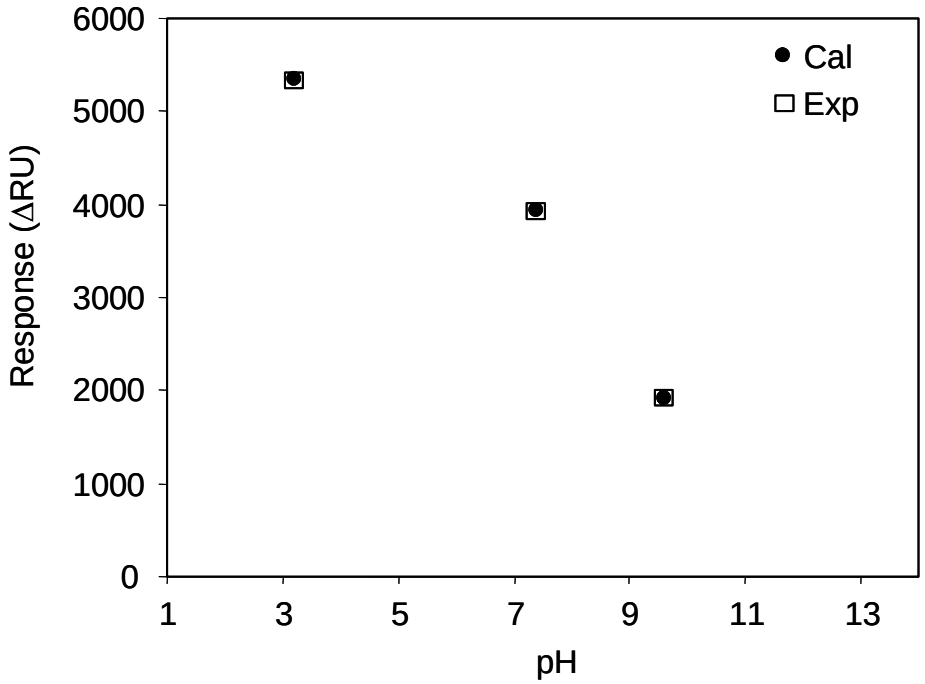

Figure 2.17 The comparison of SPR responses between calculated (Cal) and experimental (Exp) ones.

2.5 Conclusions

Anionic thermosensitive microgels, Poly(NIPAM-*co*-AAc) microgels, were prepared by aqueous free-radical precipitation copolymerization, The product was monodisperse spheres with diameter less than 200 nm, and they were responsive to both ionic strength, pH, and temperature. A series of buffer solutions including different NaCl concentrations and pHs were used to study a degree of swelling and binding of microgels onto SPR chip. SPR Biacore2000 and AFM were used to obtain information about SPR response and the number of binding microgels as a function of salt concentration. The highest salt concentration and lowest pH buffer provided the smallest size of microgel. The microgels were densely packed on the chip, keeping their original hydrodynamic size. Therefore, the smallest microgels were bound onto the chip in the largest number. The SPR response was simulated and the result had consistent correlation with experimental SPR response. The number of binding microgels was the dominant factor determining the SPR response.

References

[1] Okay, O.; Sariisik, B. S. *Eur Polym J* **2000**, *36*, 393.

[2] Okay, O.; Durmaz, S. Polymer 2002, 43, 1215.

[3] Tanaka, T. In Polyelectrolyte Gels; Harland, R. S.; Prud'homme, R. K., Eds.; ACS Symposium Series 480; American Chemical Society, Washington, DC, **1992**, p1.

[4] Siegel, R. A.; Falamarzian, M.; Firestone, B. A.; Moxley, B. C. *J. Controlled Release* **1988**, *8*, 179.

[5] Hoffman, A. S.; Afrassiabi, A.; Dong, L. C. *J. Controlled Release* **1986**, *4*, 213.

[6] Park, T. G.; Hoffman, A. S. *Appl. Biochem. Biotechnol*. **1988**, *19*, 1.

[7] Freitas, F. A.; Cussler, E. L. *Chem. Eng. Sci*. **1987**, *42*, 97.

[8] Hoffman, A.; Afrassiabi, A.; Dong, L *J. Control. Release* **1986**, *4*, 213.

[9] Gehrke, S. H *Adv. Polym. Sci*. **1993**, *110*, 81.

[10] Beltran, S.; Hooper, H. H.; Blanch, H. W.; Prausnitz, J. M. *J. Chem. Phys*. **1990**, *92*, 2061.

[11] Annaka, M.; Motokawa, K *J. Chem. Phys* **2000**, *113*, 5980.

[12] Von Hippel, P. H.; Wong, K. *Science* **1964**, *145*, 577.

[13] Saito, S.; Yukawa M. *Journal of Colloid Interface Science* **1969**, *30*, 211.

[14] Eliassaf, J. *Journal of Applied Polymer Science* **1978**, *22*, 873.

[15] Ataman, M.; Boucher, E. *Journal of Polymer Science Physics* **1982**, *20*, 1585.

[16] Florin, E.; Kjellander, R.; Eriksson, C. *Journal of Chemical Society of Faraday Trans* **1984**, *80*, 2889.

[17] Tanford, C. *The Hydrophobic Effect.* **1980**, New York, Wiley.

[18] Saito, S.; Kitamura, K. *Journal of Colloid Interface Science* **1971,** *35*, 346.

[19] Schild, H. G.; Tirrell, D. A. *Langmuir* **1990**, *6*, 1676.

[20] Park, T. G.; Hoffman A. S. *Macromolecules* **1993**, *26(19)*, 5045.

[21] Hofmeister, F. *Arch Exp Pathol Pharmacol* **1888**, *24*, 247.

[22] Von Hippel, P. H.; Schleich, T. *In structure and stability of Biological Macromolecules* **1969,** New York, Marcel Dekker: Chapter 6.

[23] Melander, W.; Horvath, C. *Archives of biochemistry and biophysics* **1977**, *183*, 200.

[24] Horne, R. A.; Almeida, J. P.; Day, A. F.; Yu, N. T. *Journal of Colloid and Iterface Science* **1971**, *35(1),* 77.

[25] Piculell, L.; Nilsson, S. *Progress in Colloid and Polymer Science* **1990**, *82*, 198.

[26] Salomaki, M.; Tervasmaki, P.; Kankare, J.; Areva, S.; Salomaki, M. *Langmuir* **2004**, *20(9)*, 3679.

[27] Ataman, M. *Colloid and Polymer Science* **1987**, *265,* 19.

[28] Dhara, D.; Chatterji, P. R. *Polymer* **2000**, *41(16),* 6133.

[29] Leontidis, E. *Current Opinion in Colloid and Interface Science* **2002**, *7(1-2)*, 81.

[30] Lee, S. B.; Song S.-C.; Jin, J.-I.; Sohn, Y. S. *Macromolecules* **1999**, *32*, 7820.

[31] Suwa, K.; Yamamoto, K.; Akashi, M.; Takano, K.; Tanaka, N.; Kunugi, S. *Colloid and Polymer Science* **1998**, *276(6)*, 529

[32] Eeckman, F.; Amighi, K.; Moes, A. J. *International Journal of Pharmaceutics* **2001**, *222(2)*, 259.

[33] Freitag, R.; Garret-Flaudy, F. *Langmuir* **2002**, *18(9)*, 3434.

[34] Frank, H. S.; Wen W. –Y. *Discussion of the Faraday Society* **1957**, *23*, 133.

[35] Samoilov, O. Y. *Water and aqueous solutions* **1972** Wiley Interscience, New York.

[36] Inomata, H.; Goto, S.; Otake, K.; Saito, S. *Langmuir* **1992**, *8*, 687.

[37] Elaissaf, J. *J. Appl. Polym. Sci.* **1978**, *22*, 873.

[38] Schild, H.; Tirreli, G. *J. Phys. Chem.* **1990**, *94*, 5154.

[39] Currie, E.; Cohen-Stuart, M.; Borisow, V. *Macromolecules*, **2001**, *34*, 1018.

[40] Nisato, G.; Munch, J. P.; Candau, S. J. *Langmuir* **1999**, *15*, 4236.

[41] Hirotsu, S.; Hirokawa, Y.; Tanaka, T. *Journal of Chemical Physics* **1987**, *87*, 1392.

[42] Otake, K.; Inomata, H.; Konno, M.; Saito, S. *Macromolecules* **1990**, *23(1)*, 283.

[43] Inomata, H.; Goto, S.; Otake, K.; Saito, S. *Langmuir* **1992**, *8*, 687.

[44] Inomata, H.; Goto, S; Saito, S. *Langmuir* **1992**, *8*, 1030.

[45] Park, T. G.; Hoffman, A. S. *Biotechnology Progress* **1994**, *10(1)*, 82.

[46] Pelton, R. H.; Chibante, P. *Colloids Surf.* **1986**, *20*, 247.

[47] Jones, C. D.; Lyon, L. A. *Macromolecules* **2000**, *33*, 8301.

[48] Pelton, R. H. *Adv. Colloid Interface Sci.* **2000**, *85*, 1.

[49] Pelton, R. H.; Chibante, P. *Colloid Surf.* **1986**, *20*, 247.

[50] Tam, K. C.; Wu, X. Y.; Pelton, R. H. *Polym. Commun.* **1992**, *33*, 436.

[51] Barrett, K. E. J. *Dispersion Polymerization in Organic Media*, Wiley, London, **1975**.

[52] Annaka, M.; Motokawa, K. *J. Chem. Phys.* **2000**, *113*, 5980.

[53] Hensen, W. N. *J. Opt. Soc. Am.* **1968**, *58*, 380.

[54] Raether, H. *Surface Plasmon on Smooth and Rough Surface and on Gratings*, Springer-Verlag, Berlin Heidelberg, **1988**, Vol. 111.

[55] Knoll, W. *Annu. Rev. Phys. Chem.* **1998**, *49*, 569.

[56] Homola, J.; Yee, S. S.; Gauglitz, G. *Sens. Actuators, B* **1999**, *54*, 3.

[57] Zhou, S.; Wu, C. *Macromolecules* **1996**, *29*, 4998.

[58] Ekgasit, S.; Yu, F.; Knoll, W. *Langmuir* **2005**, *21*, 4077.

[59] Ekgasit, S.; Thammacharoen, C.; Knoll, W. *Anal. Chem.* **2004**, 76, 561.

[60] Ekgasit, S.; Thammacharoen, Yu, F.; Knoll, W. *Anal. Chem.* **2004,** *76*, 2210.

[61] Porter, M. D.; Bright, T. B.; Allara, D. L. *J. Am. Chem. Soc.* **1987,** *109*, 3559.

CHAPTER 3
Effect of swelling degree on SPR response in standard SPR chip

3.1 Introduction

In the previous Chapter, we reported the effect of swelling and binding behavior of microgels on SPR response by using different SPR sensor chips. We found that the number of microgel is dominant factor for determining the SPR response. In order to investigate only swelling effect, the new design of unchanged number of binding microgels was introduced. Therefore, we have designed the system which can determine only the effect of swelling behavior by keeping unchanged the number of microgels in this Chapter. The increase of temperature in SPR system provided the change of swelling degree of microgel. SPR simulation based on evanescent wave suggested that the change of SPR response was not only caused by the swelling degree of microgel but also caused by the morphology of binding microgels.

Thus we would clarify the contribution of swelling of microgels to SPR response at different pHs and temperatures. The SPR phenomena would be simulated using physicochemical valuables such as evanescent field strength, the number of binding microgels which was constant in this Chapter, and refractive indexes of swollen microgels.

3.2 Equilibrium swelling of hydrogels

Swelling of gels arises from the osmotic affinity between macromolecules and solvent molecules. The capacity of hydrogels to adsorb and retain water is restricted by the crosslink density of the network, which determines its elasticity. The “equilibrium” swelling capacity of a gel is the balance of two opposing forces, namely the osmotic pressure, which swells the gel, and the elastic retraction, which restricts swelling. Flory[1] proposed an analogy between the swelling equilibrium and

the osmotic equilibrium. The original Flory-Huggin's regular solution theory, also known as liquid Lattice Theory, calculates the entropy and enthalpy change required for randomly distributing the polymer molecules on a lattice along with the solvent molecules as shown in the following scheme, Figure 3.1

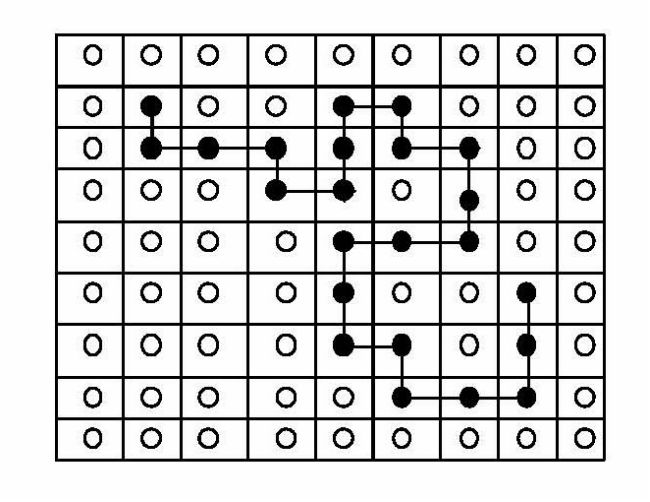

Figure 3.1 Polymer segment distributed along with the solvent in the liquid lattice.

According to his theory the net osmotic pressure (π) acting on the gel is the total force arising from polymer-polymer affinity and rubber elasticity. Thus,

$$\Pi = \mu_1 - \mu_1^0$$

$$= RT\left\{\ln(1-\varphi_2) + \varphi_2 + \chi\varphi_2^2 + V_1\left(\frac{\upsilon_e}{V_0}\right)\left(\varphi_2^{1/3} - \frac{\varphi_2}{2}\right)\right\} \qquad (3.1)$$

Here μ_1 and μ_1^0 are chemical potentials of the solvent within the gel and outside the gel, respectively. φ_2 is the volume fraction of the network, χ is the interaction parameter between the polymer and the solvent, R is the gas constant, T is the absolute temperature, V_1 is the molar volume of the solvent ν_e represents the moles of crosslinks in the network and the term $[\upsilon_e / V_0]$ is the crosslink density of the as-synthesized gel. The first three terms on the right hand side of equation (3.1) arise from the free energy change during mixing of the polymer and the solvent molecules, while the last term arises from the entropic free energy change of classical rubber elasticity assuming Gaussian chains. At equilibrium swelling, the net osmotic pressure should be zero. Hence equation (3.1) becomes

$$-\left\{\ln(1-\varphi_2)+\varphi_2+\chi\varphi_2^2\right\}=\left(\frac{V_1}{\bar{\upsilon}M_c}\right)\left\{1-\frac{2M_c}{M_n}\right\}\left(\varphi_2^{1/3}-\frac{\varphi_2}{2}\right) \qquad (3.2)$$

Here, $\bar{\upsilon}$ is the specific volume of the polymer, M_c is the molecular weight between the crosslinks and M_n the number average molecular weight. The term $\left(1-\frac{2M_c}{M_n}\right)$ is the correction factor of network imperfection resulting from dangling chain and segments.

The swelling equilibrium equation may then be solved for $\varphi_2 = 1/q_m$ with the following result

$$q_m^{5/3}=\left(V_0-\upsilon_e\right)\left(1/2-\chi_1\right)/V_1 \qquad (3.3)$$

or , from (3.2)

$$q_m^{5/3}=\left(\bar{v}M_c\right)\left(1-2M_c/M\right)^{-1}\left(1/2-\chi_1\right)/V_1 \qquad (3.4)$$

Where q, the swelling ration, is given by

$$q=\frac{volume\ of\ \ swollen\ gel}{volume\ of\ \ dry\ gel}=\frac{1}{\varphi_2} \qquad (3.5)$$

Equations (3.2-3.5) show the relationship between the swelling ratio, the crosslink density and the thermodynamic quality of the solvent. The swelling capacity of nonionic gels is limited compared to that of ionic gels. The super swelling of ionic gels is attributed to the long-range electrostatic repulsion between ionic groups that are fixed on the network. The dissociation of the ionic group influences the Donnan equilibrium of mobile counterions between those inside the gel and outside of it. The observed rise in osmotic pressure is dependent on the mobile ion concentration. Tanaka *et al.*[2] modified the Flory-Huggin's formula by including the contribution of H^+ ions dissociated from the ionizable groups. For ionic gels the osmotic pressure ($\prod$) can be written as,

$$\prod=-\frac{NkT}{V_1}\left[\varphi_2+\ln(1-\varphi_2)+\chi{\varphi_2}^2\right]+\upsilon_e kT\left[\frac{\varphi_2}{2\varphi_2}-\left(\frac{\varphi_2}{\varphi_0}\right)^{1/3}\right]+\upsilon_e fkT\left(\frac{\varphi_2}{\varphi_0}\right) \qquad (3.6)$$

Here φ_0 is the polymer volume fraction in the as-synthesized gel, *f* denotes the number of ionizable group per chain incorporated into the network. As the value of *f* increases the swelling ration increases.

In the dilute polymer solution approximation, which may not necessarily be appropriate if the concentration of electrolyte in the external solution is relatively large.

$$q_m^{5/3} = \frac{[(i/2V_u S^{1/2})^2 + (1/2 - \chi_1)/V_1]}{[\upsilon_e / V_0]} \qquad (3.7)$$

3.3 Swelling measurement

Poly(NIPAM) microgels can be prepared with a particle size distribution of narrow dispersity in the submicron size range. Thus, dynamic light scattering (DLS) is a very convenient technique for measuring swelling, and there have been many microgel papers with DLS data. However, swollen particle diameters often approach 1000 nm that is outside the sensitive range for DLS. Furthermore, swelling changes are usually computed as volume changes, so the DLS diameters must be cubed which limits the accuracy of the volumetric data.

The water content in swollen poly(NIPAM) microgels has been determined by combining the results of two light scattering techniques.[3] Static light scattering was used to give a molecular weight of the polymer per particle and dynamic light scattering was used to give the corresponding hydrodynamic volume per particle.

The first published DLS data for poly(NIPAM) microgels as function of temperature and electrolyte concentration were by Pelton et al.[4] Their results indicate that from 10°C to approximately 30°C the diameter decreases linearly by approximately one-quarter whereas from 30 to 35°C the diameter decreases by another quarter in monovalent electrolyte. The Volume Phase Transition Temperature (VPTT) is usually taken as the steepest portion of the diameter vs. temperature curve. In 0.1 M $CaCl_2$ the low temperature swelling was less than in more diluted KCl solution. Furthermore, the VPTT was lower in the presence of 0.1 M $CaCl_2$ – this is consistent with the work of Park and Hoffman[5] who have documented the influence of electrolytes on the VPTT of macrogels. Above 35°C the average diameter in 0.1 M

$CaCl_2$ dramatically increased due to the aggregation of the shrunken poly(NIPAM) microgel particles.

The extent to which a gel can swell is limited by the presence of cross-links usually based on methylenebisacrylamide (BA). McPhee et al.[5] published microgel diameter vs. temperature curves for a series of microgels with varying BA content. As expected, the swelling ratios (i.e., the diameters at 20°C divided by the diameters at 40°C) decreased with increasing BA content. The lowest BA concentration gave the smallest particles at high temperature and thus gave the highest particle concentration during gel synthesis. The swelling data were interpreted by Floy's gel theory.

3.4 Experiments

3.4.1 SPR measurement

All SPR experiments were performed on a Biacore2000 biosensor (BIAcore, Sweden). The dimensions and volume of the cell are (l x w x h = 2.4 x 0.5 x 0.05 mm) and 60 pl., respectively. All experimental data were evaluated by BIAevaluation 3.1.

Each SAM chip was placed in a Biacore2000 first, and then SPR running buffer was run until the system reached the steady state. Secondly, the SAM surface was washed with 5-μl injections of 10 mM NaOH solution twice before the binding process of microgels was started. Thirdly, 50 μl dispersions of 0.4069 wt% Poly(NIPAM-*co*-AAc) microgels were injected and measured at 20°C. And finally, in order to regenerate the surface 100 mM NaOH aqueous solution was injected twice for 1 min at the end of each experiment. Response arising from the microgels attached onto chip was taken as the difference between the SPR signals before and after interaction. Data analysis of sensorgrams was performed using BIAevaluation software.

3.4.2 Binding microgel in standard chip for swelling degree study

The number of microgels on the chip affected the SPR response exclusively in the experiments presented in the previous Chapter. However, the effect of swelling degree was not clearly assessed in such systems. Therefore, in this Chapter, the effect of swelling degree was investigated by using the same chip or standard chip, on which a certain fixed number of microgels were already bound, under different conditions. The standard chip was prepared by modified with amine-terminated SAM at first.

Then, the modified chip was placed into Biacore2000. A dispersion of microgels in citrate buffer was run though the channel of SPR sensor first. This chip was the standard chip which was used solely for all of the experiment hereafter.

The temperature was heated up from 20°C to 40°C stepwise, and the sensorgram was recorded at each temperature. Thus, SPR measurements in citrate buffer from 20°C to 40°C gave us the information to estimate the effect of temperature-dependent swelling of microgels on SPR response without disturbance by the effect of the number of microgels bound onto chip. After the experiments in citrate buffer at different temperatures, the temperature was cooled down to 20°C. Then, the buffer was changed (i.e., using the same chip) from citrate buffer to NaCl aq. and glycine buffer, sequentially and the same procedure was repeated as done in citrate buffer in order to clarify the effect of temperature-dependent swelling of microgel on SPR response in different buffers.

3.5 Results and Discussion

3.5.1 Effect of salt concentration on swelling degree

Water absorbency or degree of swelling of polyelectrolyte gel can be expressed as a function of crosslinking density through Flory's elastic theory of dilute polymer solutions as represented by eq. 3.7. Therefore, q_m is a function of the ionic osmotic pressure, the moles of crosslinking, affinity of the hydrogel with medium, and the ionic strength. The first term in the numerator of eq. 3.7 indicates the electrostatic force favoring the promotion of swelling behavior and the latter term in the numerator presents the free energy between chain network of the polymers and medium. The swelling of ionic gels is attributed to two factors. One is the long-range electrostatic repulsion between ionic groups that are fixed on the network. Another is the Donnan effect, that is, the effect of equilibrium of mobile counterions between those inside and outside of the gels. The increase of the mobile ion inside the gel is responsible for a higher degree of swelling. In the present study, the influence of ionic strength on the degree of swelling was studied by varying the concentration of NaCl from 50 to 200 mM in PBS buffer. The degree of swelling q_m was calculated as the ratio of the volume of the swollen microgel V_{gel} to that of the dry microgel $V_{\mathrm{gel}}^{(\mathrm{dry})}$.

$$q_m = \frac{V_{\mathrm{gel}}}{V_{\mathrm{gel}}^{(\mathrm{dry})}} \tag{3.8}$$

Figure 3.2 shows a linear relationship between degree of swelling$^{5/3}$ ($q^{5/3}$) and reciprocal of ionic strength (S^{-1}). This means that the relationship between degree of swelling and concentration of NaCl (i.e. ionic strength) could be satisfactorily explained by eq. 3.7

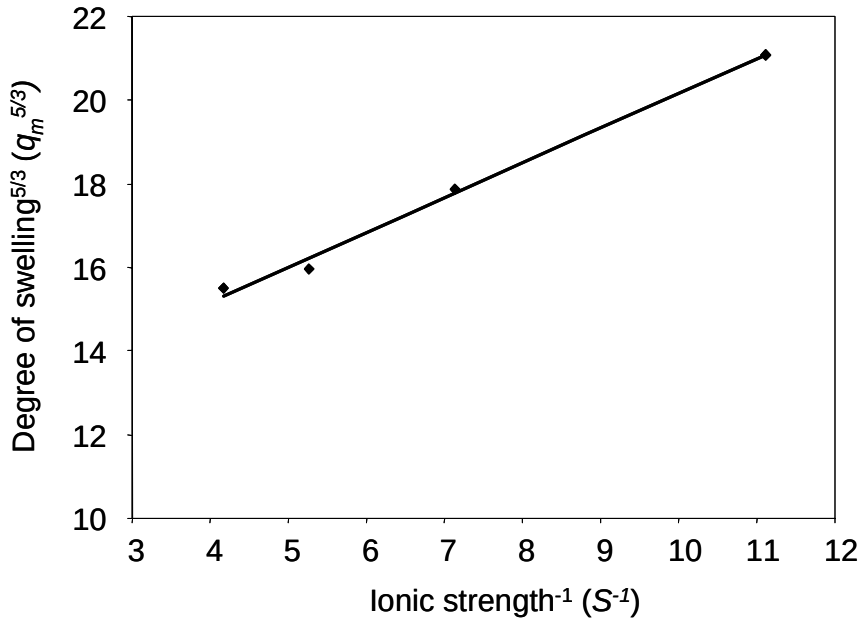

Figure 3.2 Degree of swelling of poly(NIPAM-*co*-AAc) as a function of ionic strength at 20°C.

3.5.2 The effect of swelling degree on SPR response in standard SPR chip system with microgels already bound on it.

The number of microgels on the chip affected the SPR response exclusively in the experiments presented in the previous section. The effect of swelling degree was not clearly assessed in such systems. Therefore, in this section, the effect of swelling degree was investigated by using the same chip, on which a certain fixed number of microgels were already bound, under different conditions. As previously mentioned, we confirmed that the number of binding microgels was unchanged after rinsing the chip surface with regeneration solution, as mentioned in previous Chapter (Figure 2.7). It showed us that the same chip with the fixed number of binding microgels could be used to study the effect of swelling degree on SPR response without any release of microgels at different temperatures and in different buffers. A dispersion of

microgels in citrate buffer was run though the channel of SPR sensor first. This chip was the standard chip which was used solely for all of the experiment hereafter.

The temperature was heated up from 20°C to 40°C stepwise, and the sensorgram was recorded at each temperature. Thus, SPR measurements in citrate buffer from 20°C to 40°C gave us the information to estimate the effect of temperature-dependent swelling of microgels on SPR response without disturbance by the effect of the number of microgels bound onto chip. After the experiments in citrate buffer at different temperatures, the temperature was cooled down to 20°C. Then, the buffer was changed (i.e., using the same chip) from citrate buffer to NaCl aq. and glycine buffer, sequentially and the same procedure was repeated as done in citrate buffer in order to clarify the effect of temperature-dependent swelling of microgel on SPR response in different buffers.

SPR responses with different temperatures and buffers using the single chip are shown in Figure 3.3. The temperature effect on SPR response depended on the kind of buffer solutions. In order to gain insight understandings of this system, the SPR simulation was examined.

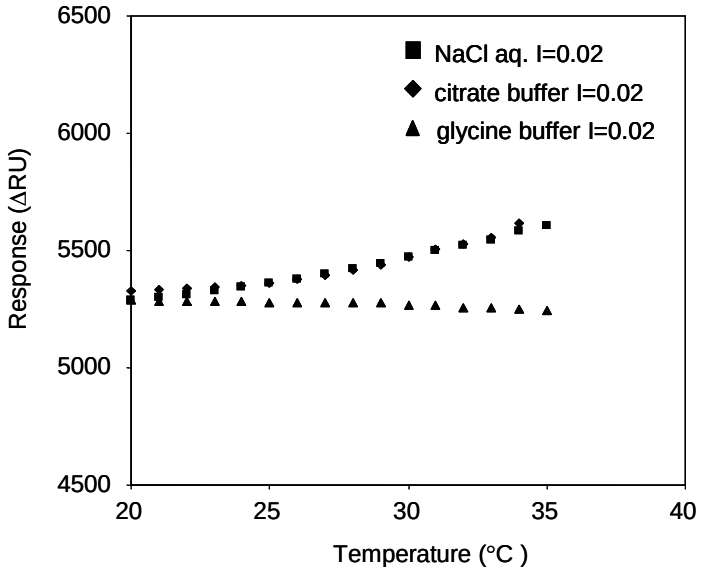

Figure 3.3 Sensorgrams of microgels as a function of temperature in various buffer solutions. 25 μl of analyte was injected with a flow rate of 5 μl/min in SPR running buffer. The same chip was used in all experiments for keeping unchanged number of microgels on the chip surface.

3.5.3 SPR simulation of SPR response of microgel on the standard chip and data processing

In this Chapter, only spherical model cannot be applicable to NaCl aq. and glycine buffer systems because the microgel had a hydrodynamic diameter larger than 139.8 nm in all temperature ranges in these mediums and could not remain unless they deformed on the standard chip. In order to get closely to a real system, flat flim model should be simulated. There are two conformations for binding microgel on the SPR chip (i.e., flat film shape and spherical shape), as shown in Figure 3.4. The detail for simulation in each model (i.e., flat film model and spherical model) will be discussed here.

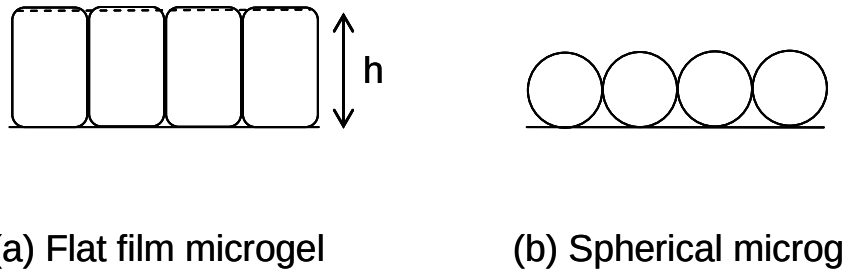

Figure 3.4 Morphology of microgel in different shape (a) Flat film microgel and (b) Spherical microgel

Based on the evanescent wave calculation, we use the change of evanescent wave resulting of binding microgel for calculating SPR response in microgel system. According to the change of evanescent field strength is very sensitive to the refractive index on the top of the metal film, the decay of evanescent field strength is using for calculating the SPR response in microgel system. The strong surface plasmon wave-generated evanescent field is governed by experimental parameters (i.e., angle of incidence and wavelength of the coupled radiation) and material characteristics (i.e., complex refractive indexes of metal film, dielectric substrate and thickness of metal and dielectric films). The magnitude and decay characteristic of the evanescent field are very sensitive to changes in any of the governing parameters. This unique characteristic makes us to use evanescent field for simulating SPR response in microgel system. We assume that there are two possible conformations of binding microgel on the SPR sensor chip surface; these are spherical and flat shape. The

difference in conformation provides the difference in the occupied volume, decay of evanescent field strength, and sensitivity. To calculate the SPR response based on evanescent wave, we have to calculate the SPR angle using Frenel reflection and transmission equation (i.e., via eq. 1.8 in Chapter 1).[6] Then, the SPR angle is used to calculate electric fields for parallel polarization (i.e., via eq. 1.11 in Chapter 1). The mean square electric field (i.e., $\left\langle \mathrm{E}^2 \right\rangle_x$ or $\left\langle \mathrm{E}^2 \right\rangle_{0,x} = \left\langle E_{xz}^2 \right\rangle + \left\langle E_{zz}^2 \right\rangle$) in each medium (i.e., gold, microgel, and buffer solution medium) using for SPR simulation could calculate from eq 1.14. All calculations were done by mathematica 6.0 programming.

The most simple and widely employed experiment set up for excitation of the surface plasmon wave at the metal/dielectric interface is set up according to the Kretschmann-Raether attenuated total reflection (ATR) configuration (Figure 1.2 in Chapter 1). In this configuration, a thin noble metal film (i.e., gold or silver with or without an adhesion promoter, for example, chromium or titanium) is deposited to the surface of a high refractive index (i.e., higher than that of the dielectric medium) prism. A parallel-polarized laser beam of the desired wavelength is coupled to the system from the prism side, and the reflected beam is monitored by a detector. The angle of incidence is varied in order to adjust the momentum of the wavevector of the coupled radiation. The surface plasmon wave at the metal/dielectric interface is excited if the wavevector of the coupled beam matches that of the surface plasmon wave. When the surface plasmon wave is excited, a substantial decrease in reflectance is observed at the surface plasmon resonance angle, θ_{SPR}.

Under the ATR condition, evanescent fields are generated at the prism/metal and metal/dielectric interfaces. The evanescent fields are strongest at the interfaces and exponentially decay as a function of the distance from the interface into the metal film and into the dielectric medium, respectively. The strength and decay characteristic of the evanescent wave function are governed by the experimental parameter (i.e., angle of incidence and wavelength of the coupled radiation) and material characteristics (i.e., complex refractive indexes of metal film, dielectric substrate and thickness of metal and dielectric films). When a dielectric medium changes from microgel layer to buffer solution, a discontinuous decay takes place.

3.5.3.1 Simulation of SPR response of microgel for flat film shape

When a surface of SPR chip is covered with a flat gel film with surface area of *S* and thickness of h, the increment of SPR response caused by the film is expressed in the following equation:

$$SPRt=S\int_0^{\infty}\left[\left\langle E^2\right\rangle_{0,x}-\left\langle E^2\right\rangle_x\right]dx \qquad (3.9)$$

where $\left\langle E^2\right\rangle_{0,x}$ and $\left\langle E^2\right\rangle_x$ are the mean square electric fields at *x* (i.e., the distance from SAM/gel interface) in buffer and swollen gel systems, respectively.

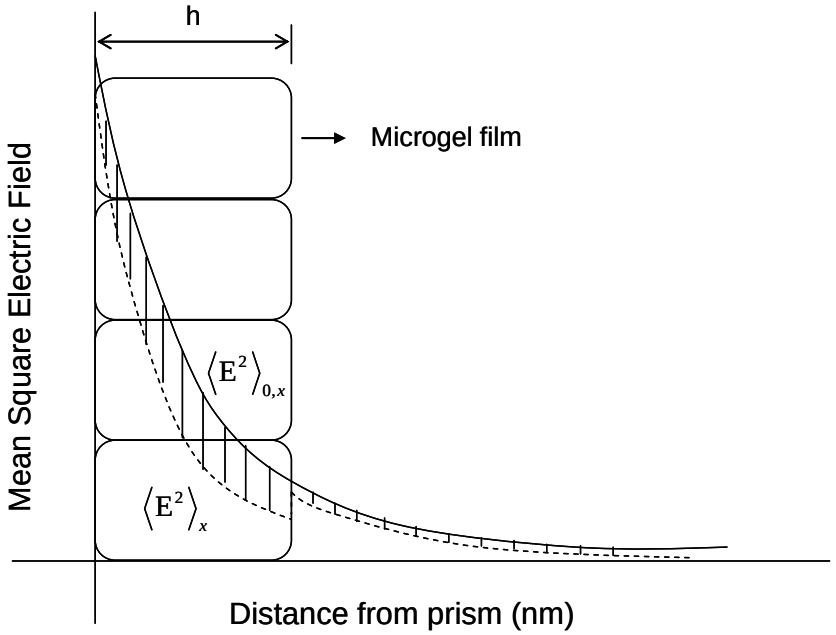

Figure 3.5 Schematic shows the different evanescent wave between passing thought in microgel film ($\left\langle E^2\right\rangle_x$) and buffer solution (without binding microgel, $\left\langle E^2\right\rangle_{0,x}$). The difference area (shadow area) is integrated and used to calculated SPR response based on evanescent wave.

Decay characteristics of mean square electric fields (MSEFs) associated with the parallel-polarized radiation with absence of flat film microgel $\left\langle E^2\right\rangle_{0,x}$ or presence of flat film microgel $\left\langle E^2\right\rangle_x$ show in Figure 3.5. The difference area (i.e., shadow area) of decay due to binding of microgel is using for SPR calculation. The SPR response which corresponds to the change in evanescent wave moduration caused by binding microgel was simulated assuming that evanescent wave entering a microgel goes straight through microgel phase.

When the number of microgels N with a diameter d is deformed to a continuous film, h is expressed in eq. 3.10

$$h = \frac{N \times \pi \times d^3}{6 \times S} \qquad (3.10)$$

3.5.3.2 Simulation of SPR response of microgel for spherical shape

The detail of SPR simulation of spherical shape has been discussed in Chapter 2. In the case of spherical shape, the calculation is different from flat film shape. Since there are two phases contact to SAM surface; these are, microgel and buffer solution, we have to integrate the total evanescent wave in different positions of passing thought, and then use the integrating value to calculate the SPR response.

SPR angle was calculated at first and then used this angle to calculate the electric fields for parallel polarization and mean square electric field (via eq. 1.10 and 1.14 in Chapter 1). The different mean square electric field (A_y) between passing thought microgel ($\langle E^2 \rangle_x$) and buffer solution (without binding microgel $\langle E^2 \rangle_{0,x}$) was calculated by integrating from the prism (x=0) to bulk solution (x=∞) (i.e., $A_y = \int_0^{\infty} \left[\langle E^2 \rangle_{0,x} - \langle E^2 \rangle_x \right] dx$).

According to spherical shape of microgel, there are differences in distribution of electric field in different positions of passing thought (Figure 2.14 in Chapter 2). In the case of spherical shape, we have to calculate mean square electric field in different position of entering into microgel, and then integrate total mean square electric field for whole microgel (i.e., $2\pi \int_0^r A_y y dy$). The integration value is SPR response only for one microgel, but for all microgels on the chip which distributed to the SPR response the integration has to multiply with the number of binding microgel (N) for one SPR chip (eq. 3.11).

$$SPRt = 2\pi N \int_0^r A_y y dy \qquad (3.11)$$

N is the number of binding microgel (particle/μm^2) observed from AFM image.

As a mentioned above, spherical model cannot be applicable to NaCl aq. and glycine buffer systems because the microgel had a hydrodynamic diameter larger than 139.8 nm in all temperature ranges in these mediums and could not remain unless they deformed on the standard chip. A film model shown in Figure 3.6 (a) was used for simulation in both of NaCl aq. and glycine buffer in which the spherical microgels were supposed to deform totally to a kind of gel film. To get closely to a real system, the SPR equation (i.e., eq. 3.9) for flat film model will be used.

When a surface of SPR chip is covered with a flat gel film with a surface area of S and thickness of h, the increment of SPR response caused by the film is expressed in eq 3.9[7-8]

When the number of microgels N with a diameter d is deformed to a continuous film, h is expressed in eq. 3.10. The profile of SPR of deformed gel had a discontinuity at h as shown in Figure 3.6 (a). Judging from the temperature dependence of hydrodynamic size, h decreased with temperature in NaCl aq., but unchanged in glycine buffer as schematically presented in Figure 3.7 (b) and (c), respectively. It means that refractive indexes of gel phase gradually increased in NaCl aq. and unchanged in glycine buffer with increasing temperature.

Simulation based on the data in Table 3.1 indicated that the calculated response increased gradually in NaCl aq. but almost unchanged in glycine buffer (Figure 3.8). The increase in SPR response with temperature in NaCl aq. was attributed to the gradual increase in refractive index like as the case of citrate buffer system. The increment of refractive index with temperature for NaCl aq. system was rather smaller than that for citrate buffer system although the increment of response with temperature was almost the same for both of NaCl aq. and citrate buffer. The space nearby the chip surface was filled with gel in gel film model but this was not the case for citrate buffer. More significant contribution of occupation of gel nearby the chip surface to the change of refractive index resulted in efficient increase in SPR response in NaCl aq. system. The h for glycine buffer system did not change with temperature and therefore caused no change in refractive index of gel phase and SPR response.

The center-to-center distance of microgels on the standard chip, which was prepared in citrate buffer at 20°C, was 139.8 nm. Due to decreasing size with increasing temperature in citrate buffer, the adjacent particles became to have some inter-particle spaces between them, keeping original shape (i.e., spherical shape), as

shown with dashed circles in Figure 3.7a. Therefore, the SPR simulation based on spherical model (i.e., eq. 3.11) was applied for simulation in citrate buffer.

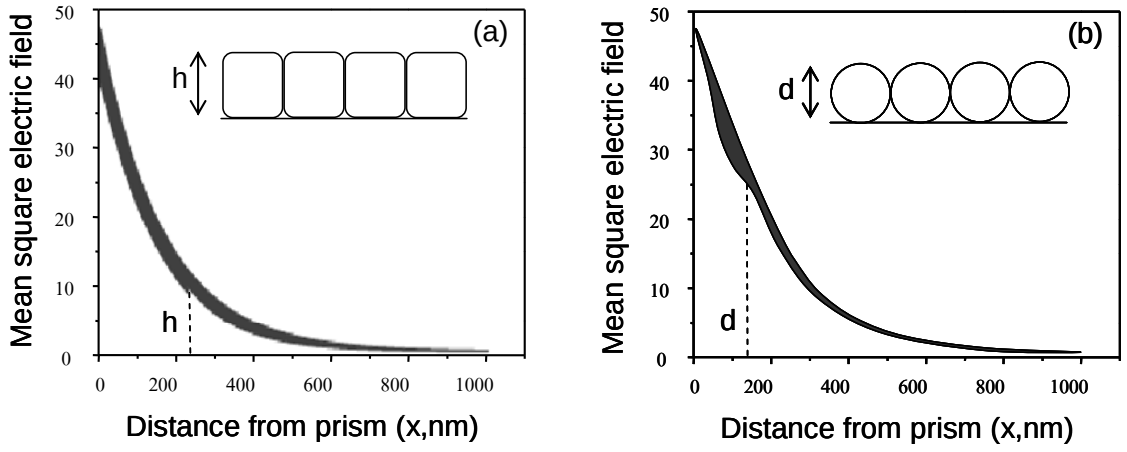

Figure 3.6 Mean square electric fields in buffer solution and microgel system; (a) film and (b) spherical models. The SPR response corresponds to the shadow area in each figure.

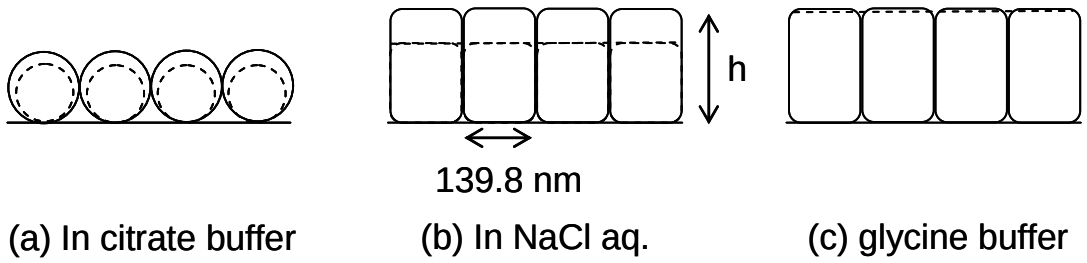

Figure 3.7 Morphology of microgels in different buffers; (a) the spherical microgels on the chip in citrate buffer (b) the gel films on the chip in both of NaCl aq., and (c) glycine buffer. Solid and dashed lines are shapes at 20°C and 40°C, respectively.

Table 3.1 The simulation parameters of SPR responses in Figure 3.7 and 3.8

Citrate buffer[a] pH 3.2

Temperature (°C)	20	25	30	34
HD (nm)	139.8	136.7	122.4	108.3
n_{gel}	1.3988	1.404	1.4326	1.4781
n_{buffer}	1.3298	1.3297	1.3296	1.3295
θ_{SPR}	71.49	71.82	73.94	77.68
SPRt in eq.3	2.03×10^9	2.07×10^9	2.15×10^9	2.23×10^9
Cal. (ΔRU)	5327.1	5432.1	5642.0	5878.2
Exp. (ΔRU)	5327.1	5363.4	5472.1	5616.8

NaCl aq[b] pH 5.7

Temperature (°C)	20	25	30	35
HD (nm)	190.2	184.0	177.3	172.2
h	291.8	264.2	236.4	216.7
n_{gel}	1.3572	1.3599	1.3634	1.3664
n_{buffer}	1.3298	1.3297	1.3296	1.3295
θ_{SPR}	69.01	69.20	69.41	69.58
SPRt in eq.4	1.00×10^9	1.02×10^9	1.07×10^9	1.11×10^9
Cal. (ΔRU)	5291.6	5388.1	5615.7	5807.9
Exp. (ΔRU)	5291.6	5359.9	5471.0	5607.7

Glycine buffer[b] pH 9.5

Temperature (°C)	20	25	30	35
HD (nm)	197.40	197.00	196.60	196.08
h	326.23	324.25	322.28	319.73
n_{gel}	1.3543	1.3544	1.3544	1.3545
n_{buffer}	1.3298	1.3297	1.3296	1.3295
θ_{SPR}	68.799	68.800	68.802	68.807
SPRt in eq.4	9.33×10^8	9.30×10^8	9.28×10^8	9.20×10^8
Cal. (ΔRU)	5286.5	5268.9	5259.8	5212.3
Exp. (ΔRU)	5286.5	5280.3	5268.9	5246.7

[a] The simulation in each temperature based on spherical model following eq. 3.11

[b] The simulation in each temperature based on film model following eq. 3.9

Simulation was done using the data in the top column of Table 3.1 and the result is shown in Figure. 3.6(b) for response per microgel and Figure 3.8 with diamond plots for calculated SPR. The values obtained from eq. 3.11 were revised by multiplying an adjusting factor to make the value (calculated SPR response) the same with experimental SPR. Temperature dependence of simulated SPR in citrate in Figure. 3.8 was very similar to that of experimental one in Figure. 3.3 The gradual increase in SPR response with temperature is attributed mainly to the increase in

refractive index of swollen microgel (n_{gel}). It was reported that the electric strength at SAM/microgel interface is inversely proportional to the refractive index in a layer near to the interface.[7-11]

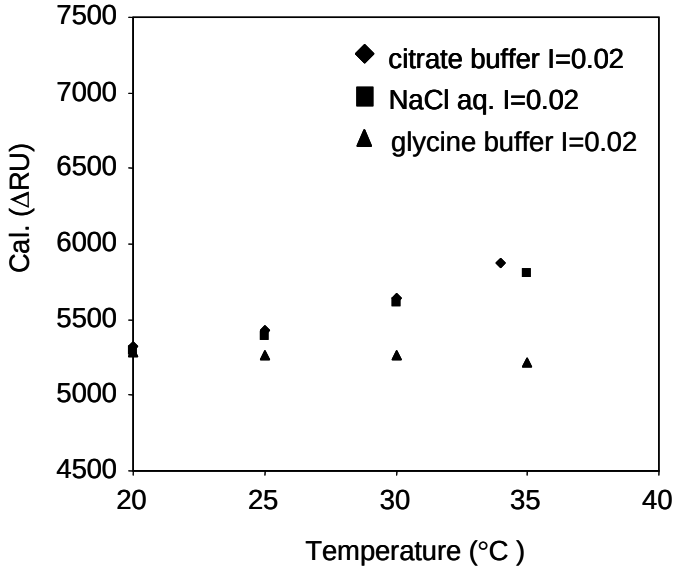

Figure 3.8 Simulation of SPR response of microgels as a function of temperature in various buffer solutions.

3.6 Conclusions

A series of buffer solutions with the different ionic strengths were used to study an effect of salt concentration on the swelling ratio. Swelling behavior affected by salt concentration could be explained Flory-Huggin's theory. SPR Biacore2000 biosensor was used to obtain information about swelling degree by varying temperature and fixing the same number of binding microgel. The low pH provided the small size of microgel and the largest number of binding microgels. Our simulation revealed that SPR response was governed by the refractive index of swollen gel and the space occupied by gel.

References

[1] Flory, P. J. *Principles of Polymer Chemistry, Cornell Unversity Press, Ithaka.* **1953**.

[2] Tanaka, T.; Fillmore, D.; Sun, S-T; Nishio, I.; Swislow, G.; Shah, A. *Phys. Rev. Lett.* **1980**, *45*, 1636.

[3] Wu, C.; Zhou, S.; Au-Yeung, S. C. F.; Jiang, S.; Makro, D. A. *Chemie* **1996**, *240*, 123.

[4] Pelton, R. H.; Pelton, H. M.; Morphesis, A.; Rowell, R. L. *Langmuir* **1989**, *5*, 816.

[5] McPhee, W.; Tam, K. C.; Pelton, R. *J. Colloid Interface Sci.* **1993**, *156(1)*, 24.

[6] Hansen, W. N. *J. Opt. Soc. Am.***1968**, *58*, 380.

[7] Jeenanong, A.; Kawaguchi, H. *Colloid Surf. A: Physicochem. Eng. Asp.* **2007**, *302*, 403.

[8] Jeenanong, A.; Kawaguchi, H. *Colloid Surf. A: Physicochem. Eng. Asp*. In press.

[9] Ekgasit, S.; Thammacharoen, C.; Knoll, W. *Anal. Chem.* **2004**, *76*, 561.

[10] Ekgasit, S.; Thammacharoen, C.; Yu, F.; Knoll, W. *Anal. Chem.* **2004**, *76*, 2210.

[11] Ekagsit, S.; Yu, F.; Knoll, W. *Langmuir* **2005,** *21*, 4077.

Chapter 4
Protein Adsorption to 2D-arrayed microgels on SPR chip

4.1 Introduction

Poly(*N*-isopropylacrlyamide) (poly(NIPAM)) gel is one of the most attractive polymer materials in the last two decades. Since poly(NIPAM) gel changes its volume in water, at 32°C, which is close to room temperature or body temperature, efforts have been made to utilize this character especially in the biomedical and biotechnologyical fields. Our group[1-3] found that the poly(NIPAM) favored the adsorption of protein when the thermosensitive surface of microgel become hydrophobic above the lower critical solution temperature (LCST). During the last decade, the measurement of surface binding equilibrium and kinetics has become a very popular approach for the study of protein interactions.[4-8] There are many publications on protein adsorption onto polymer surface[9-11]; however, there have been no research reports on kinetic adsorption of protein onto temperature- and pH-sensitive microgel surface

As mentioned in the Chapters 2 and 3, we found the microgel could be bound onto SAM surface strongly. We would design two-dimensional (2D) arrayed microgel to study protein adsorption onto stimuli-responsive surface. Since SPR allows the direct visualization of these macromolecular interactions in real-time, the data contain information on the rate and equilibrium binding constants that describe the interaction being investigated. Microgels composed of poly(*N*-isopropylacrylamide-*co*-acrylic acid) with different acrylic acid contents were prepared. The dispersion of microgels with higher AAc content exhibited affinity with human immunoglobulin G (IgG). 2D arrayed microgel was prepared and IgG adsorption on the array was compared with above mentioned adsorption in dispersion of microgels. Surface plasmon resonance (SPR) was used to investigate the kinetic parameters of protein binding onto 2D-

arrayed microgels. The association and dissociation rate constants at various pHs were obtained.

4.2 Biomolecular Interaction analysis with SPR

The surface plasmon resonance detection principle allows detection of refractive index changes close to the sensor surface in real time. If these refractive index changes are caused due to binding of a molecule species in solution to a molecule species immobilized onto the sensing surface, real time monitoring of this process allows deduction of chemical rate and affinity constants of the interaction. The investigation of highly specific interaction between a biomolecule and its biological counterpart is called 'Biomolecular Interaction Analysis' (BIA). The method itself is named 'affinity biosensing' and the sensors are 'affinity sensors'.[12] In typical experiments, one of the interacting species is covalently attached to the sensor surface, giving the biosensor the biospecificity. That member of the specific binding pair is known as the 'ligand', or, often, more intuitively called the 'receptor', although this term is originally used only for acceptor molecules on a cell surface. The 'analyte' is injected onto the surface and the binding is recorded with respect to time. This is known as the association phase. In the dissociation phase, the analyte solution is replaced by buffer solution and the loss of bound analyte from the surface is monitored.[13]

The signals versus time plots are evaluated by application of a mathematical model to the curves; Langmuir adsorption isotherms are often suitable for the description of biomolecular interaction measurements. Deviations from the Langmuir model can be caused by the failure of the interacting system to be adequately described by a single unified binding step (e.g., the system exhibiting a conformational changes after forming the complex with altered dissociation constant; two slightly different species of receptors are present with different rate constants, so called surface heterogeneity),[14] mass transport phenomena in the flow chamber[15] and probably by employment of a hydrogel matrix used for receptor immobilization.[16-18] These effects can be modeled by more complex mathematical models [14,19] but the application needs to be reviewed and should only be taken into consideration if the nature of the participating binding partners or the experimental procedure itself definitely requires the use of a more complex model. Since complex

models almost always describe interaction measurements better than a simpler model -in terms of reduced sum of squared residuals between measurement and fit curve- it appears tempting to employ these models. However, the deduced rate and affinity constants are not necessarily closer to the true values. This is determined by application of the right model[20] and importantly by proper experimental design and execution[19,21] Ultimately, the prerequisites for Langmuir-like adsorption behaviors are often fulfilled in biomolecular interaction experiments and thus the Langmuir isotherm is often the appropriate model for mathematical description of the measurements.

SPR biosensors are the most widely employed, where SPR, as a surface-oriented method, allow real-time analysis of biospecific interactions without the use of labeled biomolecules. The SPR biosensor technology has been commercialized and has become a central tool for characterizing and quantifying biomolecular interactions. Since the first demonstration, in 1983, of the viability of SPR bionsensing[22] , SPR detection of biospecific interactions as developed until the appearance, in 1994, of the first analysis methods for surveying biomolecular interactions in real-time.[23] These methods have been improved for the study of kinetic and thermodynamic constants of those interactions. Generally, SPR biosensing relies on the immobilization of the biological receptor at the chemically modified gold surface, which is in contact with a buffer solution.[24] Upon addition of a specific ligand to the solution, binding occurs close to the gold surface, allowing for SPR detection due to mass increase, and consequent change in the refractive index in this region.[25] The shift in the resonance angle acts as a mass detector and the continuous angular interrogation in the SPR-sensing device allow for the real-time monitoring of binding, provide kinetic data on the biospecific interaction. Prism-based SPR biosensors using angular interrogation have been employed in studies of antigen-antibody[26-29], protein-protein[30-31] , protein-DNA interactions[32] and epitope mapping.[33-34] Many other biomoleuclar studies are presently among the applications of SPR biosensing, which has become a part of modern analytical methods.

The features of SPR biosensor are:

a. Versatility: SPR sensor platforms can be constructed for detection of any analyte, providing a biomolecular recognition element recognizing the analyte available; analyte does not have to exhibit any special properties such as fluorescence or characteristic adsorption.

b. **No labels required**: binding between the biomolecular recognition element and analyte can be observed directly without the use of radioactive or fluorescent labels because SPR is based on detecting the difference in dielectric constant at the sensor surface.

c. **Speed analysis**: the binding event can be observed in real-time providing potentially rapid response.

However SPR biosensors exhibit two limitations:

a. **Specificity of detection**: specificity is solely based on the ability of biomolecular recognition elements to recognize and capture analyte. Biomolecular recognition elements may exhibit some type of non-specific affinity to non-target molecules. If the non-target molecules are present in a sample at a high concentration, sensor response due to the non-target analyte molecules will disturb the signal which one would like to analyze.

b. **Sensitivity to interfering effects**: similar to other affinity biosensors relying on measurement of dielectric constant changes, SPR biosensor measurement can be compromised by interfering effects which produce refractive index variations. These include non-specific interaction at sensor surfaces. In addition extremely small substances might need a large amount of ligand to capture a lot of targets to increase the response.

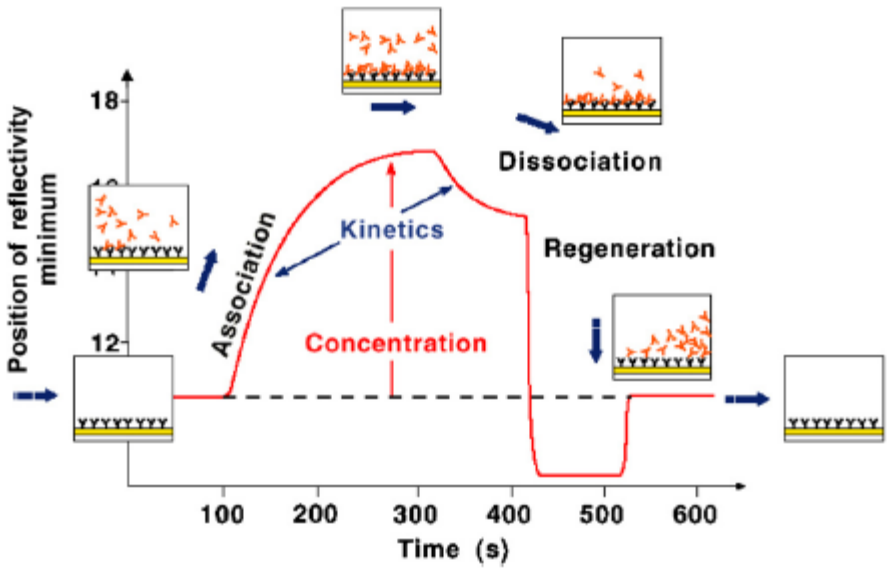

Figure 4.1 Schematic of kinetic analyses of bioaffinity interaction using SPR spectroscopy and a gold surface that is functionalized with biomolecular receptors.

4.3 Biosensing hydrogels for SPR detection

SPR is an evanescent wave technique being sensitive for a distance of some hundred nanometers from the surface. Therefore biomolecular interactions which shall be measured by SPR need to occur close to the surface. This is achieved by immobilizing one interaction partner on the surface and supplying the other in solution. In virtually all studies until the late 1980s, the sensing layer of biological recognition molecules was attached directly to the SPR sensor surface by physical adsorption.[35] The biomolecular interactions studied have been those between immunoglobulin G (IgG) and anti-IgG,[36-37] human serum albumin (HSA) and anti-HSA,[38] bovine serum albumin (BSA) and anti-BSA.[39] However, although the method of physical adsorption fulfils the basic need of immobilization to the sensing surface, it suffers from some severe drawbacks.[40-41]

- The attachment is not stable; the molecules may be removed from the surface or may diffuse along the surface
- There is a tendency of denaturation and loss of function for sensitive biomolecules
- Randomly oriented attachment; recognition sites may face downwards
- The surface is prone to promote nonspecific adsorption of analyte molecules

Later studies have used organic coupling layers between the sensor metal surface and the biomolecule receptors to aid in receptor immobilization and alignment. Morgan and Taylor[42] have immobilized streptavidin on a biotinylated gold film (after treatment with chromic acid the surface of a gold film is biotinylated by immersion in a solution of d-biotin nitrophenyl ester). Biotinylated sex hormone binding globulin antibodies (α-SHBG) were bound to the streptavidin and served as a bio-specific sensing layer for SHBG antigens. The sensor worked efficiently, but the biotinylation of one biomolecule species is mandatory. Häussling *et al*[43]. employed self assembled monolayers (SAM) of alkanethiols on gold. The alkanethiols were functionalized with biotin and the binding of streptavidin to the biotin was studied. It was found that the higher the packing density of the biotin in the SAM was, the less effective, indicated that steric restrictions hamper the binding to a 2D sensing layer. Nevertheless, it was also shown that the coverage of gold with alkanethiol SAMs can passivate the gold surface against nonspecific protein adsorption. Self-assembled monolayers consisting of alkanethiols are suited for the immobilization of almost

every protein, thus the application of the system biotin-streptavidin is not obligatory.[44] The most versatile strategy for covalent immobilization of proteins employs carboxylate-terminated SAMs. Addition of 1-ethyl-3-(3-dimethylaminopropyl) carbodiimide (EDC) and N-hydroxysuccinimide (NHS) to the SAM results in the formation of NHS esters. Lysines of proteins react with the ester and form an amide bond.[45] However, this approach still suffers from the random orientation of the immobilised molecules. For instance, Wadu-Mesthridge *et al.*[46] have proven with atomic force microscopy (AFM) that IgG binds to a SAM in various orientations. Only 30% of the immobilized IgG molecules were able to interact specifically with their biological counterpart.

In view of these shortcomings the application of hydrogels for biosensing purposes is favorable for many reasons. A hydrogel is a polymeric material which swells in water and retains a significant fraction of water within its structure (e.g. a lightly cross-linked derivative of poly(acrylic acid) can absorb approximately a hundred fold water compared to its own mass,[47] but which will not dissolve in water. Hydrogel materials resemble, in their physical properties, living tissue more than any other class of synthetic biomaterial. In particular, their relatively high water contents and their soft, rubbery consistency give them a resemblance to living soft tissue.[48] Often, for biosensing and specifically for SPR applications hydrogels are employed in crosslinked form; dissolution is only prevented by the covalent attachment to the substrate. Depending on the structure of the polymer, the single polymer chains can be fixed to the surface either by a certain fraction of reactive groups along the chain or by their terminal group. The hydrogel is strongly swollen in aqueous media -often buffers for biosensing purposes- and thus provides binding sites for biomolecule immobilization in a three-dimensional arrangement. The mixture of loosely packed polymer chains and buffer solution provides a solution-like environment preventing proteins from denaturation. The 3D attachment of biomolecules leads to higher sensitivity and dynamic range of the SPR biosensor because the receptor density per sensor surface area is larger compared to a flat surface.[49] Additionally, the extended hydrogel matrix allows more efficient exploitation of the evanescent SPR field. Since analyte molecules can diffuse into the polymer matrix, the actual orientation of the receptor molecules is less relevant compared to flat sensor surfaces.

However, this issue also highlights a disadvantage of hydrogels: when main interest is in kinetic data, long diffusion pathways in the 3D matrix may lead to an

undesirable deceleration of receptor-analyte complexation, especially in case fast kinetics are analysed.[50] Moreover, rebinding effects can affect the apparent dissociation constant in a kinetic measurement.[51]

Nevertheless, the outstanding advantages of hydrogels are convincing, therefore that the BIAcore SPR biosensor was already equipped with a dextran hydrogel functionalized sensor surface at it's launch in 1990.

4.4 Experiments

4.4.1 Synthesis of poly(NIPAM-*co*-AAc) microgel particles having different acrylic acid contents

Preparation of poly(*N*-isopropylacrylamide-*co*-acrylic acid) microgels was described in Chapter 2 and the recipe was shown in Table 4.1

4.4.2 Characterization of microgel and chip surface

After polymerization, all prepared microgels were refined by dialysis followed by repetitive centrifugation-decantation-redispersion and finally dispersed in each pH solution. Hydrodynamic diameters of particles were determined by dynamic light scattering (DLS) using a laser particles analyzer system (PAR-III, Otsuka Electronic Co.). The size and shape of dried particles were characterized by field emission transmission electron microscopy (TECNAI F20, Philips Electron Optics Co.).

4.4.3 Determination of protein loading of microgels.

The total protein loading on the microgel in dispersions were examined by BCA (Bicinchoninic Acid) analysis. Briefly, an amount of microparticles 5 mg was redispersed in 500 ul of 100 ppm IgG. The proteins were dissolved in buffer with different pHs at ionic strength 0.005. The mixtures were incubated at each fixed temperature (i.e., 20°C and 40°C) for a given time (1h). All mixtures were centrifuged to separate polymer particles from the supernatants after the adsorption process. The adsorbed amount of IgG adsorption was determined from the difference between the initial and the final concentration of IgG in the supernatant. The IgG concentration in supernatant was measured using BCA protein assay.

4.4.4 Protein adsorption behavior onto microgel surface

Real-time kinetic interaction between IgG and microgel surface was analyzed using SPR Biacore2000. SIA kit Au glasses were cleaned with piranha solution (H_2O_2/H_2SO_4 = 1:3 by volume) and thoroughly rinsed with Milli-Q water and ethanol sequentially. The Au sensor chip was covered with amine-terminated self-assembled monolayer (SAM). SPR biacore 2000 was used to prepare microgel monolayer surface. Each 0.05% wt/wt of microgel dispersion at pH 3 was injected into SPR system. IgG (0.1mg/ml, pH 3) was injected onto microgel surface at 20°C. The flow rate of microgel dispersion and protein solution was 5 μl/s. To regenerate microgel surface, 100 mM NaOH aqueous solution were injected twice at the end of each protein adsorption, and then another buffer and protein (i.e., pH 5, 7, and 9, respectively) were injected and done the same procedure at pH 3.

Association and dissociation rate constants were determined by nonlinear fitting of individual sensorgram data using the BIA evaluation 3.1 software (Pharmacia Biotech, Uppsala, Sweden). The model fits the association phase of a 1:1 interaction (Langmuir) to the integrated rate equation: $R = (k_aCR_{max}[1\text{-}e\text{-}(k_aC + k_d)t])/(k_aC + k_d)$, where R is the SPR signal in RU at time t and C is the concentration of the analyte and R_{max} is the maximum analyte binding capacity in RU.[52] More details of kinetic equilibrium have shown in Appendix.

4.4.5 Fabrication of microgel array for SPR imaging

The microgel array was fabricated by the following procedure. In step 1, Au-coated chip (Toyobo) was immersed into 50 mM ethanolic solution of 11-amino-1-undecanethiol hydrochloride for 24h at room temperature to create a thiol surface. The obtained thiol-modified surface was rinsed with ethanol and Mili-Q water. In step 2, this surface was manually spotted by microgel dispersion with different AAc content and kept for 24h at room temperature.

4.4.6 Imaging experiments

The fabricated microgel array was placed in the SPR imaging instrument (Toyobo). For surface preparation, 10 mM NaOH was injected into the SPR instrument three times for 1 min before experiments. The SPR running buffer and the sample in the same buffer were applied to the sensor chip surface at a flow rate of 100

μl/min at 25°C. The SPR image and signal data were obtained with the MultiSPR inter Analysis Program (Toyobo). The SPR difference images and the line profile were constructed by Scion Image (Scion).

The morphology of microgel monolayer before and after binding of protein was observed by atomic force microscopy (AFM) in contact mode with a SPR300/SPI3700 (SII Nano-Technology Inc.).

4.5 Results and Discussion

4.5.1 Characterization of microgel particles

The TEM micrograph of the purified microgel is depicted in Figure. 4.2 showing that particles were monodisperse and displayed smooth spherical shape (under dehydration state). The particle sizes measured by dynamic light scattering (DLS) and by electron microscopy are showed in Table I. The size of microgels increased with increasing acrylic acid content. The introduced carboxyl groups have a strong effect on the swelling behavior in water of poly(NIPAM-*co*-AAc) hydrogels.[53]

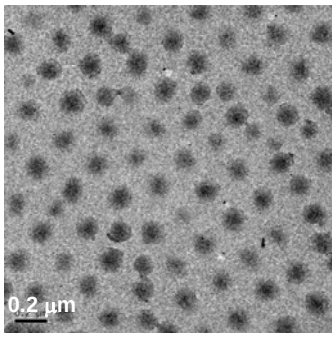

Figure 4.2 TEM of poly(NIPAM-*co*-AAc) microgel particles. The content of AAc is 5wt.% with presence of SDS.

4.5.2 Effect of environmental temperature and pH on adsorption of IgG protein onto poly(NIPAM-*co*-AAc) microgel in dispersion state

Since the prepared microgels contained NIPAM segments, it is expected that the suspensions respond to temperature. In Figure. 4.3, the amount of IgG adsorbed onto microgel particles at different pHs and temperatures is shown. First, we noticed

that there is a difference in IgG adsorption between 20°C and 40°C for poly(NIPAM) (N). Basically, the binding amount of IgG increased by elevating temperature from 20°C to 40°C for all the cases. The adsorption amount at 40°C was two times as much as that at 20°C for pH 5 and pH 7. This is because poly(NIPAM) becomes more hydrophobic as temperature is higher than LCST. Therefore, the hydrophobic interaction leads to the higher binding amount of IgG. There is no different adsorption at pH 9 due to electrostatic repulsion effect caused by the same negatively charged in both of particles and IgG molecules. However, with the AAc content increasing in the microgels, the effect of the temperature on the loaded amount of IgG becomes weak. This means that the adsorption of IgG to the poly(NIPAM-*co*-AAc) microgels is mainly governed by the electrostatic interaction and hydrogen bonding at the condition. In result, there was little effect of temperature on the IgG binding to the microgels with AAc segments. The difference in size between 20°C and 40°C becomes less with increasing AAc content (see Table 4.1).

Table 4.1 Feed amount of monomers used in the microgel preparation and diameter of obtained particles

Sample no.	Monomer feeds				Hydrodynamic Diameter (nm) in water		Diameter of dry particle (nm)
	NIPAM (g)	AAc (g)	BIS (g)	C_{AAc}(%wt)	20°C	40°C	
N	1.44	-	0.17	0	150.2	-	117.0
NA5	1.44	0.072	0.17	5	196.7	163.5	150.3
NA10	1.44	0.144	0.17	10	245.3	223.1	218.7
NA15	1.44	0.216	0.17	15	315.1	295.3	287.2

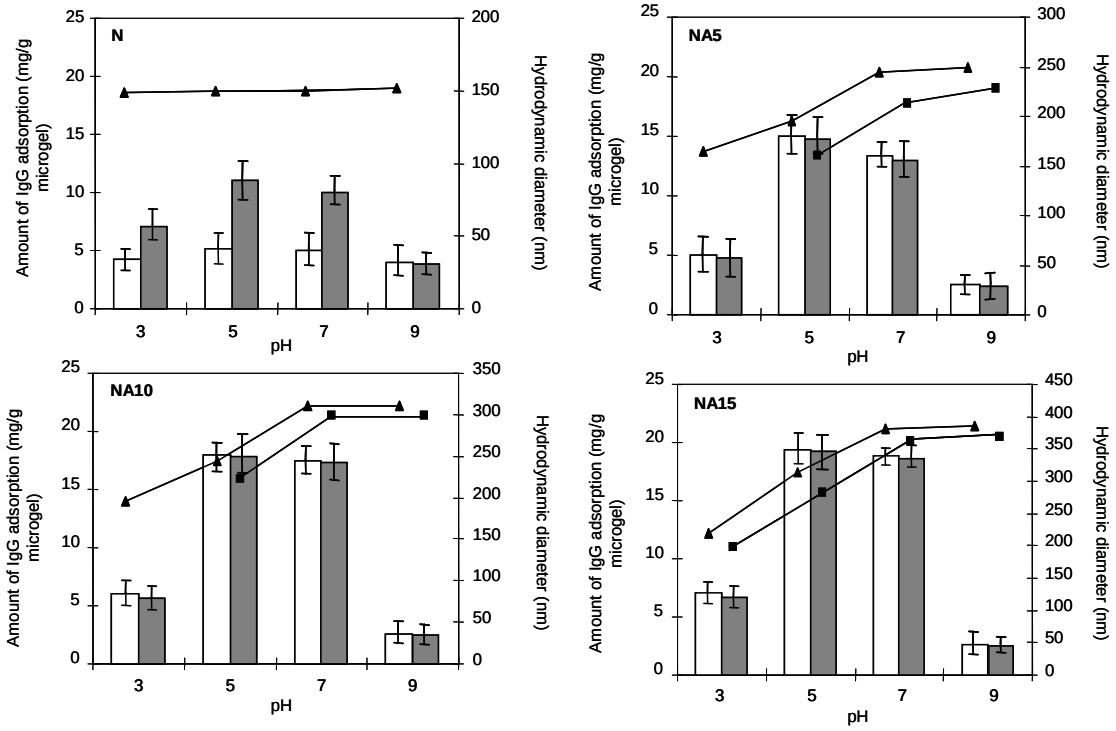

Figure 4.3 Amounts of IgG adsorption onto poly(NIPAM-*co*-AAc) microgel in dispersions at temperature of 20°C (□) and 40°C (■) at various pHs. Initial concentration of IgG was 0.1 mg/ml. The values are the mean of three experiments; error bars indicate the standard deviation. Hydrodynamic sizes presented with plots and lines.

4.5.3 Protein adsorption onto 2D-arrayed microgels

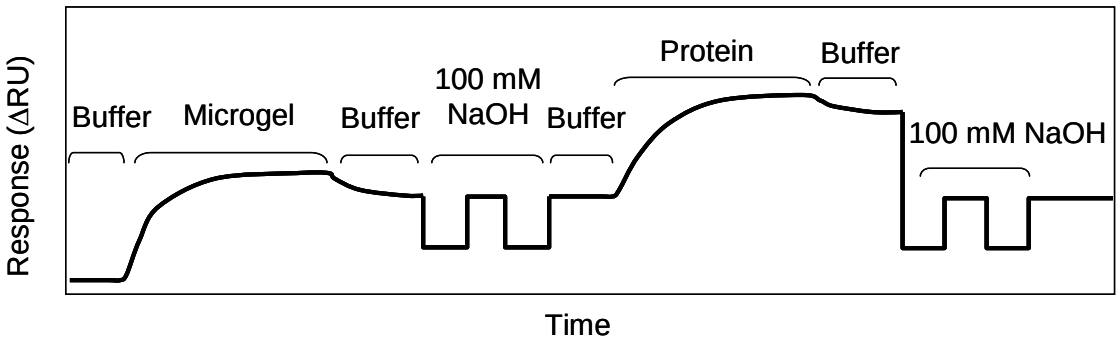

Figure 4.4 Schematic illustration of protein adsorption onto 2D-arrayed microgel surface

A series of the microgels contained different AAc contents were used for study of protein adsorption. 2D-arrayed microgel surface was prepared by injection of dispersed microgel.[54-55] The SPR sensor chip modified with SAM was mounted as part of a flow cell. First, SAM surface was washed with buffer pH 3. Second, the

microgel dispersion was injected into flow cell. The microgels were bound onto surface, and those which did not bind directly onto SAM surface were removed with regeneration solution (i.e., 100mM NaOH). Finally, the protein was injected into flow cell and then bound onto microgel array. The 2D-arrayed microgel surface was regenerated using 100 mM NaOH and then similar IgG binding was done with other pH buffers (i.e., pH 5, pH 7, and pH 9, respectively). The morphology of surface before and after binding IgG was confirmed by using AFM (Figure 4.5)

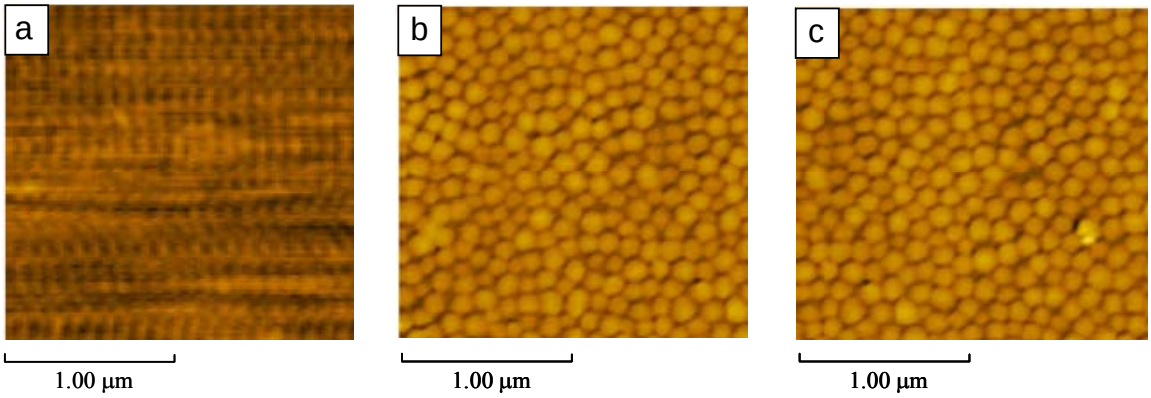

Figure 4.5 AFM images of (a) SAM surface and (b) microgel surface before and (c) after binding IgG.

In order to discuss the influence of the charge of protein on adsorption behavior, the amount of adsorbed IgG onto the poly(NIPAM) surface was studied by using SPR at different pHs. Figure. 4.6 shows SPR response arising from the IgG binding onto the microgel surface (NA5) after exposure to a IgG solution with different pHs. The adsorption of IgG was dependent on the charged state both of the microgel and IgG molecule at each pH. The adsorption was lowest at pH 9 due to the same sign charge between the microgels surface and IgG.

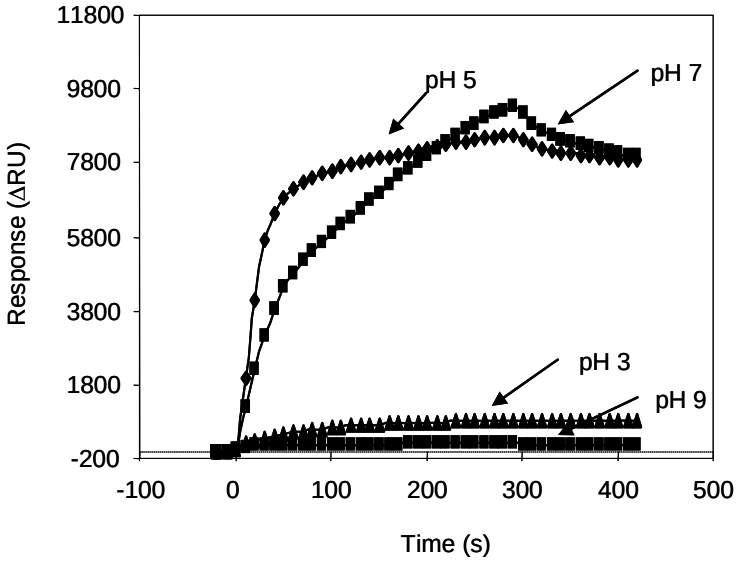

Figure 4.6 Sensorgrams of the IgG adsorptions onto 2D-arrayed poly(NIPAM-*co*-AAc) microgel surface (NA5) in various pH buffers. 25μl of 0.1 mg/ml of IgG solution was injected at 20°C with a flow rate 5μl/min in SPR running buffer.

At pH 3, although there are opposite charged between IgG and microgel surface, the lowest adsorption could obtain. It is due to that the electrostatic repulsion among IgG molecules. The results obtained here indicate that the electrostatic repulsion among IgG molecules is significant factor to decide how the IgG molecules adsorbed at this surface. Both pH 5 and pH 7 gave the same amount of IgG adsorption. However, there was difference in rate of adsorption between pH 5 and pH 7. The details will be discussed in the kinetic section. The adsorption of IgG onto microgel surfaces was studied as a function of pH and temperature, shown in Figure. 4.7 The significant temperature dependence was obtained on poly(NIPAM) surface. The adsorbed amount of IgG increased by raising temperature from 20°C to 40°C for all pH ranges. The thermosensitive behavior of poly(NIPAM) is governed by hydrophilic to hydrophobic character change when temperature rises from values below to above the LCST. Therefore, hydrophobic interactions are likely to have a contribution when the hydrophobic character of the polymer increased at temperature above LCST especially near pI of IgG.[1]

The different responses resulted from differently charged IgG without AAc segment having the same negative charge all pH ranges. The effect of temperature on the IgG adsorption becomes lower with the presence of AAc. It is due to the loss of temperature sensitive property at higher AAc content. The hydrodynamic size of microgel was also used to confirm this point. With the higher AAc content the

difference in size between 20°C and 40°C becomes lower (see Table 4.1). The microgel is possible to be dissociated and lost thermosensitive property even low pH. IgG adsorption increases as the amount of AAc increases. The small IgG adsorption was also observed at pH 3 even the opposite sign charge of microgel and protein. The maximum adsorption was observed at around pH 5.0. At this pH, the charges of microgel surface and IgG molecule are opposite. The electrostatic interaction between microgel surface and IgG molecule resulted in the high adsorption at both pH 5 and pH 7. These results in SPR sensor presented the same tendency to those of the dispersion (BCA analysis). It revealed that protein adsorption onto 2D-arrayed microgels could give us the information about the general adsorption on dispersed particle. Thus, the kinetic study of IgG adsorption onto 2D-microgel surface could also be investigated by using SPR.

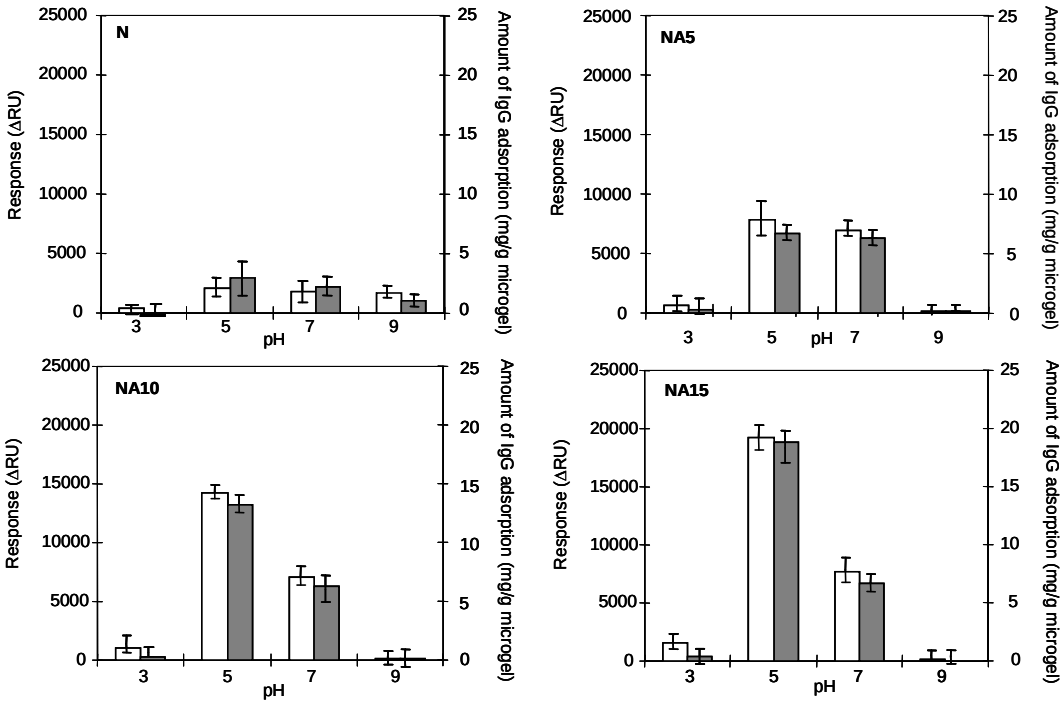

Figure 4.7 Amounts of IgG adsorption onto 2D-arrayed poly(NIPAM-*co*-AAc) microgel at temperature of 20°C (□) and 40°C (■) at various pHs. Initial concentration of IgG was 0.1 mg/ml. The values are the mean of three experiments; error bars indicate the standard deviation.

4.5.4 K Kinetic study of IgG adsorption onto 2D-arrayed microgel for poly(NIPAM-*co*-AAc) containing 5% of acrylic acid contents (NA5)

To investigate the kinetic parameters, IgG concentrations of 20, 40, 80, and 160 nM were examined under a flow rate of 50 μl/min for SPR measurement. As shown in Figure 4.8., different concentrations of the IgG induced different binding responses. The values of the binding rate coefficient k_a and the dissociation rate coefficient k_d were given in Table 4.2

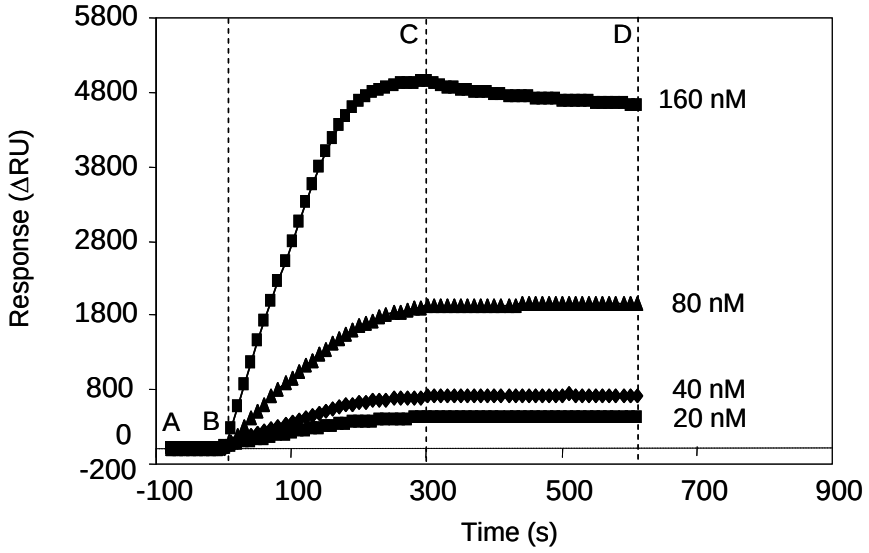

Figure 4.8 Kinetics of IgG adsorption onto microgel surface (NA5). IgG was bound to the 2D-arrayed microgels at pH 5. Real-time binding was measured for IgG at the concentrations indicated. The SPR response gives the amount of surface-bound component at each stage of the reaction, namely (A and B) baseline response; (B and C) association phase; and (C and D) dissociation phase.

Table 4.2 Values of the binding and dissociation rate constants for interaction of IgG and microgel surface (NA5) at various pHs

pH	k_a ($M^{-1}s^{-1}$)	k_d(s^{-1})	K_A(M^{-1})	K_D(M)
3	$(2.37 \pm 0.3) \times 10^4$	$(9.47 \pm 0.5) \times 10^{-5}$	$(2.50 \pm 0.2) \times 10^8$	$(4.00 \pm 0.1) \times 10^{-9}$
5	$(5.04 \pm 0.2) \times 10^4$	$(3.46 \pm 0.3) \times 10^{-4}$	$(1.45 \pm 0.1) \times 10^8$	$(6.88 \pm 0.1) \times 10^{-9}$
7	$(2.38 \pm 0.5) \times 10^4$	$(7.12 \pm 0.4) \times 10^{-4}$	$(3.35 \pm 0.2) \times 10^7$	$(2.99 \pm 0.2) \times 10^{-8}$
9	$(1.78 \pm 0.6) \times 10^4$	$(6.11 \pm 0.5) \times 10^{-4}$	$(2.92 \pm 0.2) \times 10^7$	$(3.43 \pm 0.2) \times 10^{-8}$

As above mentioned, IgG binding onto microgel surface (NA5) gave the highest response in both pH 5 and pH 7. However, there was difference in the binding rate coefficient k_a and the dissociation constant k_d between two pHs. The k_a of pH 5 was 2.1 times larger than the k_a of pH 7. It was due to the less charge of IgG at pH 7, which is near pI of IgG. The electrostatic interaction between IgG and microgel at pH 7 was less than that of pH 5. The affinity constant (K_A) of pH 5 was also higher than that of pH 7. K_A was the highest at pH 3. It was implied that the IgG molecules which can avoid the electrostatic repulsion among themselves strongly adsorbed onto microgel surface. It was due to the strongest positive charge of IgG at pH 3. However, only small amount of IgG molecules could overcome the electrostatic repulsion among themselves and adsorb strongly onto microgel surface. At pH 9, the k_a and K_A were the lowest among those at other pHs, the response of binding was also the lowest. Due to electrostatic repulsion between IgG molecule and microgel surface, the IgG adsorbed onto microgel slowly including weak interaction at pH 9.

4.5.5 SPR imaging of IgG adsorption for poly(NIPAM-*co*-AAc) microgels containing 0%, 5%, 10%, and 15% of acrylic acid contents (N, NA5, NA10, and NA15)

The SPR imaging response was measured for the adsorption of IgG from aqueous buffer solution at pH 5 onto a bare gold-coated substrate. Initially, incident angle was adjusted for clear image. The angle was selected, for all areas of interest, and the reflected light intensity at this angle was monitored simultaneously in real time. Five representative response curves from five areas of the sensing surface are shown in Figure 4.9. After establishing a steady baseline with the carrier buffer (pH 5), IgG solution (1mg/mL) in the exactly same buffer was injected and replaced with the carrier buffer.

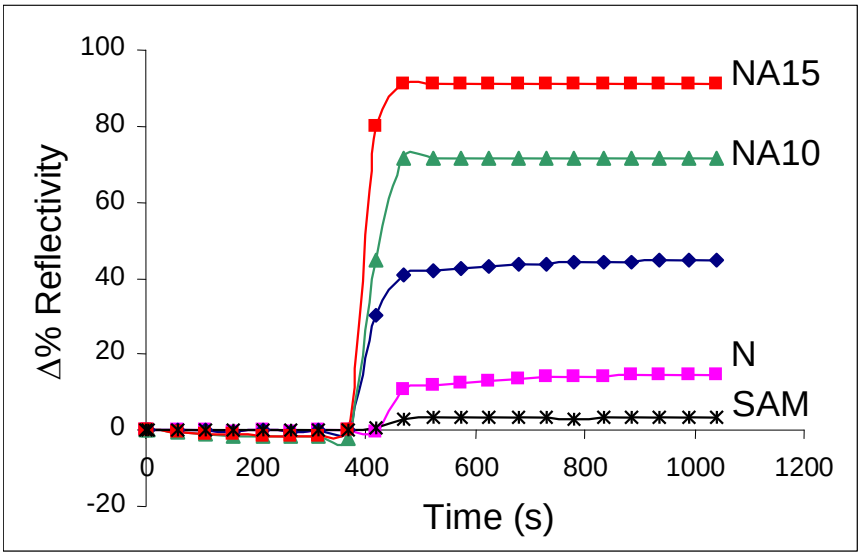

Figure 4.9 Change in percent reflectivity over time as IgG solution and buffer were sequentially injected over a microgel array. Initially, adsorption of IgG on the microgel surface is observed as a continuous flow of IgG solution is introducted to the array. A steady state is reached where the rates of IgG adsorption and desorption are equal. This curve was obtained by averaging the change in percent reflectivity measured at four microgel array elements relative to the SAM background.

Figure 4.10 shows a SPR image of microgel array and simultaneous, real-time events of IgG binding to the array spots. A four-spot microgel array was prepared on a self assembled monolayer (SAM) on a gold-coated substrate. First a microgel array was made by using manual pipette to spot the dispersion of microgel having different acrylic content. Then IgG solution with 1mg/mL was injected into the SPR flow cell. The SPR image evolved rapidly (within 5 min of injection of the IgG) into the SPR image shown in Figure 4.10. The brightening of Figure 4.10a (in four cycles) in the SPR image relative to their starting intensities indicates the presence of additional microgel associated with the surface due to binding IgG in these regions. From the plot profiles shown in Figure 4.9, it can be seen that the signal from the background did not change so much and the contrast between the spots and the background due to the binding IgG was clear, illustrating that only slight nonspecific attachment of IgG to SAM surface occurred. The intensities of brightening increased with increasing AAc content. This result suggested that the binding affinity of IgG increases with increasing AAc content. The average difference in reflected intensity for the spots containing both microgel and IgG, was 18.5, 42, 77, and 96% for N, NA5, NA10, and NA15, respectively.

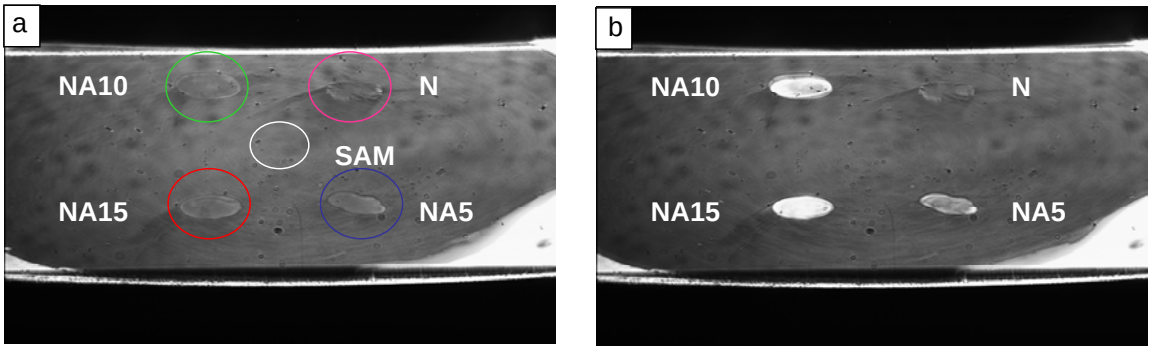

Figure 4.10 The SPR difference image of binding microgel for four-spots having different AAc contents 0%, 5%, 10%, and 15% for N, NA5, NA10, and NA15, respectively (a) and binding IgG on microgel arrays.

4.6 Conclusions

A series of poly(N-isopropylacrylamide-*co*-acrylic acid) with different acrylic acid contents were prepared for IgG adsorption analysis. Two-dimensional (2D) arrayed microgel was prepared and IgG adsorption on the microgel at different pHs and temperatures was investigated using SPR Bicore2000. The pH dependent adsorption was explained by the contribution of electrostatic force. IgG adsorption onto microgel dispersion also measured using BCA protein analysis. The results of SPR analysis after eliminating the influence of chip surface gave the same tendency to those in the dispersion. The kinetic study of IgG adsorption could be studied from SPR. Although the IgG could be adsorbed onto microgels the same amount at pH 5, there was difference in kinetic adsorption. The IgG adsorption at pH 5.0 provided the rate value which was larger than that of pH 7.0. The data from kinetic study represented the essential information for understanding the binding event of IgG onto microgel system. In addition, the adsorption of IgG has been also monitored by using SPR imaging. The different brightening in each spot indicated that the affinity of IgG adsorption increased with increasing AAc contents.

References

[1] Kawaguchi, H.; Fujimoto, K.; Muzuhara, Y. *Colloid Polym. Sci.* **1992**, *270*, 53.

[2] Kawaguchi, H.; Fujimoto, K.; Saito, M.; Kawasaki, T.; Urakami, Y. *Polym. Int.* **1993**, *30*, 225.

[3] Kawaguchi, H. *Prog. Polym. Sci.* **2000**, *25*, 1171.

[4] Fagerstam, L. G.; Frostel, A.; Karlsson, R.; Kullman, M.; Larsson, A.; Malmqvist, M.; Butt, H. *J. Mol. Recognit.* **1990**, *3*, 208.

[5] Schuck, P.; *Annu. Rev. Biophys. Biomol. Struct.* **1997**, *26*, 541.

[6] Rich, R. L.; Myszka, D. G.; *J. Mol. Recognit.* **2001**, *14*, 273.

[7] Cooper, M. A. *Nat. Rev. Drug. Discov.* **2002**, *1*, 515.

[8] Svitel, J.; Balbo, A.; Mariuzza, R. A.; Gonzales, N. R.; Schuck, P. *Biophysical Journal.* **2003,** *84*, 4062.

[9] Zhou, F.; Huck, W. T. S. *Phys. Chem. Chem. Phys.* **2006**, *8*, 3815.

[10] Sonesson, A. W.; Callisen, T. H.; Brismar, H.; Elofsson, U. M. *Colloids and Surfaces B: Biointerfaces.* **2007**, *54*, 236.

[11] Pasche, S.; Voros, J.; Griesser, H. J.; Spencer, N. D.; Textor, M. *J. Phys. Chem. B.* **2005**, *109*, 17545.

[12] Malmqvist, M.; Granzow, R. *Mothods* **1994**, *6(2)*, 95.

[13] Szabo, A.; Stolz, L.; Granzow, R. *Phys. Rev.***1995**, *120(1)*, 130.

[14] Morton, T. A.; Myszka, D. G.; Chaiken, I. M. *Anal. Biochem.* **1995**, *227*, 176.

[15] Christensen, L. L. H. *Anal. Biochem.* **1997**, *249*, 153.

[16] O'Shannessy, K. J.; Winzor, D. J. *Anal. Biochem.* **1996**, *236*, 275.

[17] Schuck, P. *Biophys. J.* **1996**, *70,* 1230.

[18] Witz, J.; *Anal. Biochem.* **1999**, *270,* 201.

[19] Karlsson, R. and Fält, A. *J. Immunol. Methods* **1997**, *200*, 121.

[20] Schuck, P. *Curr. Opin. Biotechnol.* **1997a**, *8*, 498.

[21] Rich, R. L.; Myszka, D. G. *Curr. Opin. Biotechnol.* **2000**, *11*, 54.

[22] Liedberg, B.; Nylander, C.; Lundstrom, K. *Sens. & Actuat*. **1983**, *4*, 299.

[23] "BIAcore Instument Handbook", (Pharmacia Biosensor AB, 1994) Uppsala, Sweden.

[24] Johnsson, B.; Lofas, S.; Lindquist, G. *Anal. Biochem.* **1991**, *198*, 268.

[25] Fagerstam, L. G.; Frostel-Karlsson, A.; Karlsson, R.; Persson, B.; Ronnberg, I. *J.* Chrom. **1992**, *597*, 397.

[26] Altschuh, D.; Dubs, M. C.; Weiss, E.; Zeder-Lutz, G.; Van Regenmortel, M. H. V. *Biochemistry*, **1992**, *31*, 6298.

[27] Lasonder, E.; Bloemhoff, W.; Welling, G. W. *J. Chrom. A*, **1994,** *676*, 91.

[28] Lasonder, E.; Schellekens, G. A.; Koedijk, D. G. A. M.; Damhof, R. A.; Welling-Wester S.; Feijlbrrief, M.; Scheffer, A. J.; Welling, G. W. *Eur. J. Biochem*. **1996**, *240*, 209.

[29] Houshmand, H.; Froman, G.; Magnusson, G. *Anal. Biochem*. **1999**, *268*, 363.

[30] Wu, Z.; Johnson, K.; Choi, Y.; Ciardelli, T. L. *J. Biol. Chem*. **1995**, *270*, 16045.

[31] Lessard, I. A. D.; Fuller, C.; Perham, R. N. *Biochemistry*. **1996**, *35*, 16863.

[32] Cheskis, B.; Freedman, L. P. *Biochemistry*. **1996**, *35*, 3309.

[33] Dubs, M. C.; Altschuh, D.; Van Regenmortel, M. H. V. *J. Chrom*. **1992**, *597*, 391.

[34] Saunal, H.; Van Regenmortel, M. H. V. *J. Immunol. Meth*. **1995**, *183*, 33.

[35] Garland, P. B. *Rev. Biophys.* **1996**, *29*, 91.

[36] Liedberg, B.; Nylander, C.; Lundström, I. *Sens. Actuators*, **1983**, *4*, 299.

[37] Geddes, N. J.; Martin, A. S.; Caruso, F. Urquhart, R. S. Furlong, D. N. Sambles, J. R.; Than, K. A.; Edger, J. A. *J. Immunol. Methods*. **1994**, *175,* 149.

[38] Kooyman, R. P. H.; Kolkman, H.; Van Gent, J.; Greve, J. *Anal. Chim. Acta.* **1988**, *213*, 35.

[39] Mayo, C. S.; Hallock, R. B. *J. Immunol. Methods.* **1989,** *120,* 105.

[40] Löfås, S.; Johnsson, B.; Edström, A.; Hansson, A.; Lindquist, G.; Hilgren, R.-M.; Stigh, L. *Biosens. Bioelectron.* **1995**, *10,* 813.

[41] Garland, P. B. *Q. Rev. Biophys.* **1996**, *29*, 91.

[42] Morgan, H.; Taylor, D. M. *Biosens. Bioelectrons.* **1992**, *7*, 405.

[43] Häussling, L.; Ringsdorf, H.; Schmitt, F.-J.; Knoll, W. *Langmuir* **1991**, *7,* 1837.

[44] Wink, T.; Zuilen, S. J. V.; Bult, A.; Benekom, W. P. V. *The Analyst* **1997**, *122,* 43R.

[45] Patel, N.; Davies, M. C.; Hartshome, M.; Heaton, R. J.; Roberts, C. J.; Tendler, S. J. B.; Williams, P. M. *Langmuir*, **1997**, *13*, 6485.

[46] Wadu-Mesthridge, K.; Amro, N. A.; Liu, G. Y. *Scanning* **2000**, *22*, 380.

[47] Omidian, H.; Hashemi, S. A.; Sammes, P. G.; Meldrum, I. *Polymer* **1999**, *40*, 1753.

[48] Hoffman, A. S.; Horbett, T. A.; Ratner, B. D. *Acad. Sci.* **1977**, *283*, 372.

[49] Granzow, R.; Reed, R. *Bio/Technology* **1992**, *10*, 390.

[50] Schuck, P. *Annu. Rev. Biopmol. Struct.* **1997b**, *26*, 541.

[51] Nieba, L.; Krebber, A.; Plückthun, A. *Anal. Biochem.* **1996**, *234,* 155.

[52] O'Shannessy, D. J.; Burke, M. B.; Soneson, K. K.; Hensley, P.; Brooks, I. *Anal. Biochem.* **1993**, *212*, 457.

[53] Kratz, K.; Hellweg, T.; Eimer, W. *Colloid. Surf. A: Physicochem. Eng. Asp.* **2000**, *170*, 137.

[54] Jeenanong, A.; Kawaguchi, H. *Colloid. Surf. A: Physicochem. Eng. Asp*. **2007**, *302*, 403.

[55] Jeenanong, A.; Kawaguchi, H. *Colloid. Surf. A: Physicochem. Eng. Asp*. In press.

Chapter 5
Concluding Remarks

This dissertation is aimed to understand how Surface Plasmon Resonance (SPR) sensor detects the stimuli-sensitive behavior of microgels. pH- and thermo-sensitive microgel was synthesized, and its behavior was investigated by SPR. The SPR results could give interesting information about stimuli-sensitive behavior under various environmental conditions. SPR simulation based on evanescent field introduced the quantitative expression that described the relationship between SPR response and physicochemical valuables (i.e., refractive index, evanescent field strength, and the number of binding microgels). As achievements of the studies carried out in this thesis, the following important results should be remarked.

Chapter 2 described the influence of ionic strength, pH, and temperature on the binding behavior and SPR response of poly(NIPAM-*co*-AAc) microgels. Anionic thermosenstive microgels, poly(NIPAM-*co*-AAc) microgels, were prepared by aqueous free-radical precipitation copolymerization. The product was monodisperse spheres with diameter less than 200 nm, which was a suitable size for measuring SPR. Series of buffer solutions including different NaCl concentrations (i.e., 50, 100, 150, and 200 mM) and pHs (citrate buffer pH 3.2, NaCl aqueous pH 5.7, glycine buffer pH 9.6) were used to study the stimuli-sensitive behavior and binding of microgels onto SPR chip. SPR Biacore2000 and AFM were used to obtain information about SPR response and the number of binding microgels as a function of pH and salt concentration. The highest salt concentration and low pH provided the smallest size of microgels, which could allow the SPR chip to obtain the largest number of binding microgels. According to our SPR simulation, the number of binding microgels was the dominant factor for determining the SPR response. We also found that the temperature has a significant effect on the SPR response due to swelling degree. At

higher temperature, the smaller microgels provided the larger number of binding and the higher SPR response.

In Chapter 3, we discussed the effect of temperature and pH on the swelling degree of poly(NIPAM-*co*-AAc) microgels by using the same chip (i.e., the chip binding the same number of microgels). In the previous chapter, we have studied the effect of swelling degree and binding behavior of microgels on SPR response by using different SPR sensor chips. Although the number of binding microgels was the dominant factor, the swelling degree of microgels might also have an affect on SPR response. To investigate only the swelling effect, a new design with unchanged number of binding microgels was introduced. We clarified the contribution of swelling degree and morphology of binding microgel to SPR response at different temperatures and pHs. The SPR phenomena would be simulated with different binding shapes of microgels (i.e., flat film microgel and spherical microgel). SPR simulation could explain how the difference in morphology of binding microgel and swelling degree of microgel affect the SPR response by keeping the number of binding microgels constant.

Since the poly(NIPAM-*co*-AAc) microgels could attach strongly onto the SPR sensor chip, we fabricated 2D-arrayed microgel, which is a stimuli-responsive surface, to study the protein adsorption at different pHs and temperatures. A series of poly(*N*-isopropylacrylamide-*co*-AAc) with different acrylic acid contents were prepared for IgG adsorption analysis. The IgG adsorption onto 2D-arrayed microgel was compared to that of the microgel dispersion system. Both systems gave the same tendency in IgG adsorption. The IgG adsorption increased with increasing AAc contents. At different pHs, the IgG adsorption gave high adsorption at pH 5 and 7. However, there was a difference in the rate of adsorption. Since the SPR sensor can observe the binding event in real-time, we used the 2D-arrayed microgel to study the kinetics of adsorption of IgG. The data from kinetic study provided the essential information for understanding about the binding event of IgG onto microgel system. We could image the IgG adsorption at different spots, which have different acrylic acid contents, simultaneously. The different brightening in each spot indicated that the affinity of IgG adsorption increases with increasing AAc contents.

The author hopes that the SPR calculation based on evanescent field theory conducted in this thesis will make a contribution to the future development of SPR detection in both chemical SPR sensor and bio-sensor. Moreover, the 2D-arrayed microgels could be responsive surface. This array should be applied for bio-analytical system in future work.

Appendix

Kinetic and equilibrium theory of SPR sensorgrams

Since the SPR detector is a continuous, real-time detector, the possibility for assessing the kinetics of interaction exits. As noted earlier, the interaction observed is between an immobilized ligand and a soluble ligate.

For the reversible interaction,

$$A + B \underset{k_d}{\overset{k_a}{\longleftrightarrow}} AB \qquad \text{(A-1)}$$

Association rate $$\frac{d[AB]}{dt} = k_a[A][B] \qquad \text{(A-2)}$$

Dissociation rate $$-\frac{d[AB]}{dt} = k_d[AB] \qquad \text{(A-3)}$$

At equilibrium, association and dissociation rates are equal, so

$$k_a[A][B] = k_d[AB] \qquad \text{(A-4)}$$

Which can be rearranged to give

$$\frac{k_d}{k_a} = \frac{[A][B]}{[AB]} = K_D \quad \text{(i.e., the equilibrium dissociation constant)} \qquad \text{(A-5)}$$

or $$\frac{k_a}{k_d} = \frac{[AB]}{[A][B]} = K_A \quad \text{(i.e., the equilibrium association constant)} \qquad \text{(A-6)}$$

The formation of surface complex in the SPR sensor system between the analyte A and the surface bound ligand B can be represented by the scheme

$$A_{bulk} \underset{k_m}{\overset{k_m}{\rightleftharpoons}} A_{surface} + B \underset{k_d}{\overset{k_a}{\rightleftharpoons}} AB \qquad \text{(A-7)}$$

Where k_m is the constant for mass transport to and from the surface (the rate constant for mass transport is the same in both directions) and k_a and k_d are the rate constants for the formation of complex.

The observed rate of complex formation may be written

$$\frac{d[AB]}{dt} = k_f [A_{bulk}][B] - k_r [AB] \qquad \text{(A-8)}$$

Here, k_f and k_r are the effective forward and reverse rate constants respectively, given by

$$k_f = \frac{k_a k_m}{k_a [B] + k_m} = \frac{k_a}{1 + k_a [B]/k_m} \qquad \text{(A-9)}$$

and

$$k_r = \frac{k_d k_m}{k_a [B] + k_m} = \frac{k_d}{1 + k_a [B]/k_m} \qquad \text{(A-10)}$$

Note that both the forward and reverse rate constants show the same dependence on mass transport. This means that a mass transport-controlled association is in principle always followed by a mass transport-controlled dissociation. Mass transport limitations dominate in the early phase of association (when the concentration of free ligand sites is high) and correspondingly in the late phase of dissociation. The observed rate during both association and dissociation is reduced in comparison with the interaction-controlled rate by a factor of $1/(1+k_a[B]/k_m)$, so that "true" (interaction-controlled) kinetics are observed close to zero free ligand concentration. Dissociation kinetics are best measured from the initial phase of dissociation from a surface saturated with analyte.

Note also that mass transport-limitation during dissociation is dependent on the association rate constant for the interaction, not on the dissociation rate constant. Comparative dissociation kinetics under conditions where mass transport limitations dominate can thus be used for affinity ranking in terms of association rate constants.

If the rate is fully mass transport-controlled (i.e., $k_a[B] >> k_m$), the rate equation becomes

$$\frac{d[AB]}{dt} = k_m [A] - \frac{k_m k_d}{k_a [B]} . [AB] \qquad \text{(A-11)}$$

Under these condition, the initial association rate ($[AB] \approx 0$) depends only on the analyte concentration [A]. Since this is maintained at a constant value in real-time BIA, the initial association is linear and the rate can be used as an "affinity independent" measure of analyte concentration.

If the mass transport is much faster than interaction-controlled association ($k_a[B] << k_m) \approx 1$), the analyte at the surface is maintained at the same concentration as in the bulk phase, and the measured forward and backward rate constants approximate to the constants for interaction kinetics. Under these conditions, the rate equation can be written as

$$\frac{d[AB]}{dt} = k_a [A][B] - k_d [AB] \qquad \text{(A-11)}$$

The concentration of unoccupied ligand [B] is the difference between the total amount of ligand on the surface $[B]_0$ and the amount of complex:

$$[B] = [B]_0 - [AB] \qquad \text{(A-12)}$$

Substituting in the rate equation for the formation of AB:

$$\frac{d[AB]}{dt} = k_a [A]\left([B]_0 - [AB]\right) - k_d [AB] \qquad \text{(A-13)}$$

If the total amount of ligand $[B]_0$ is expressed in terms of the maximum analyte binding capacity of the surface, all concentration terms can then be expressed as SPR response in RU, eliminating the need to convert from mass to molar concentration:

$$\frac{d[R]}{dt} = k_a C\left(R_{max} - R\right) - k_d R \qquad \text{(A-14)}$$

Where dR/dt is the rate of change of the SPR signal

C is the concentration of analyte

R_{max} is the maximum analyte binding capacity in RU and R is the SPR signal in RU at time t

This equation may be rearranged to give

$$\frac{d[R]}{dt} = k_a C R_{max} - \left(k_a C + k_d\right) R \qquad \text{(A-15)}$$

Thus a plot of dR/dt against R will theoretically be a straight line with slope $-(k_aC+k_d)$ for interaction-controlled kinetics. The initial binding rate (at R=0) is

directly proportional to the analyte concentration and can be used for concentration measurements.

After the pulse of analyte has passed over the sensor chip surface, the surface-bound complex dissociates in a zero-order reaction. Assuming that re-association of released analyte is negligible (i.e., that mass transport of analyte from the surface is not rate limiting and that released analyte is effectively washed out by the buffer flow):

$$\frac{dR}{dt} = -k_d R \qquad \text{(A-16)}$$

Separating variables and integrating gives

$$R_t = R_0 . e^{-k_d (t-t_0)} \qquad \text{(A-17)}$$

or

$$\ln \frac{R_0}{R_t} = k_d \left(t-t_0 \right) \qquad \text{(A-18)}$$

Where R_t is the response at time t and R_0 is the response at an arbitrary starting time t_0 (not necessarily the beginning of the dissociation phase). Equation (A-17) can be used for non-linear regression analysis of the dissociation phase of a single sensorgram.

From equation (A-17)

$$\frac{dR}{dt} = -k_d R_0 . e^{-k_d (t-t_0)} \qquad \text{(A-19)}$$

or

$$\ln \left(\frac{dR}{dt} \right) = \ln \left(-k_d R_0 \right) - k_d \left(t-t_0 \right) \qquad \text{(A-20)}$$

Plotting $\ln(R_0/R_t)$ or $\ln(dR/dt)$ against $t-t_0$ thus gives a straight line with slope k_d or $-k_d$ respectively. These plots are sometimes referred to simply as “dissociation plots”.

Equilibrium arises when association of analyte with the surface is balanced by dissociation of the surface-bound complex, so that the net rate of complex formation is zero. Since the analyte is continuously added to and removed from the system by a flow, the situation here is a steady state rather than equilibrium according to the strict

definition of the terms. The analysis is the same however, and the more familiar term equilibrium is used throughout this discussion.

At equilibrium the equation will be

$$\frac{dR}{dt} = k_a C\left(R_{max} - R_{eq}\right) - k_d R_{eq} = 0 \qquad \text{(A-21)}$$

$$k_a C\left(R_{max} - R_{eq}\right) = k_d R_{eq} \qquad \text{(A-22)}$$

$$\frac{k_a}{k_d} = K_A = \frac{R_{eq}}{C\left(R_{max} - R_{eq}\right)} \qquad \text{(A-23)}$$

A plot of R_{eq}/C against R_{eq} thus gives a straight line from which R_{max} and K_A can be calculated. This plot is analogous to a standard Scatchard plot. Parameters which calculated from BIAevaluation software are shown in Table A.1.

Table A.1 Parameters and reporting parameters from BIAevaluation solfware.

Parameters		Reporting parameters		
T_{on}	Starting time for sample injection (s)	K_A	k_a/k_d	Equilibrium binding constand (affinity)
T_{off}	Ending time for sample injection (s)	K_D	k_d/k_a	Equilibrium dissociation constand
Conc	Analyte concentration (M)	R_{eq}	$\frac{k_a \times Conc \times R_{max}}{\left(k_a \times Conc \times k_d\right)}$	Steady state binding level
R_{max}	Maximum analyte binding capacity (RU)	k_{obs}	$k_a \times Conc + k_d$	Observed rate constant
K_a	Association rate constant ($M^{-1}s^{-1}$)			
K_d	Dissociation rate constant (s^{-1})			
RI	Bulk refractive index contribution (RU)			

Bibliography

Journal publications related to this thesis

1. Anan Jeenanong, Haruma Kawaguchi
   "SPR response of stimuli-sensitive microgel on sensor chip"
   Colloid and Surfaces A: Physicochem. Eng. Aspects, 302, 403-410 (2007).
2. Anan Jeenanong. and Haruma Kawaguchi
   "Effect of pH and temperature on the behavior of microgel in SPR sensor"
   Colloid and Surfaces A: Physicochem. Eng. Aspects, 315, 232-240 (2008).
3. Anan Jeenanong. and Haruma Kawaguchi
   "Protein Adsorption to 2D-arrayed microgels on SPR chip"
   Transactions of Materials Research Society of Japan, In press.

International Conferences

1. Anan Jeenanong.* and Haruma Kawaguchi., "SPR response of temperature and pH- sensitive microgel on sensor chip," 4th East Asian Polymer Conference, Tianjin, China (2006).
   (5/28-31, 2006)
2. Anan Jeenanong.* and Haruma Kawaguchi., "Effect of NaCl, pH, and temperature on the behavior of microgel in SPR sensor," 234th American Chemical Society National Meeting, Boston, USA. (2007).
   (8/19-23, 2007)
3. Anan Jeenanong.* and Haruma Kawaguchi., "Protein Adsorption to 2D-arrayed microgels on SPR chip," The Doyama Symposium on Advanced Materials, Tokyo, Japan (2007).
   (9/5-8, 2007)